12-1-2013

Recovering Bioresources from Integrated Photo-Bioelectrochemical System

Li Xiao
University of Wisconsin-Milwaukee

RECOVERING BIORESOURCES FROM INTEGRATED PHOTO-BIOELECTROCHEMICAL SYSTEM

by

Li Xiao

A Dissertation Submitted in

Partial Fulfillment of the

Requirements for the Degree of

Doctor of Philosophy

in Engineering

at

The University of Wisconsin-Milwaukee

December 2013

ABSTRACT
RECOVERING BIORESOURCES FROM INTEGRATED PHOTO-BIOELECTROCHEMICAL SYSTEM

by

Li Xiao

The University of Wisconsin-Milwaukee, 2013
Under the Supervision of Professor Zhen He

Compared to traditional wastewater treatment technologies, the electricity generation is one of the most important advantages of bioelectrochemical systems (BES). However, due to its high cost and low energy production, BES technologies are still far away from feasible application. The main purpose of this work was to investigate ways to improve the electricity generation and reduce the cost of BES technologies. We focused on microbial fuel cells (MFCs) and microbial electrolysis cells (MECs) as two representative BES technologies. In order to improve the energy performance of MFCs, an accurate evaluation of the energy is necessary. However, the common evaluation methods of the energy performance in most MFC related studies prevent the meaningful comparison between different MFCs, and hence impede the further development of MFC technologies. So this study developed a new parameter, normalized energy recovery, to evaluate the energy performance of MFCs. Electrode materials are the main expense for the construction of BES and they have a significant effect on the performance of BES. Crumpled graphene and carbon/iron-based nanorod catalyst are relatively low-cost materials, so were applied in BES to improve their performance. Also, a novel system, integrated photo-bioelectrochemical (IPB) system, was developed to integrate algal

technology and MFCs. The IPB system can efficiently remove the organics and nutrients in the wastewater and produce electricity and biomass.

Table of Contents

LIST OF FIGURES

LIST OF TABLES

LIST OF ABBREVIATIONS

AC	Activated carbon
AEM	Anion exchange membrane
BES	Bioelectrochemical system
CC	Carbon cloth
CE	Coulombic efficiency
CEM	Cation exchange membrane
CNT	Carbon nanotube
COD	Chemical oxygen demand
CR	Coulombic recovery
CV	Cyclic voltammetry
DO	Dissolved oxygen
EIS	Electrochemical impedance spectroscopy
FO	Forward osmosis
GO	Graphene oxide
HER	Hydrogen evolution reaction
HRT	Hydraulic retention time
IPB	Integrated photo-bioelectrochemical
LSV	Linear sweep voltammetry
MCC	Microbial carbon capture cell
MEC	Microbial electrolysis cell
MFC	Microbial fuel cell
N/A	not available
N/D	not detected
NER	Normalized energy recovery
OCP	Open-circuit potential
ORR	Oxygen reduction reaction
PAMFC	Photosynthetic algal microbial fuel cell
PBS	Phosphate buffer solution
PFC	Photomicrobial fuel cell
PTFE	Polytetrafluoroethylene
PVC	Polyvinyl chloride
r-GO	Reduced graphene oxide
SCOD	Soluble chemical oxygen demand
SEM	Scanning electron microscopy
SHE	Standard hydrogen electrode
SSM	Stainless steel mesh
TEM	Transmission electron microscopy

ACKNOWLEDGEMENTS

I owe my gratitude to all the people who have supported and encouraged me during my years here at UW-Milwaukee. My utmost gratitude undoubtedly will go to my advisor, Professor Zhen He (Jason). Jason has not only taught me how to design and conduct experiments, but also trained me how to communicate and present the results effectively. His weekly literature report turned out to be very beneficial for me in the early stage of my research. Jason was also very supportive in my job/postdoc search. I am grateful to have such a knowledgeable and inspiring advisor who made my PhD research life stimulating and productive.

I would like to thank all the members in the Evironmental Biotechnology & Bioenergy Laboratory (EBBL): Fei, Kyle, Kristen, Jackie, Suqing, Bo, Zheng, Qingyun, Jian, Mary, Ananta, Patrick, Yiran, Suri. They have made the EBBL a very pleasant and coherent place to work. They were always ready to help me and were happy to discuss any issues in research. Without their help, I could not imagine I could finish any of my projects or have any vacation in the past over three years. I am also thankful to my collaborators: Prof. Jiaxing Huang, Prof. Erica Young, Dr. Zhenhai Wen, et al., who taught me a lot in their fields.

I would like to thank my thesis committee members: Prof. Jin Li, Prof. Qian Liao, Prof. Erica Young and Prof. Nanduri for their valuable comments on my proposal and final thesis. Three of them (Profs. Li, Liao and Nanduri) were also lecturers in many of my graduate classes, and I thank them and other teachers for my educations received here. I also especially thank Dr. Young for her support and collaboration on my IPB project.

I would like to thank my friends in Milwaukee, especially Wei, Jie and Nan. They have helped me go through the highs and lows in Milwaukee, especially helped me get accustomed to the life in my early days here. We also had a lot of fun time together. Lastly and most importantly, I would like to thank my family for their constant support and encouragement. Throughout the years my parents have always been very supportive in my career and life. My husband, Liang, has been a large part of my life, and I feel very happy to have him by my side moving forward.

1 Introduction

1.1 Energy issues

With global industrialization and rising population, the demand for energy is increasing rapidly. The International Energy Agency (IEA) forecast that global energy consumption by 2030 would be increased by another 60% compared to 2001 [1]. Although huge energy sources are on exploitation, the energy use per capita started decreasing since 2010 but the price of energy is still increasing all the time (Figure 1). Figure 2 shows that fossil fuels are still the main energy sources today, but these sources are not sustainable, as the formation of fossil fuels takes millions of years while the energy demand in industry and people's daily life increases exponentially. In the 20^{th} century, global population quadrupled and our energy demand went up 16 times [2]. The exponential energy consumption is exhausting our fossil fuel supply at an alarming rate. So renewable energy sources, such as sunlight, wind, and geothermal heat, attract people's attention since they can be continually replenished. But only 9% of current global energy consumption comes from renewable sources including hydroelectric power, wood, biofuels, wind, waste, geothermal and solar energy (Figure 2). Energy Information Administration (EIA) predicted that about half of the global energy demand could be met by renewable sources by the year 2050 [3]. Among the renewable sources, organics in the wastewater treated by bioelectrochemical systems (BES) could be an important one. The BESs are unique systems capable of converting the chemical energy of organic waste into other forms of energy, such as electrical energy in microbial fuel cells (MFCs) and hydrogen energy in microbial electrolysis cells (MECs) [4].

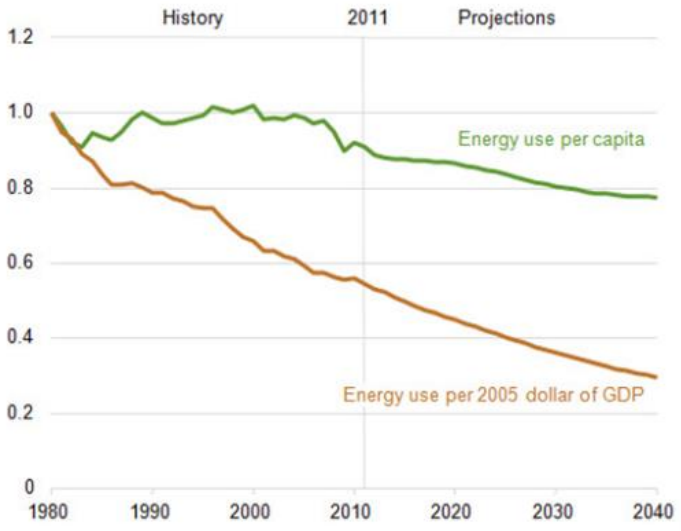

Figure 1. Energy use per capita and per dollar of gross domestic product, 1980-2040 (index, 1980 = 1) [5].

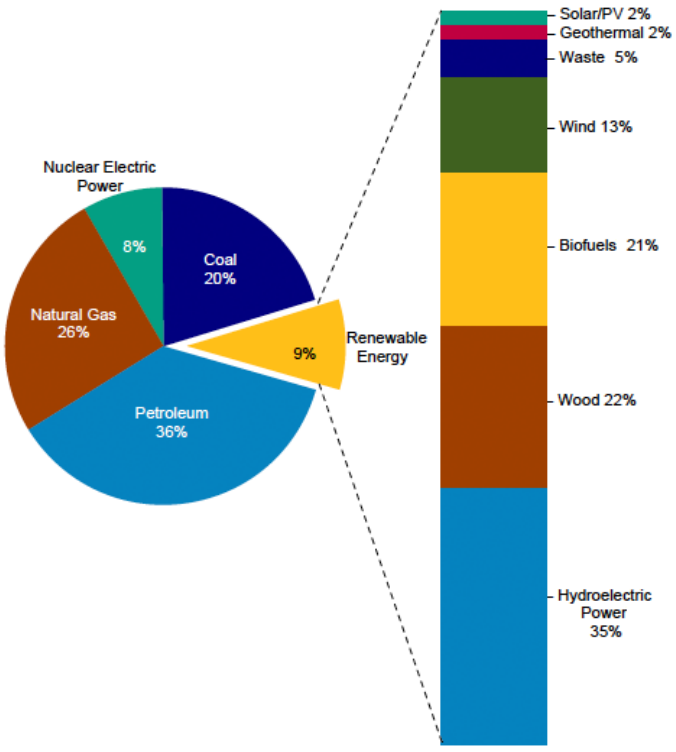

Figure 2. Primary energy production by sources [5].

1.2 Microbial fuel cells

Wastewater contains a high content of organic matter and nutrients, which can be used as sources of energy to offset the energy consumption in wastewater treatment. Therefore, as a type of BES technology, microbial fuel cells (MFCs), which convert the energy stored in the chemical bonds of organic compounds to electrical energy, has raised great interest of research in related fields in recent years [6]. MFCs usually use bacteria as biocatalysts to degrade organic matter and facilitate the electron transfer. In 1911, Potter observed the current produced by the bacteria, which opened the door to the studies of microbial fuel cells [7]. In the late 1990s, Kim and coworkers demonstrated that bacteria could be used in a biofuel cell as a method of determining the concentration of lactate in water [8], and then electricity generation in an MFC could be sustained by using some industrial wastewater [9]. From then on, MFC was not only a novel technology to produce electricity, but also a feasible method to treat wastewater.

1.2.1 Principle of MFCs

A schematic diagram of an MFC system is shown in Figure 3. Two chambers (anode chamber shown as a pink box and cathode chamber shown as a blue box in Figure 3) are separated by a membrane (cation exchange membrane, CEM or anion exchange membrane, AEM, shown as a yellow line in Figure 3). The two electrodes (anode electrode and cathode electrode, shown as black bars in Figure 3) are connected by a wire containing a load (e.g., a resistor).

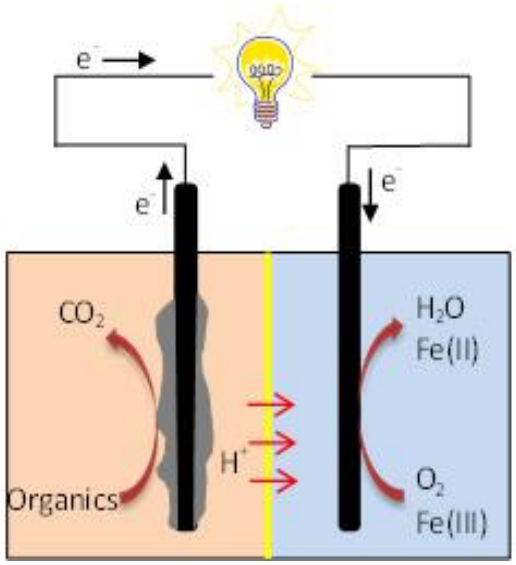

Figure 3. A schematic diagram of an MFC (pink box: anode chamber; blue box: cathode chamber; yellow line: membrane; black bars: electrodes)

In the anode chamber, bacteria oxidize the organic matter and transfer the electrons to the anode electrode (see half reaction (1)). Then the electrons go through the outside circuit to the cathode electrode and are accepted by an electron acceptor (e.g. O_2 or Fe(III)) in the cathode chamber (half reaction (2)) to generate current. The electron transport is driven by the difference in the redox potential between the aerobic cathode reaction and the anaerobic anode reaction. Under the standard condition, the maximum voltage of an MFC is about 1.2 V.

$$\text{Anode: Organics} \rightarrow CO_2 + H^+ + e^- \qquad (1)$$

$$\text{Cathode: } O_2 + H^+ + e^- \rightarrow H_2O \qquad (2)$$

1.2.2 The expression for the performance of MFCs

The first observation one makes about the electricity production from MFCs is the voltage, which can be measured by a voltage meter. The working voltage of an MFC is commonly 0.3-0.8V, varied by the external resistance (R) [10]. Current is another important parameter in any electricity generation device. For an MFC, current can be calculated from voltage and external resistance (Table 1). The amount of energy extracted from wastewater by an MFC is also an essential consideration for its performance, which can be expressed by Coulombic efficiency (CE) and Coulombic recovery (CR). The Coulombic efficiency is calculated as the ratio of total amount of coulombs actually produced and the coulombs contained in the removed organics, while the Coulombic recovery is calculated as the ratio of total amount of coulombs actually produced and the total coulombs contained in feeding organics. The actually transferred coulombs can be determined by integrating the current over time. The total coulombs contained in removed/feeding organics can be calculated as the theoretical coulombs of transferred electrons if all removed/feeding organics participate in the half reaction (2) (see explicit expressions in Table 1).

The energy performance of MFCs is usually expressed as power, which can be calculated by multiplying current and voltage. In order to compare MFCs of different configurations and sizes, power density is often shown in the MFC related studies instead of power. The power density is widely used in electrical sources studies, such as fuel cells, and can be calculated from power divided by the surface area of the electrode or the volume of the cell. However, an MFC is not only an electricity generation device but also a wastewater treatment unit. So energy density based on the volume of treated wastewater or removed

organics is also an important parameter to evaluate the energy performance of MFCs and we call it normalized energy recovery (Table 1). Other commonly used parameters for wastewater treatment plants are also important in MFCs studies, such as hydraulic retention time, organic loading rate, etc. The main parameters for evaluating the performance of MFCs are listed in Table 1.

Table 1. Parameters for evaluating performance of MFCs

Parameters	**Units**	**Calculation/measurement**
Electrode potential	V	Φ, measured between electrode and reference electrode
Voltage	V	U, measured between two ends of the applied external resistance
Open circuit voltage	V	OCV, voltage at infinite resistance
Current	A	I=U/R, R is external resistance
Power	W	$P=I^2R$ or P=IU
Current density	A/m^2	$I_A=I/A$, A is projected electrode surface area
Current density	A/m^3	$I_V=I/V$, V is the volume of the cell
Power density	W/m^2	$P_A=P/A$
Power density	W/m^3	$P_V=P/V$
Coulombic efficiency	%	$CE=(I\times t)/(96485\times\Delta COD\times 4)$, t is time, ΔCOD is the amount of removed organics in moles expressed in chemical oxygen demand (COD)
Coulombic recovery	%	$CR=(I\times t)/(96485\times COD\times 4)$, COD is the amount of total feeding organics in moles expressed in COD
Internal resistance	Ω	R_i, calculated from $P_{max}=OCV^2R/(R_i+R)^2$, P_{max} is maximum power
Normalized energy recovery	kWh/m^3	$NER_V=P/Q$, Q is wastewater flow rate
Normalized energy recovery	kWh/kg COD	$NER_S=P/(\Delta COD\times Q)$
Hydraulic retention time	hour	HRT=V/Q
Organic Loading rate	$kg/m^3/day$	$OLR=COD\times Q/V$
Organic removal rate	$kg/m^3/day$	$ORR=\Delta COD\times Q/V$
Organic removal efficiency	%	$ORE=(1-\Delta COD/COD)\times 100$

1.2.3 Materials used in MFCs

A typical MFC consists of three main physical components including an anode electrode, a cathode electrode and a separator (note that in membrane-less MFCs the separator is taken out for reducing the internal resistance and construction cost [11]). Therefore, in order to improve the performance of MFCs, large amount of efforts were made to explore more effective materials for MFCs. Some commonly used materials are listed in Table 2.

Table 2. Some common materials used in MFCs

Electrode	**Catalyst**	**Separator**
Graphite plate/rod	Pt	Cation exchange membrane
Graphite fiber	Co/FeCoTMPP	Anion exchange membrane
Carbon brush	Fe/FeCu/CoPc	Nafion membrane
Carbon paper	Co/Fe/NCNT	Microfiltration membrane
Carbon cloth	MnO_x	Ultrafiltration membrane
CNTs	Co-OMS-2	Bipolar membrane
Stainless steel	Ruile	J-Cloth

Anode electrode materials must be conductive, biocompatible and chemically stable in the reactor solution [12]. And materials with high surface area are preferred for anode electrodes, which are good for the attachment of bacteria. Therefore, carbon based materials are popular for anode electrodes, such as carbon paper, graphite rod and carbon brush [12]. The simplest anode materials are graphite plates or rods, which are cheap, easy to handle and have a well-defined surface area. Much higher surface area is achieved by using carbon brush, which is made from carbon fibers. The surface area is estimated to be 18200 m^2/m^3-brush volume for the small carbon brush, and 7170 m^2/m^3-

brush volume for the large carbon brush [13]. With the development of nanotechnologies, some unique and excellent properties of some nano-materials have received great interest in applying on anode electrode. For example, Qiao and coworkers evaluated a carbon nanotube (CNT)/polyaniline (PANI) composite as the anode material for high power MFCs and they also synthesized a nanostructured polyaniline (PANI)/mesoporous TiO_2 composite as the anode in Escherichia coli MFCs [14][15].

Basically, the anode materials can also be applied as cathode materials. However, depending on the cathode reaction, there are different requirements for cathode electrodes. For example, electrodes with catalytic activity are required to reduce the over potential of the oxygen reduction, while electrodes with high surface area and good biocompatibility are required for biocathode reactions. The most commonly used catalyst for cathode electrodes is Pt, which is very expensive. To reduce the cost of MFCs, a large number of catalysts are used to replace Pt, such as manganese oxides, metal tetramethoxyphenylpophyrin (CoTMPP and FeCoTMPP) and metal phthalocyanine (FePc, CoPc and FeCuPc) [16][17].

Except membrane-less MFCs and sediment MFCs, the separator is also an important material in most MFCs. Currently, cation/anion exchange membranes (CEM/AEM) are widely used in MFCs. These membranes are used to separate the anode and cathode chambers, as well as to selectively transfer ions between anode and cathode chambers. In order to increase the efficiency, some special membranes are introduced to MFC technology. Heijne et al. applied a bipolar membrane in a flat plate MFC in 2006 [18]. In contrast to the CEM/AEM which can only transfer cation or anion ions, the bipolar membrane consists of cation and anion exchange sections jointed together [18]. Forward

osmosis (FO) membrane is a semi-permeable membrane used to induce flow from high-water potential part to low-water potential part. In 2011, Zhang et al. developed an osmotic MFC with an FO membrane as a separator for wastewater treatment and water extraction [19].

1.2.4 Configurations of MFCs

A lot of different configurations have been developed for MFCs. A basic and widely used design is an "H" type MFC (Figure 4A). It is built with two glass bottles jointed by an ion exchange membrane such as CEM, AEM or Nafion. It is easy to set up, operate and control, so it is a good choice to do some fundamental researches on MFCs, such as examining power production using new materials, testing the effect of different cultures on the anode and so on. However, because of the tube between the two glass bottles, the distance between the electrodes is long and the membrane area is small. So the efficiency of "H" type MFC is not very high.

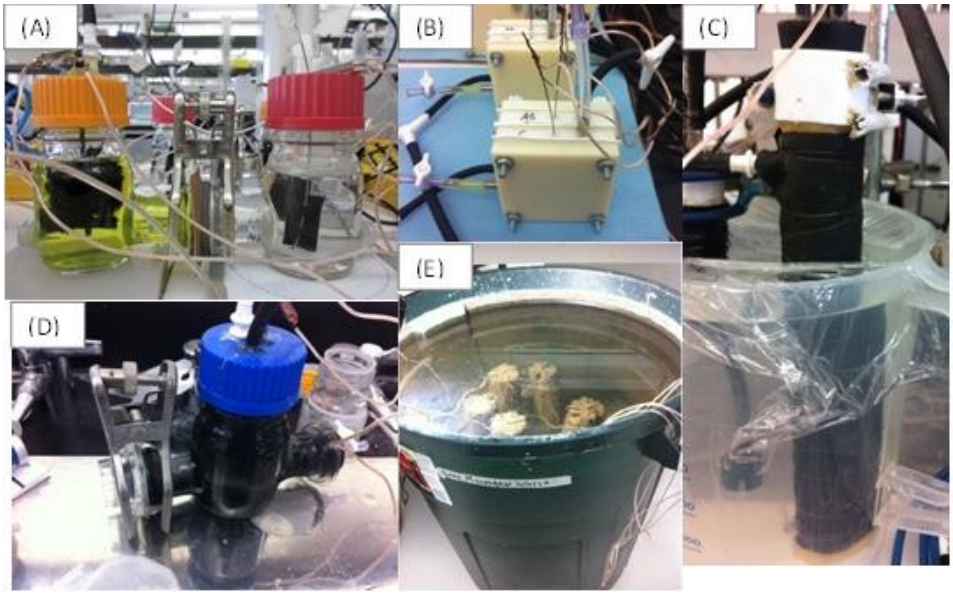

Figure 4. Several configurations of microbial fuel cells in our lab (A: “H” type MFC; B: plat MFC; C: tubular MFC; D: single chamber; E: sediment MFC)

In order to improve the efficiency, two chambers directly connected by a membrane without the tube can form a flat MFC (Figure 4B). In this case, the distance between two electrodes becomes much shorter and the membrane area is larger than that in the “H” type MFC. Another commonly used configuration is tubular MFC (Figure 4C). It is constructed based on a CEM or AEM tube with a certain diameter and height. One can also add a PVC tube to support the membrane tube. Usually the inside of the tube is the anode chamber and the outside is the cathode. It has very high membrane area and is easily scaled up.

There are two configurations that do not have membrane, single chamber MFC (Figure 4D) and sediment MFC (Figure 4E). For the single chamber MFC, the anode chamber is separated from the air-cathode chamber by a gas diffusion layer allowing for a passive oxygen transfer to the cathode. Without the membrane, the ion transfer becomes easy, so

the internal resistance of single chamber MFC is much lower than that of a two-chamber MFC with a membrane. However, with the time of operation, the cathode electrode is gradually contaminated by the anode bacteria and the activity of catalysts on the cathode electrode declines. So the performance could be diminished with time. Sediment MFC can be easily used in the river and lake. There are two layers in a sediment MFC, a solid layer (sludge) as anode and a liquid layer as cathode. It is almost the simplest MFC and can provide electricity to power some sensors under the water.

1.2.5 Factors on the performance of MFCs

There are a lot of factors affecting the performance of MFCs. One of the most important facts is the reactor design, including configurations, size and materials. The first thing in designing an MFC is choosing a suitable configuration based on your requirements and environmental conditions. Several commonly used configurations of MFCs are described in section 1.2.4. For example, “H” type MFC is good for fundamental research while tubular MFC is suitable for scaling up, and if you want to set an MFC in the lake to provide electricity for some sensors in the bottom of the lake, sediment MFC is a good choice. Size is also a very important factor for MFCs. Large surface area electrodes usually improve the rate of the electrode reaction. Large membrane area is good for ion transfer. But the larger size MFCs always produce less power density. The distance between anode and cathode electrodes also affects the ion transfer, and the shorter distance leads to lower internal resistance and produce more electricity. Materials also have large influence on the performance of MFCs, which are described in section 1.2.3.

For example, an MFC with carbon fiber brush as anode electrode produced over two times as much power density as an MFC with carbon paper in one study by Logan and coworkers[13].

Another set of factors is operational parameters including wastewater properties, flow rate and external resistance. The properties of wastewater include substrate type and concentrations of nutrients, pH, temperature and conductivity. Except the substrate type, the wastewater can be pretreated to achieve an optimal set of properties for the operation of MFCs.

Substrates are food sources for the microbial communities in the anode, and electron sources for electricity generation in MFCs. So substrate is an important factor in the performance of MFCs. Acetate is a simple substrate, which is widely used as carbon source in MFCs because of its inertness towards alternative microbial conversions (fermentations and methanogenesis) at room temperature [20]. Glucose, as the simplest fermentative substrate, is another common substrate used in MFCs. Some special wastes, such as dye, corn stover, and farm manure, have also been applied in MFCs [20]. Compared to complex substrates, such as domestic wastewater, MFCs with pure and simple substrates usually show significantly higher performance [21]. The different substrate concentrations can also lead to different power generation and Coulombic efficiency.

Temperature and pH are the two most important factors for the activity of bacteria and the potential of the reaction happening on the electrodes. A neutral pH is preferred by anode bacteria, while low pH can increase the rate of the cathode reaction [22]. Different

bacteria require different temperatures: thermophilic bacteria can live in MFCs at a temperature around 55 ℃ [23]. For bacteria commonly used in MFCs, the optimum temperature range is 30-37 ℃ [24]. However, higher temperature means more energy input, and lower temperature sometimes does not affect the energy performance much; Liu et al. found that decreasing the temperature from 32 to 20 ℃ only reduced the power output of an MFC by 9% [24]. So with the consideration of the expense, room temperature (around 20 ℃) is widely used in MFC related works. High conductivity, usually achieved by increasing the ionic strength of the solution, can decrease the internal resistance of an MFC and improve the ion transfer. Power density was increased from 720 to 1330 mW/m^2 by increasing the solution ionic strength from 100 to 400 mM [24]. But additional cost is associated with adding salt into the wastewater to increase the conductivity and removing salt in the post-treatment to get clean water.

Flow rate determines the hydraulic retention time (HRT) of the MFCs when the reactor cell is fixed. At the same time, the flow rate also affects the organic loading rate of MFCs. The high flow rate leads to a low HRT but a high organic loading rate. The high flow rate provides more substrates for MFCs and a better mixing condition of wastewater. Moon et al. studied the effect of the flow rate on the performance of MFCs and found that the power density was increased as the flow rate was increased up to 0.65 ml/min [25]. When the flow rate was increased to 1 ml/min, the MFCs showed lower power density than at 0.65 ml/min [25]. The poor performance of MFCs at the high flow rate may be due to the faster growth of the fermentative bacteria than of the electrochemically active bacteria acidifying the anode [25].

External resistance is also an important factor in the electricity generation by MFCs. The highest voltage is obtained at the infinite resistance, which is called open circuit voltage. A low external resistance leads to a low voltage but high current, which results in a high electrode reaction rate. When the external resistance equals to the internal resistance, MFCs produce the maximum power. So depending on the function of MFCs, different external resistances need to be chosen. For example, the low external resistance is applied on the MFCs used for hydrogen production or desalination, which requires high current.

1.3 Microbial electrolysis cells

In about one hundred years of BES development, a lot of functions were found beyond producing electricity and consuming organic matter in wastewater, such as desalination, softening water and hydrogen production. Microbial electrolysis cell (MEC), whose final product is hydrogen gas, is one of many well-known BES technologies (Figure 5).

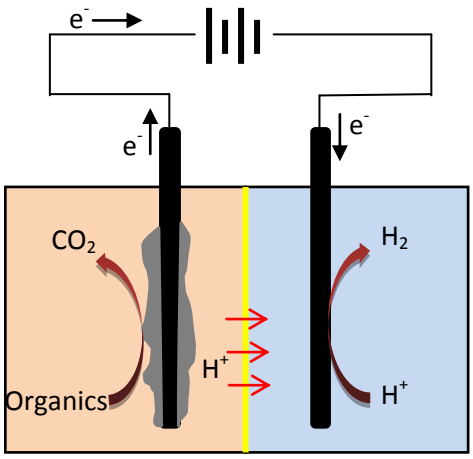

Figure 5. Schematic diagram of a microbial electrolysis cell (pink box: anode chamber; blue box: cathode chamber; yellow line: membrane; black bars: electrodes)

Whilst MFCs produce an electric current from the microbial decomposition of organic compounds, MECs partially reverse the process to generate hydrogen or methane from organics by applying an external power supply. Because of the electric potential supplied by the anode reaction, MECs require an additional voltage as low as 0.2 V from external sources to reduce protons to hydrogen gas, which is a significant advantage compared to hydrogen production via water electrolysis [26]. MECs offer opportunities to recover hydrogen as an energy carrier from biomass and wastewater; in particular, MECs can use fermenting products from biohydrogen-producing processes and thus maximize hydrogen production if linked to biohydrogen production.

1.4 Objectives of the thesis

The main objective of this thesis was to research ways to improve energy performance of bioelectrochemical systems (BES). The specific objectives were: (1) develop a new concept/parameter to evaluate the energy performance of MFCs; (2) modify electrodes of BES with novel nano-materials; (3) design a new type of BES by integrating algal bioreactors and MFCs.

2 Evaluation of normalized energy recovery (NER) in tubular microbial fuel cells

(This section is under review for publication in Journal of Power Sources)

2.1 Introduction

Microbial fuel cells (MFCs), which combine wastewater treatment and energy recovery in a single system, hold a great promise to become an energy-efficient technology for sustainable wastewater treatment [27]. The direct electricity generation with aid of microbial respiration of an electrode in an MFC has some advantages over conventional energy-recovering technologies such as anaerobic digestion. Thus, there have been intensive studies of MFCs in the aspects of microbiology, electrochemistry, materials of electrodes and membranes, and system development and operation in the past decade [28]. The performance of "electricity generation" in an MFC is usually described by the data of voltage, current and power. With incorporating the factors of electrode surface area or reactor liquid volume, current and power is also presented in densities (e.g., A m^{-3} and W m^{-3}). Significant efforts have been made to improve the maximum power density in MFCs. Although energy information was mentioned in some prior publications and energy efficiency has been defined before [29][30], there has been a lack of proper presentation of energy data in most MFC studies [31]. Energy, which is often shown in joule (J) or kilowatt hour (kWh), is a key parameter to evaluate the performance of the MFCs that are designed focusing on energy recovery. Reporting energy data will also facilitate communication between MFC researchers and wastewater industries; the latter usually use kWh or kWh m^{-3} to evaluate energy consumption by wastewater treatment [32].

To help with presenting energy data in MFCs, a new parameter - normalized energy recovery (NER) was recently proposed [21]. NER is expressed in two units: NER_V in kWh m^{-3}, based on the volume of the treated wastewater in an MFC (or power divided by wastewater flow rate, Eq. 1), and NER_S in kWh $kgCOD^{-1}$, based on the amount of organic substrates (measured as chemical oxygen demand, COD) removed in an MFC (or power divided by removed COD and wastewater flowrate, Eq. 2). Compared with power density, NER excludes the factor of the reactor size and involves the information of wastewater flow rate and organic removal efficiency, which may make NER more suitable for cross-wise comparison between different MFCs designed for wastewater treatment. Moreover, presenting NER data will also help to establish an energy balance in MFCs, which can reveal the gap of both knowledge and development for MFCs to be an energy-neutral or -positive treatment technology. Therefore, the use of NER will provide an effective approach to quantitatively understand the energy performance of MFCs.

$$NER_V = \frac{Power}{Wastewater\ \ flow\ rate} \qquad \text{(Eq.1)}$$

$$NER_S = \frac{Power}{Removed\ COD \times Wastewater\ \ flow\ rate} \qquad \text{(Eq.2)}$$

A recent review paper has examined energy data (expressed in NER) from the MFC publications appeared in the past twelve years, and its analyses had some interesting indication [21]. For example, the MFCs generally recover a low NER (< 1.0 kWh m^{-3} or 1.0 kWh $kgCOD^{-1}$) with a few exceptions of higher NER values. Although the maximum power densities seem to decrease with increasing reactor size, there was no significant difference in NER among the analyzed MFC studies. The MFC fed with acetate recover

more energy than those with more complicated substrates, and no significant difference in the NER_V was observed between the MFCs fed with different acetate concentrations, while the NER_S from the low-strength substrate (acetate < 500 mg L^{-1}) is higher than that with acetate > 500 mg L^{-1}. However, those findings are indications rather than conclusions, because it is hard to draw any firm conclusions based on the NER data from various MFC studies with significant difference in reactor configurations/operation, electrode/membrane materials, substrates and microbiology. There is need for well-designed experiments to verify some of those findings and to help us better understand the energy performance of MFCs.

In this study, we have evaluated energy recovery in tubular MFCs with different reactor dimensions or substrates. The tubular configuration was chosen because it has been well investigated before and much information on system operation has been obtained [33][34]. We think that tubular MFCs have potential to be further scaled up; the first MFC pilot used tubular configuration [28], and our ongoing project on MFC scaling up also adopted tubular reactors. Thus, evaluation of energy recovery in tubular MFCs will be of great interest to its further development. All MFCs in this study were continuously operated, and both power densities and NER data were analyzed. This work presents the first systematic investigation of energy performance (in the unit of NER) in MFCs.

2.2 Materials and methods

Tubular MFC setup

Multiple tubular MFCs with different dimensions (shown in Table 3) were constructed similarly to our previous MFCs [34]. Cation exchange membrane (CEM, Ultrex CMI7000, Membranes International, Inc., Glen Rock, NJ, USA) was used to make a tube containing a polyvinyl chloride (PVC) tube as an interior supporter. Carbon brush (Gordon Brush Mfg. Co., Inc., Commerce, CA, USA) was used as the anode electrode; before use, the carbon brush was pretreated by being immersed in acetone overnight and then heated at 450 ℃ for 30 min. The cathode electrode was a layer of carbon cloth coated with activated carbon (AC, as the cathode catalyst) wrapping the CEM tube. To coat the catalysts on the cathode electrode, AC powder was mixed with polytetrafluoroethylene (PTFE) solution and then applied to the surface of carbon cloth by using a brush to achieve a final loading rate of ~5 mg AC cm^{-2}; the coated carbon cloth was heated at 370 ℃ for 30 min. The anode and cathode electrodes were connected by copper wires to an external circuit across a resistance box.

Table 3. Experimental conditions of four groups of the tubular MFCs used in this study. V_{anode} is the anode liquid volume, COD_{in} is the influent COD concentration, HRT is hydraulic retention time, and $COD_{Loading}$ is the COD loading rate.

		MFC Configuration			**MFC Operation**					
		Diameter (cm)	Length (cm)	V_{anode} (mL)	COD_{in} (mg L^{-1})	Substrate	Stage I		Stage II	
							HRT (h)	$COD_{Loading}$ (kg m^{-3} d^{-1})	HRT (h)	$COD_{Loading}$ (kg m^{-3} d^{-1})
1	A	3.81	20	400	390	Acetate	13.3	0.70	13.3	0.70
	B	5.08	20	700	390	Acetate	23.3	0.40	13.3	0.71
	C	7.62	20	1700	390	Acetate	56.7	0.16	13.3	0.70
2	A	3.81	10	180	390	Acetate	6	1.56	13.0	0.72
	B	3.81	20	400	390	Acetate	13.3	0.70	13.3	0.70
	C	3.81	100	1800	390	Acetate	60	0.15	13.3	0.70
3	A	3.81	20	400	195	Acetate	13.3	0.35	N/A	N/A
	B	3.81	20	400	390	Acetate	13.3	0.70	N/A	N/A
	C	3.81	20	400	2341	Acetate	13.3	4.21	N/A	N/A
4	A	3.81	20	400	195	Acetate	13.3	0.35	N/A	N/A
	B	3.81	20	400	192	Glucose	13.3	0.35	N/A	N/A
	C	3.81	20	400	192	Waste water	13.3	0.35	N/A	N/A

Operating conditions

Four groups of MFCs (shown in Table 3) were operated in a continuously-fed mode at a room temperature (~ 20 ℃). The anode compartments were inoculated with the anaerobic sludge from a municipal wastewater treatment plant (South Shore, Milwaukee, WI). Except an MFC in the group 4 that used the actual wastewater (primary effluent from South Shore Water Reclamation Facility), the anode feeding solution in other MFCs was prepared as (per L of DI water): NH_4Cl, 0.15 g; NaCl, 0.5 g; $MgSO_4$, 0.015 g; $CaCl_2$, 0.02 g; $NaHCO_3$, 0.1 g; KH_2PO_4, 0.53 g; K_2HPO_4, 1.07 g; trace elements, 1 mL [35]; and acetate or glucose with a designated concentration as shown in Table 1. All four groups of MFCs were operated with the same anolyte flow rate of 0.5 mL min^{-1} in the stage I, resulting in different hydraulic retention time (HRT) in the different-size MFCs. Both group 1 and 2 were continued to the stage II, in which the anolyte flow rate was adjusted

to achieve the same HRT of 13.3 h in all MFCs. The anolyte was recirculated at a rate of 100 mL min^{-1} in all MFCs. The cathode compartments were filled with 25-mM phosphate buffer solution (PBS, containing 1.3 g L^{-1} KH_2PO_4 and 2.7 g L^{-1} K_2HPO_4) and aerated with air. When the pH of the catholyte increased above 10, 50% of the catholyte was replaced with fresh PBS.

Measurement and analysis

The MFC voltage was recorded every 5 minutes by a digital multimeter (2700, Keithley Instruments, Inc., Cleveland, OH, USA). The polarization test was performed by varying external resistance. The concentration of chemical oxygen demand (COD) was analyzed by a DR/890 colorimeter (Hach Company, Loveland, CO, USA). The pH was measured by using a bench-top pH meter (Oakton Instrument Co., Ltd., USA). Power density (W m^{-3}) and current density (A m^{-3}) were calculated based on the liquid volume of the anode compartment. The NER_V (kWh m^{-3}) was calculated based on the volume of treated water, and NER_S (kWh $kgCOD^{-1}$) was calculated based on the mass of removed COD. Energy data were statistically analyzed for comparison by using two-sample t-test.

2.3 Results and discussion

Energy recovery in tubular MFCs with different dimensions

Reactor size and dimension is a key parameter in MFC design and development. Diameter and length are two critical factors in determining the size of a tubular MFC. Thus, we investigated the NER in the tubular MFCs with different diameters or lengths (to achieve different sizes).

(1) Tubular MFCs with different diameters

The MFCs in the Group 1 had the same length of 20 cm but different diameters varying from 3.81 cm to 7.62 cm, resulting in different anode liquid volumes (Table 3). Figure 6 shows the power or energy curves along increasing current densities in the stage I in which all MFCs received the same amount of the anolyte (at the same flow rate of 0.5 mL min^{-1}). We observed that the maximum current density and the maximum power density decreased with increasing the MFC's diameter (and thus the anode liquid volume); it should be noted that those two parameters were calculated based on the anode liquid volume, and thus a smaller volume could result in a higher density. However, the energy data showed that the MFC with the largest diameter (7.62 cm) produced a higher maximum NER_V, compared with the MFC with smaller diameters, and there was no significant difference in the maximum NER_S among these three MFCs (Figure 8A). The power and energy curves in the stage II (Figure 7) show some difference from the stage I. When the anolyte flow rate was adjusted to achieve the similar HRTs for the three MFCs in the stage II, the smaller MFCs generated higher maximum power densities than the 7.62-cm MFC, and there was no significant difference in the maximum power density

between the 3.81-cm and the 5.08-cm MFCs (Figure 8B). Likewise, the results of the maximum NER exhibited similar trends like the maximum power densities. In more details, the 7.62-cm MFC produced the lowest maximum NER_V (0.021 ±0.001 kWh m^{-3}) and the lowest maximum NER_S (0.089 ±0.001 kWh $kgCOD^{-1}$), while the other two MFCs recovered 0.048 ±0.001 kWh m^{-3}/0.181 ±0.002 kWh $kgCOD^{-1}$ and 0.048 ±0.001 kWh m^{-3}/0.187 ±0.006 kWh $kgCOD^{-1}$, respectively.

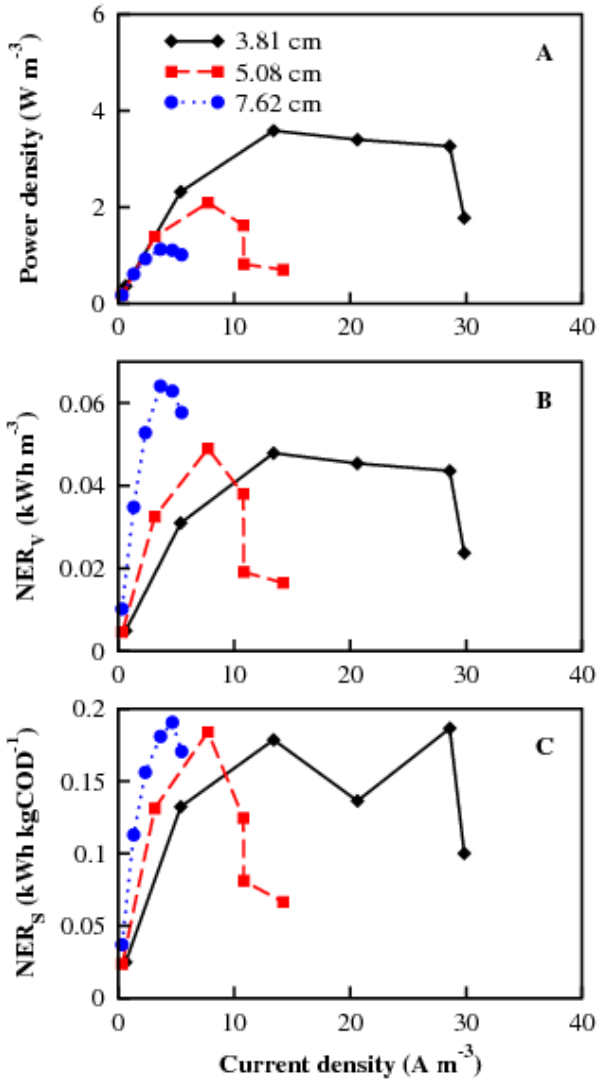

Figure 6. Variation of power or energy data along current density in the MFCs with different diameters at the same anolyte flowrate: (A) power curves; (B) NER_V; and (C) NER_S.

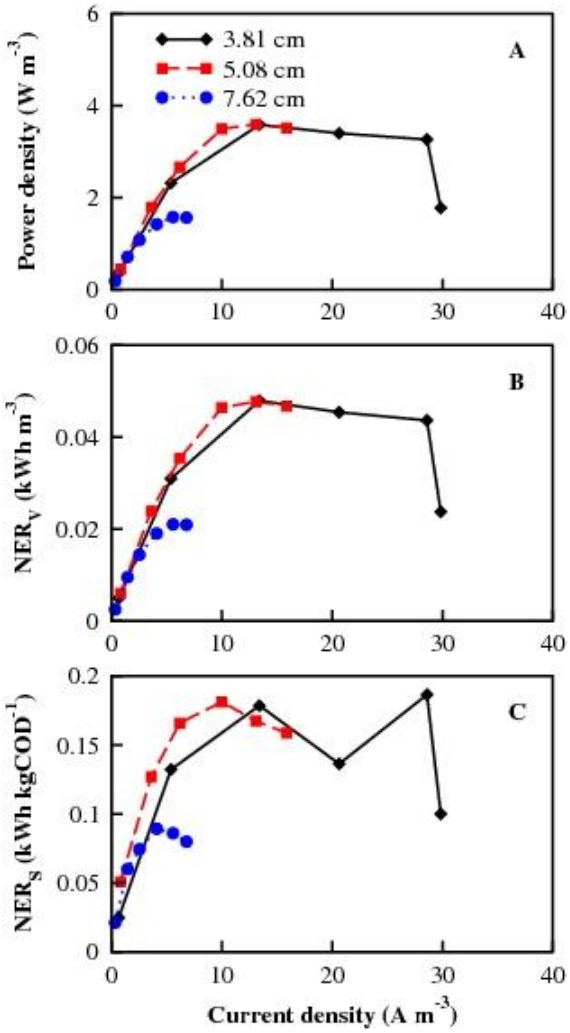

Figure 7. Variation of power or energy data vs. current density in the MFCs with different diameters at the same anolyte HRT: (A) power curves; (B) NER_V; and (C) NER_S.

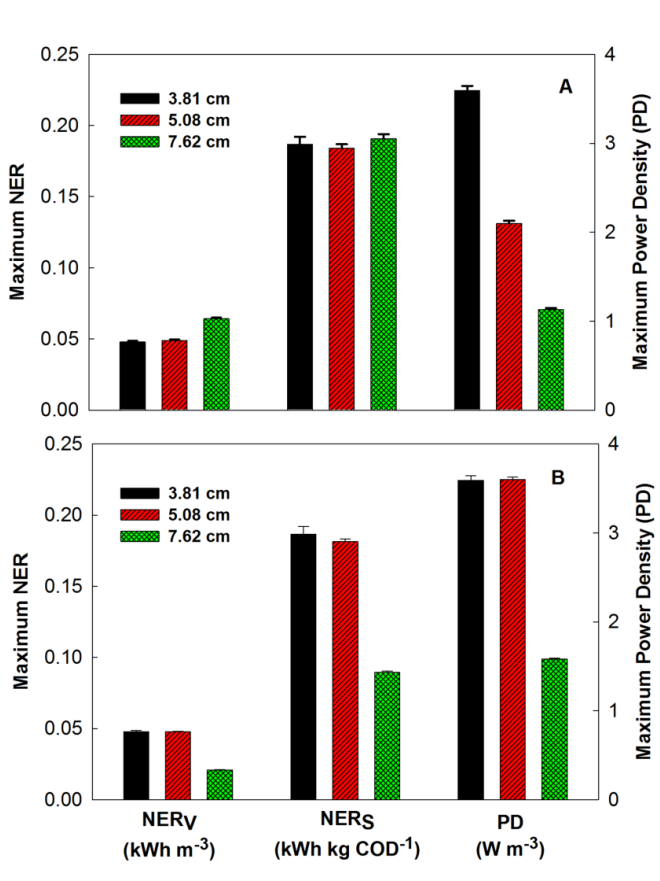

Figure 8. Comparaison of the maximum power density (PD) or the maximum NER in the MFCs with different diameters: (A) at the same anolyte flowrate; and (B) at the same anolyte HRT.

The above results confirmed that, although small MFCs generally produce a higher maximum power density, they do not always have advantages in energy recovery compared with larger-scale MFCs. This encourages further scaling up of MFC system. With the same anolyte flow rate, the three MFCs with different diameters (and thus different sizes) were treating the same amount of synthetic solution within the same time period. As a result, a larger MFC would allow a longer HRT and thus a lower organic loading rate, resulting in better treatment and energy recovery. The effects of HRT and organic loading rate on energy recovery were also demonstrated when the HRT (as well

as organic loading rate) was adjusted to be similar among the three MFCs in the stage II: the 7.62-cm MFC with a shorter HRT and a higher organic loading rate exhibited lower energy recovery. It should be noted that, at the same HRT, the smaller MFCs would treat much less wastewater than the larger MFCs. Those results indicate that the treatment capacity should be considered when evaluating the MFC performance, because the primary function of an MFC is thought to be wastewater treatment. The objective of this study was to examine the effect of MFC dimensions on energy recovery, rather than identifying the optimal dimensions (e.g., optimal diameter for a tubular MFC). The 7.62-cm diameter would not be an optimal diameter, because of its worse performance at a higher organic loading rate, possibly due to a larger distance between the anode and the cathode electrodes. The 5.08-cm diameter seems to be better in terms of energy recovery and has been used in our other ongoing research of tubular MFCs, but an optimal diameter requires further investigation.

(2) Tubular MFCs with different lengths

The effect of MFC size on energy recovery was further investigated in the MFCs with the same diameter of 3.81 cm but different lengths varying from 10 to 100 cm, thereby resulting in different anode liquid volumes (Group 2 in Table 3). Similar to the Group 1, the Group 2 MFCs were also operated in two stages with the same anolyte flow rate or the same HRT (or organic loading rate). The performance of the maximum power density still follows the similar trend as the Group 1: with the same anolyte flow rate, the smallest MFC produced the highest maximum power density (4.65 ± 0.02 W m^{-3}), which

was 1.3 times of that from the 20-cm MFC or 2.6 times of the maximum power density in the 100-cm MFC; while at the same HRT, the maximum power density from the 10-cm MFC was 4.80 ± 0.16 W m^{-3}, about 1.3 or 1.9 times of that from the 20-cm MFC or the 100-cm MFC (Figure 9). The maximum NER increased with the increasing lengths in the stage I, while showed the opposite trend in the stage II. In the stage I, the longest MFC produced the highest maximum NER_V of 0.108 ± 0.001 kWh m^{-3} and the highest maximum NER_S of 0.317 ± 0.003 kWh $kgCOD^{-1}$; in the stage II, the shortest MFC generated the highest maximum NER_V of 0.063 ± 0.002 kWh m^{-3} and the highest maximum NER_S of 0.236 ± 0.005 kWh $kgCOD^{-1}$.

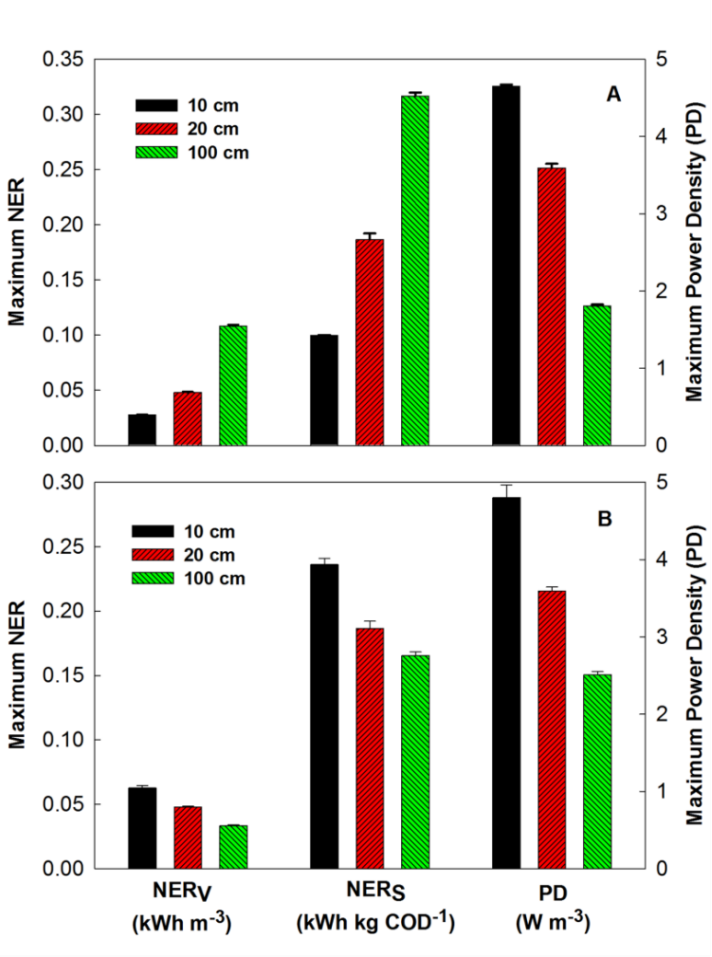

Figure 9. Comparaison of the maximum power density (PD) or the maximum NER in the MFCs with different lengths: (A) at the same anolyte flowrate; and (B) at the same anolyte HRT.

The results obtained from the Group 2 MFCs confirm that increasing MFC size does not necessarily decreases energy recovery, and HRT/organic loading rate obviously affects energy recovery. Similarly to the Group 1, a larger MFC (or a longer MFC) in the Group 2 enabled a longer HRT of the anolyte at the same feeding rate, resulting in better energy recovery. With the same HRT, the longer MFC could have a larger internal resistance due to more electrode/membrane materials used, which may lead to lower energy recovery. Again, the different-size MFCs treated different amount of the anolyte at the same HRT,

and a tradeoff between treatment capacity and energy recovery will need to be considered in the future design of MFC system.

When we put the Group 1C and the Group 2C MFCs together, we obtained two MFCs with similar size (1700 vs. 1800 mL) but totally different dimensions (diameters and lengths). The Group 2C MFC outcompeted the Group1C MFC in both power density and energy recovery, and the difference between the two is significant. For example, at the same flow rate of the anolyte, the maximum NER of the Group 2C MFC was 0.108 ± 0.001 kWh m^{-3} or 0.317 ± 0.003 kWh kg COD^{-1}, much higher than that of the Group 1C MFC (0.064 ± 0.001 kWh m^{-3} or 0.191 ± 0.003 kWh kg COD^{-1}). Although the slightly longer HRT in the Group 2C MFC would contribute to its better performance, the difference may also indicate that increasing the distance between the electrodes could change some key factors (most likely the internal resistance) that affect the MFC performance more significantly than extending the reactor length. This implies that to design a tubular MFC, it may be more important to control its diameter (to below a certain value) than its length, and the tubular MFCs can be further scaled up by extending its length, instead of enlarging its diameter.

Effects of substrates on energy recovery

The Group 3 and 4 MFCs were used to investigate the effects of substrate concentrations and types on energy recovery. In the Group 3, three concentrations (expressed in COD with acetate as an organic source), 195, 390 and 2341 mg L^{-1}, were chosen, and the anolyte was fed into the MFCs with the same dimensions and HRTs (Table 3). The MFC

fed with 390 mg L^{-1} produced the highest maximum power density (13.99 ± 0.21 W m^{-3}); while in energy recovery, the 390-mg L^{-1} MFC still had the highest maximum NER_V (0.187 ± 0.003 kWh m^{-3}), followed by the 2341- and the 195-mg L^{-1} MFCs, and the lowest concentration yielded the highest maximum NER_S (1.092 ± 0.012 kWh $kgCOD^{-1}$) (Figure 10A). The NER_V results indicate that, when treating the same amount of wastewater, a higher organic concentration (e.g., 390 vs. 195 mg L^{-1}) will lead to higher energy recovery; however, the maximum NER_V may not always increase with increasing organic concentrations (e.g., 390 vs. 2341 mg L^{-1}), likely due to the inherent limitation (e.g., internal resistance) of the MFC. When the energy recovery was expressed in NER_S, the maximum NER_S increased with decreasing organic concentration. Considering both NER_V and NER_S, the low concentrations (195 and 390 mg L^{-1}) resulted in better performance of energy recovery than the high concentration (2341 mg L^{-1}). Since the tested low concentrations are within the range of domestic wastewater, we think that domestic or other low-strength wastewaters could be better substrates for MFCs than the high-strength wastewaters, which support what we found in the prior studies [34][36].

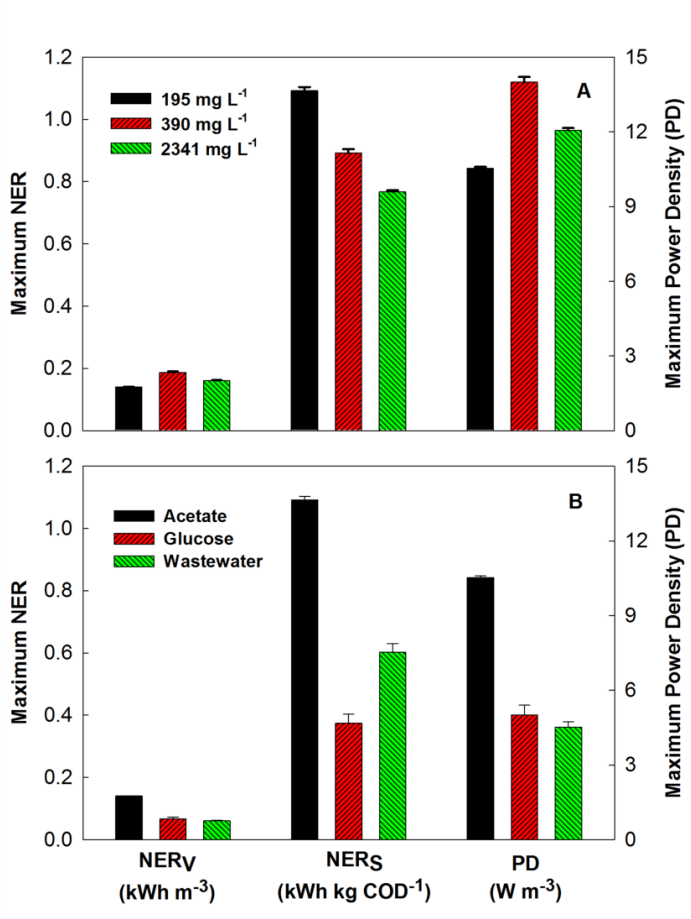

Figure 10. Comparaison of the maximum power density (PD) or the maximum NER in the MFCs with different substrates: (A) different concentrations of acetate; and (B) different substrate types.

The Group 4 MFCs were fed with three types of organic sources, acetate, glucose, and primary effluent of domestic wastewater. Because low-strength substrates had better energy recovery and the primary effluent used in this study had an average concentration of 192 mg L^{-1} (COD), we prepared both acetate and glucose solutions with a concentration of ~ 195 mg L^{-1} (Table 3). The results confirmed what we observed previously [21] that the acetate-fed MFC exhibited much better performance in both power density and energy recovery than either glucose- or wastewater-MFCs (Figure

10B). In more details, the maximum power density in the acetate-fed MFC was 10.53 ± 0.06 W m^{-3}, more than twice those from the glucose-fed MFC (5.00 ± 0.40 W m^{-3}) and the wastewater-fed MFC (4.52 ± 0.21 W m^{-3}). Likewise, the highest maximum NER_V (0.140 ± 0.001 kWh m^{-3}) and the highest maximum NER_S (1.092 ± 0.012 kWh $kgCOD^{-1}$) were obtained in the MFC fed with acetate. The MFCs with glucose or wastewater had similar maximum power densities and the maximum NER_V; the wastewater generated a higher maximum NER_S than the glucose, possibly due to the less COD removal in wastewater than glucose (NER_S is calculated based on the removed COD).

The maximum NER and NER_V vs NER_S

For the purpose of energy recovery, the maximum NER will be a key parameter to report. Similar to the maximum power density that is most often reported in the MFC studies, the maximum NER represents the performance of electricity generation with a focus on energy. Although a higher maximum power density does not necessarily mean a higher maximum NER in the cross-wise comparison, the maximum NER may be estimated from the maximum power under a certain condition because of the relationship between power and energy. We found that the maximum NER_V always occurred at the same current density (or the same external resistance) as the maximum power density in the tested MFCs. This is because that NER_V is determined by power and wastewater flow rate, and the latter does not change under different current densities. The maximum NER_S behaves differently from the maximum NER_V. For example, the MFC fed with 390 or 2341 mg L^{-1} COD showed their maximum power density or the maximum NER_V at current densities

of 26.45±0.20 and 24.55±0.10 A m^{-3} (both under 50-ohm resistance), respectively; their maximum NER_S occurred at current densities of 17.88±0.13 and 16.70±0.05 A m^{-3}, respectively (both under 100-ohm resistance). This difference was caused by different COD removal efficiencies at different current densities (Figure 11A).

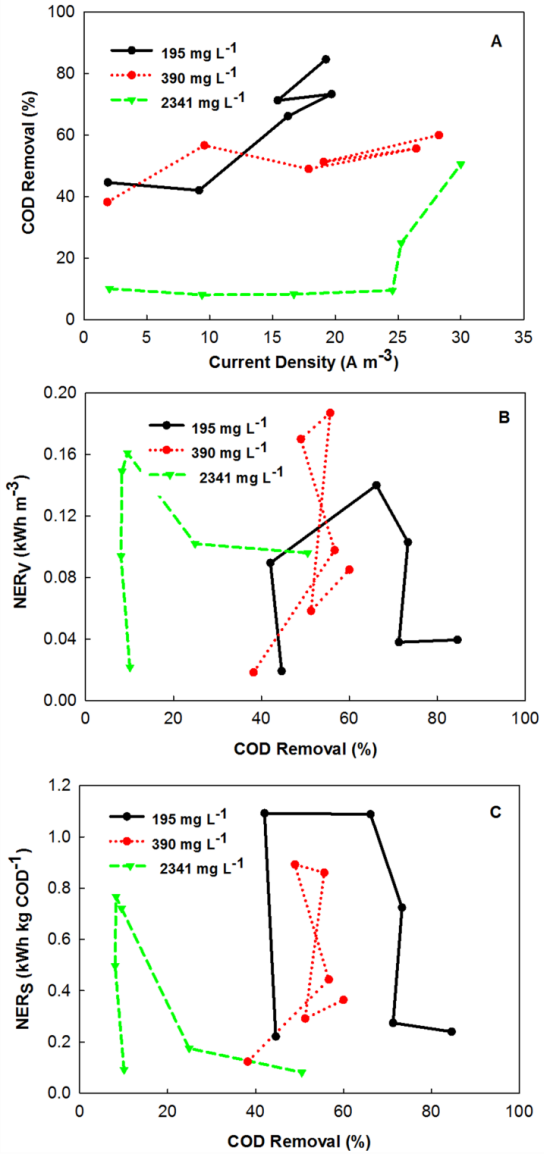

Figure 11. The energy recovery and COD removal efficiency in the MFCs fed with different concentration of acetate: (A) variation of COD removal efficiency along current density; (B) variation of NER_V with COD removal efficiency; and (C) variation of NER_S with COD removal efficiency.

In the cross-wise comparison, both the maximum NER_V and the maximum NER_S showed similar trends of variation among different conditions when we altered the dimensions of the MFCs (Group 1 and 2). However, when the anode substrates were changed (concentrations or types), those two parameters showed differently. For example, the maximum NER_V of the 390 mg L^{-1}-MFC was higher than that of the 195 mg L^{-1}-MFC, but its maximum NER_S was lower. Another example is that, the maximum NER_S of the wastewater-MFC was higher than the glucose-MFC, while the maximum NER_V between the two was not significantly different. Although NER_S includes the information of the conversion efficiency of organic compounds to electric energy, it may be "artificially improved" or become larger when the COD removal becomes worse (less COD is removed). It may not be a fair comparison to claim a "better" MFC if it shows a larger NER_S while achieves a lower COD removal efficiency. It is of interest to further investigate and understand the difference and interaction between NER_V and NER_S. At this moment, as we previously suggested [21], we think both parameters should be reported in an MFC study that focuses on energy recovery.

From the difference between NER_V and NER_S, we notice some potential issues about COD removal efficiency and the maximum NER. We have identified that the primary function of an MFC is wastewater treatment, and thus organic removal must be taken into the consideration of evaluating an MFC system. Using the Group 3 MFCs as an example, the COD removal efficiency increased with the increasing current density (or decreasing external resistance) (Figure 11A). Especially, the COD removal efficiency remained below 10% until the external resistance was reduced to 30 Ω (from 1000Ω) when the removal efficiency increased to 25% and then to 50% at 20 Ω. The MFCs with lower

concentrations of acetate achieved 60% or 85% of COD removal at their highest current densities (or lowest external resistance of 20 Ω). However, the maximum NER appears with a relatively lower COD removal efficiency: 8-10% in the MFC fed with 2341 mg L^{-1}, 48-56% in the MFC of 390 mg L^{-1}, and ~ 66% in the 195 mg L^{-1} MFC (Figure 6B and C). Therefore, a question arises: which parameter should we pursue, the maximum NER or the maximum COD removal? The maximum NER brings in the benefit of high energy recovery, while the maximum COD removal gives us more environmental benefit. The answer to this question requires a detailed analysis and comparison of economic benefit between those two conditions, which is a great challenge to the current stage of MFC development (given its scale and the available information on operation of larger-size systems). Our initial thought (without additional analysis) is that, because of generally low energy recovery in an MFC system, it may be more important to achieve high organic removal efficiency. Energy recovery is still important, but it may not be the most important task of an MFC system.

2.4 Conclusions

The results of this study have provided valuable information though evaluating (maximum) NER in tubular MFCs. Unlike the maximum power density that is obviously affected by the MFC size, we obtained the mixed messages about the relationship between the maximum NER and the anode liquid volume: when varying the reactor diameter, the MFCs with different size showed comparable maximum NER at the same anolyte flow rate, and some difference at the same HRT; when the length of the reactor

was altered, the maximum NER decreased with the decreasing anode liquid volume at the same anolyte flow rate, and exhibited the opposite trend at the same HRT. This finding encourages the further scaling up of MFCs, because energy recovery does not decrease with increasing MFC size under a certain conditions. The NER data from the substrate tests indicate that the low-strength substrate (e.g., domestic wastewater) may be more suitable for MFC treatment. The discrepancy between the maximum NER and the maximum COD removal brings up the question whether an MFC system treating wastewater should pursue high energy recovery or high contaminant removal. Given the current fact that MFCs generally have low energy recovery, contaminant removal may be more important, although further analysis will be required.

3 Nano-materials modified electrodes

3.1 Crumpled graphene particles for microbial fuel cell electrodes

(This section has been published as: Xiao, L., Damien, J., Luo, J., Jang, H. D., Huang, J. and He, Z. (2012) Crumpled graphene particles for microbial fuel cell electrodes. ***Journal of Power Sources.*** 208, 187-192.)

3.1.1 Introduction

Wastewater contains a high content of organic matter that can be used as a source of energy to offset energy consumption by treatment processes [37]. The use of microbial fuel cells (MFCs) offers one of the most promising approaches for extracting useful energy from wastewater. Through bioelectrochemical reactions, MFCs can convert the energy stored in the chemical bonds of organic compounds to electrical energy [12]; however, the low power output of MFCs currently restricts their practical applications. Research towards improving MFC power production focuses on understanding microbial activities, optimizing MFC configuration and operation, reducing electrochemical limitation, and exploring new materials for electrodes and membranes. Among these, electrode materials (including electrodes and their modifying materials) are of special interest because of rapid developments in material sciences [38][39].

The key criteria for electrode materials in MFCs include high surface area, high conductivity, good stability (resistant to chemical and microbes), and low cost [12]. Electrodes can also be modified by coating additional materials to achieve those properties [40]. The most commonly used materials for anode electrodes are carbonbased, such as carbon paper, carbon cloth, and graphite felt [39], because they are inexpensive,

easy to use, and have a defined surface area. Carbon materials can be modified with nanoparticles to improve the power density [41][42]. Cathode electrodes, on the other hand, require catalytic ability to reduce terminal electron acceptors, in addition to those properties described with anode electrodes. Cathode electrodes can also be modified with nanomaterials to improve catalyst activities and/or facilitate catalyst support [43]. The most popular catalyst for cathode electrodes is platinum (Pt), an expensive noble metal. Several other catalysts have been studied, such as manganese oxides, metal tetramethoxy phenylephrine (CoTMPP and FeCoTMPP), and metal phthalocyanine (FePc, CoPc and FeCuPc) [17]. These alternatives can achieve a comparable performance to Pt, but their long-term stability requires further examination, especially for the presence of metals like iron and manganese, which could be involved in a microbial metabolism. Therefore, it is necessary to explore more options for simple and stable materials used for preparing electrodes in MFCs.

Since the isolation of graphene in 2004, researchers have found a variety of unique and desirable properties for electrochemical applications – high electrical conductivity, large surface area, applicable electrocatalytic activities, and low production costs [44][45][46]. As a result, graphene is studied as an electrode material in many electrochemical applications, such as solar cells, lithium-based rechargeable batteries, and ultracapacitors [47][48][49]. Recently, Zhang and his co-workers reported the improved electrochemical performance of a dual-chamber MFC operated with a graphene-modified anode electrode [50], and Huang and his co-workers found that graphene oxide nanoribbons could enhance extracellular electron transfer in bioelectrochemical systems [51]. These studies revealed the great potential of using graphene to improve electrode performance in MFCs.

The graphene material is made by thermal annealing of graphene oxide (GO), which is prepared by a modified Hummers' synthesis [52]. Such prepared graphene materials are usually called chemically modified graphene, or reduced GO(r-GO), as they are more defective than pristine graphene [53]. Regular r-GO is made by thermal exfoliation of GO at 200 ◦C and the resulting material is typically flat sheet with wrinkles (Figure 12B). We have developed a new type of r-GO particles by crumpling the sheets into crumpled paper ball-like structure by an aerosol-assisted capillary compression process [54]. In the synthesis, the soft GO sheets were subject to near isotropic compression during rapid evaporation of the aerosol droplets and subsequently reduced by in situ heating. The particles' morphology resembles crumpled paper balls (Figure 12C). While regular sheet-like graphene materials are prone to aggregation, making their surface area and processability sensitive to the materials' processing history, the crumpled particles are remarkably aggregation-resistant in both solution and solid state and have a much more stable, consistently higher surface area and excellent solution processability that aremuchless sensitive to processing history. Like crumpled paper balls, crumpled graphene (i.e., r-GO) particles can also tightly pack into a three-dimensional (3D), porous structure without significantly losing surface area. Therefore, it is expected that electrodes modified with the crumpled graphene particles should have a much higher surface area than those modified with regular graphene sheets, resulting in a much better MFC performance.

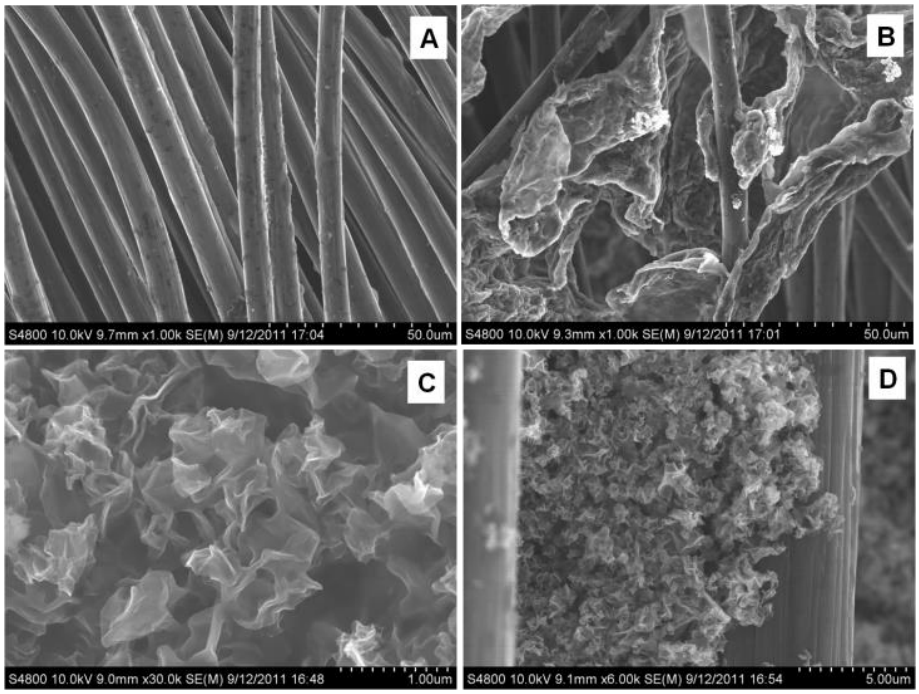

Figure 12. Morphologies of electrodes: (A) carbon fiber of carbon cloth; (B) r-GO sheets on carbon cloth; (C) r-GO particles before being applied; and (D) r-GO particles on carbon cloth.

In this study, we systematically examined electricity generation with the graphene-modified (anode or cathode) electrodes and employed electrochemical techniques such as cyclic voltammetry and electrochemical impedance spectroscopy to characterize the electrochemical properties of the electrodes. For comparison, we tested an activated carbon (AC)-modified anode electrode and platinum-modified and unmodified cathode electrodes (carbon cloth – CC) in parallel with the graphene-modified electrodes.

3.1.2 Materials and methods

Electrode modification

The details of preparation and characterization of r-GO particles can be found in our previous publication [54]. The base material, carbon cloth (PANEX®30PW03, Zoltek Corporation, St. Louis, MO, USA) was used for modification. For anode tests, carbon cloth modified with regular r-GO sheets, crumpled r-GO particles and AC were tested. For cathode tests, carbon cloth modified with regular r-GO sheets, crumpled r-GO particles, and Pt/C (10% Pt in black carbon powder) were measured. An unmodified carbon cloth (CC) electrode was also used in the cathode test as a control. The project surface area for each electrode was 4.5 cm^2 each side. For modification, 45 mg r-GO particles were mixed with 0.5 mL deionized water in a 5-mL centrifuge tube and the mixture was sonicated for 30 min. Then 0.3 mL Nafion solution was added into the mixture, which was sonicated again for 5 min. This mixture was applied to both sides of the carbon cloth and dried in air for 24 h. The final loading rate of the modifying material was 5mg cm^{-2}. Other modified electrodes were prepared by the same method with the same loading rate.

MFC construction and operation

Two-chamber microbial fuel cells were built with glass bottles jointed by a cation exchange membrane (CEM) (Ultex CMI 7000, Membranes International, Inc., Glen Rock, NJ, USA). Each chamber had a liquid volume of 120 mL. Three electrodes were installed in the same chamber to minimize the effect of the (different) counter electrode on MFC

performance. For example, the anode-MFC for the anode electrode test contained the r-GO particles-, the r-GO sheets- and the AC-modified electrodes in its anode chamber and one single cathode electrode (carbon brush, Gordon Brush Mfg. Co., Inc., Commerce, CA, USA) in the cathode chamber. In contrast, the cathode-MFC for the cathode electrode test had the r-GO particles-, the r-GO sheets- and the Pt- (or CC) modified electrodes in the cathode chamber and one single anode electrode (carbon brush) in the anode chamber. Before use, carbon brush electrodes were pre-treated by immersing in acetone overnight and heating at 450 ℃ for 30 min. We did not find obvious effects of the location of electrode placement on electricity generation, although there was a slight difference in the distance between different electrodes and the membrane. The multiple electrodes in the same chamber were connected individually with copper wires to their common counter electrode. One resistance decade box was connected in each electrical circuit to adjust the external resistance between each electrode couple. Both the anode and the cathode chambers were continuously stirred with magnetic bars. A reference electrode (Ag/AgCl) was installed in the testing chamber for in situ electrochemical analysis.

The MFCs were operated in batch mode at room temperature (about 20 ℃). The anodes were inoculated with the anaerobic sludge from a local municipal wastewater treatment plant (South Shore, Milwaukee, WI, USA). The nutrient solution in the anode chamber contained (per 1 L of tap water): sodium acetate, 0.5 g; NH_4Cl, 0.3 g; NaCl, 1 g;$MgSO_4$, 0.03 g; $CaCl_2$, 0.04 g; $NaHCO_3$, 0.2 g; KH_2PO_4, 5.3 g; K_2HPO_4, 10.7 g and 1mL trace elements [55]. The anode solution was replaced (~80%) when the voltages of all three electrode couples dropped below 4mV. The cathode of the anode-MFC was filled with

1M potassium ferricyanide, while the cathode of the cathode-MFC was filled with 100 mM phosphate buffer solution (5.3 g L^{-1} KH_2PO_4 and 10.7 g L^{-1} K_2HPO_4) and aerated with air flow.

Measurement and analysis

The cell voltage was recorded every 5min by a digital multimeter (2700, Keithley Instruments, Inc., Cleveland, OH, USA). A potentiostat (Reference 600, Gamry Instruments, Warminster, PA, USA) performed the polarization curve at a scan rate of 0.8mV s^{-1} for anode electrode tests and 0.2mV s^{-1} for cathode electrodes tests. The power density and current density were calculated based on the anode liquid volume. The total charge produced in one batch cycle was calculated by integrating current with time (the period of a cycle). The cyclic voltammogram (CV) was also performed using the Gamry reference 600 potentiostat at a scan rate of 5mV s^{-1} in two ways: the in situ test was conducted in the (anode) MFC that used the anode electrode as a working electrode, the cathode electrode as a counter electrode and an Ag/AgCl reference electrode (200mV vs. SHE), and vice versa for the cathode MFC; the ex situ test was conducted in an electrochemical cell that contained a glassy carbon electrode modified with r-GO particles or Pt powder as a working electrode, a Pt wire as a counter electrode and an Ag/AgCl reference electrode. The gas phase of the electrochemical cell was flushed with either oxygen or nitrogen gas. The r-GO particles, carbon cloth and graphene-modified electrodes were imaged using a scanning electron microscope (SEM) (Hitachi S4800, Japan).

Electrochemical impedance spectroscopy (EIS)

The impedance spectra were collected at the open-circuit potential (OCP) of the anode and the cathode using a Gamry reference 600 potentiostat. An ac voltage signal of 10mV was applied in a frequency range from 100 kHz to 5 mHz. EIS measurements were conducted in a three-electrode mode by recording the impedance spectrum of the anode, with the cathode acting as a counter electrode (CE) in the anode-MFC, and vice versa for the cathode-MFC. The reference electrode was Ag/AgCl. The EIS data was analyzed using ANALEIS with an equivalent circuit containing two time constants. Rs represents solution resistance, Rp1 is related to pore resistance of coating layer, and Rp2 is the reaction (polarization) resistance at the coating/substrate interface.

3.1.3 Results

Graphene-modified anode electrodes

(1) Electricity generation

Electricity generation was observed from all three anode electrodes in the anode-MFC and the graphene modification exhibited a beneficial effect on the MFC performance. Batch operation resulted in a profile of current production, with a rapid increase upon the replacement of the fresh anode solution and a gradual decrease due to the depletion of the substrate. At an external resistance of 100 Ω, all three current profiles exhibited a similar trend of increase and decrease, although at different levels (Figure 13A). The current generations were clearly affected by the substrate consumption because three anode

electrodes were in the same anode chamber. Each cycle of current production lasted for about 20 hours. The currents reached peak values of 1.30 ± 0.04 mA, 1.05 ± 0.09 mA and 0.57 ± 0.03 mA for the r-GO particles-, the r-GO sheets- and the AC-modified electrodes, respectively. The total charges produced in one cycle amounted to 50.5 ± 7.3 C for the r-GO particles-modified electrode, 44.5 ± 9.0 C for the r-GO sheets-modified electrode, and 27.8 ± 5.9 C for the AC-modified electrode. The anode-MFC was operated for more than three months and electricity generation with all three anode electrodes was stable, suggesting good stability and reproducibility of the tested electrode materials.

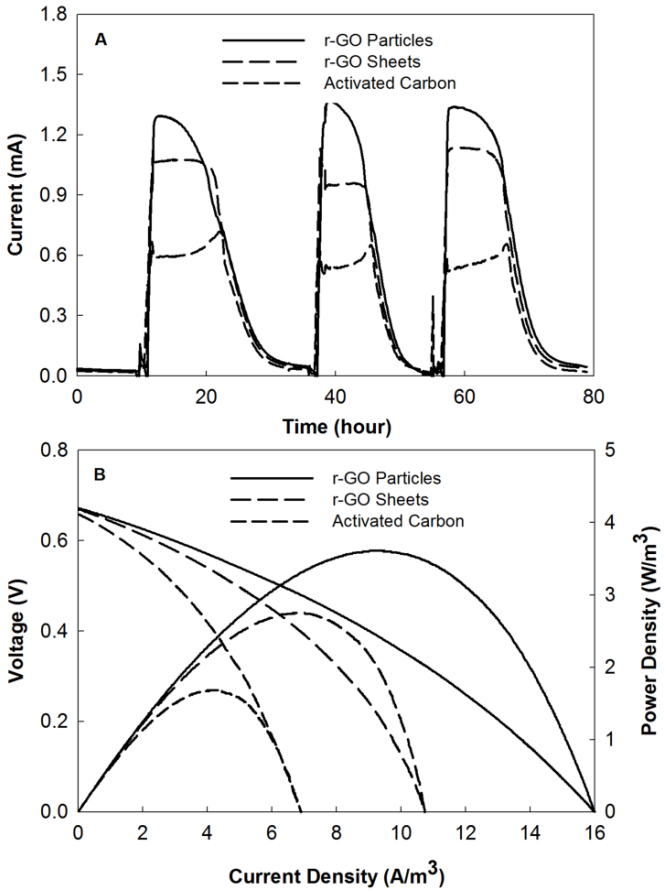

Figure 13. Electricity generation with graphene-modified anode electrodes: (A) current generation at 100 Ω; and (B) polarization curves.

Polarization tests confirmed the difference in electricity generation from three modified anode electrodes. As shown in Figure 13B, the open cell voltages (OCV) of three electrodes were almost the same (~ 0.66 V), comparable with OCVs in other MFC studies. However, the maximum power densities were apparently different. The AC-modified anode electrode produced 1.7 W m^{-3}, which was 61% of the r-GO sheets - modified anode electrode (2.7 W m^{-3}) and 46 % of the r-GO particles-modified anode electrode (3.6 W m^{-3}). Accordingly, the AC-modified anode electrode generated the lowest short-circuit current of 6.9 A m^{-3}; while the r-GO particles- and the r-GO sheets-modified anode electrodes produced 16.0 and 10.8 A m^{-3}, respectively.

(2) Electrochemical analysis

The electrochemical behaviour of the modified anode electrodes in the anode-MFC was analyzed by using CV and EIS. The *in situ* voltammograms of the r-GO particles-modified and the r-GO sheets-modified anode electrodes showed larger currents than that of the AC-modified anode electrode, indicating either an enhanced surface area or an optimized structure (Figure 14). By fitting the data of the Nyquist plots (Figure 15), we obtained the values of each parameter (Table 4). The solution (ohmic) resistances, R_s resulting from the ionic resistance of electrolyte, the intrinsic resistance of active materials, and the contact resistance, were generally lower than 10 Ω for all three modified anode electrodes. The pore resistance of the coating layer (R_{p1}) behaved very differently, with the highest value of 182 Ω from AC-modified anode electrode and the lowest value of 16 Ω from r-GO particles-modified anode electrode. Similarly, the highest polarization resistance (R_{p2}) of 304 Ω also occurred from the AC-modified anode

electrode; while the r-GO particles-modified anode electrode had 33 Ω, almost one tenth of that of the AC-modified anode electrode. Both resistances with the r-GO sheets-modified anode electrode were higher than those of the r-GO particles-modified anode electrode but much lower than those of the AC-modified anode electrode.

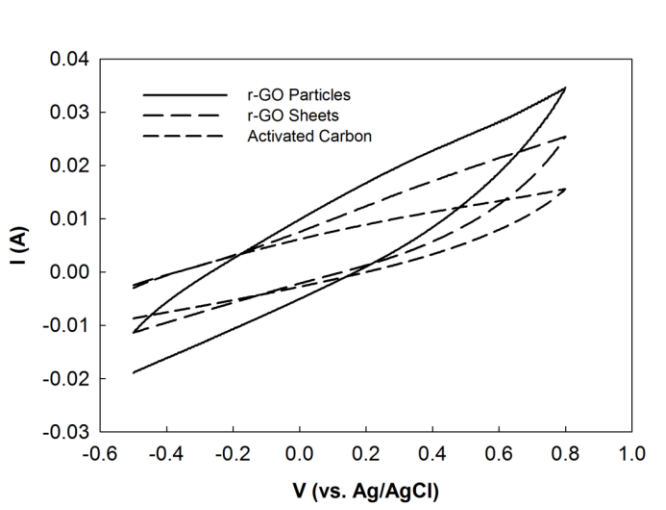

Figure 14. Cyclic voltammetry of the modified anode electrodes.

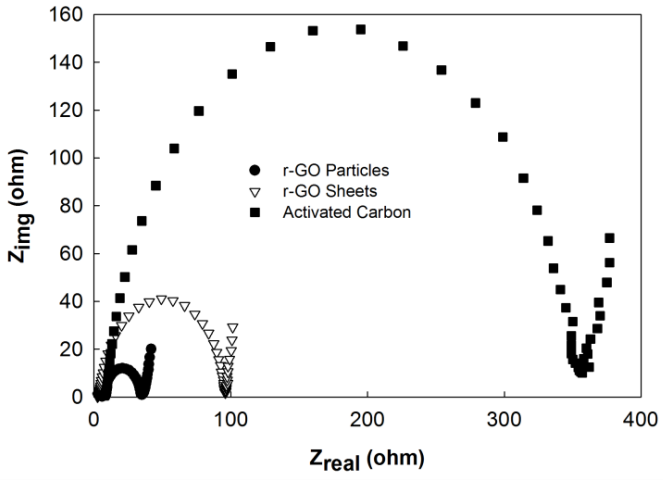

Figure 15. EIS (Nyquist plots) of the modified anode electrodes.

Table 4. The fitting parameters of EIS data for the MFCs with modified electrodes

	Modifying material	**R_s (Ω)**	**R_{p1} (Ω)**	**R_{p2} (Ω)**
Anode-MFC	r-GO particles	6.0	15.7	32.8
	r-GO sheets	3.3	59.2	71.4
	AC	8.0	182.1	303.8
Cathode-MFC	r-GO particles	6.6	21.0	29.2
	r-GO sheets	8.8	34.4	38.5
	CC	11.0	52.5	16680

Graphene-modified cathode electrodes

(1) Electricity generation

To examine the graphene modification for cathode reactions, two groups of cathode electrodes were studied in the cathode-MFC: first, r-GO particles-, r-GO sheets- and Pt/C-modified cathode electrodes; and second, r-GO particles-, r-GO sheets- and unmodified CC cathode electrodes. Polarization tests were employed to determine the overall performance of graphene materials compared with either Pt/C or CC. In the first group, the Pt/C-modified cathode electrode exhibited the best performance, while the r-GO particles- and the r-GO sheets-modified cathode electrodes behaved almost identically (Figure 16). The OCV of the r-GO particles- and the r-GO sheets-modified cathode electrode were about 0.65 V, lower than 0.75 V of the Pt/C-modified cathode electrode. Likewise, the maximum power density of either the r-GO particles- or the r-GO sheets-modified cathode electrode (2.9 W m^{-3}) was 60% of the Pt/C-modified cathode electrode (4.8 W m^{-3}). Compared with the unmodified electrode (CC), the use of r-GO particles or r-GO sheets had clearly improved the MFC's performance (Figure

17B). The maximum power densities of the r-GO particles- and the r-GO sheets-modified cathode electrodes were 3.3 W m^{-3} and 2.5 W m^{-3}, respectively, significantly higher than 0.3 W/m^3 with the unmodified cathode electrode.

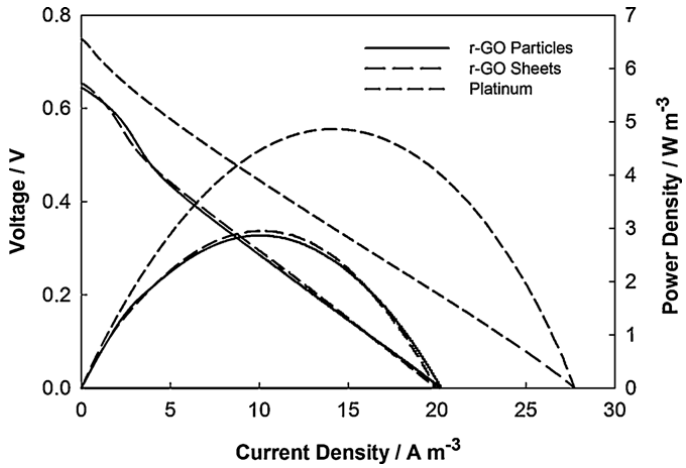

Figure 16. Polarization curves with the modified cathode electrodes in the cathode-MFC. Pt cathode was used as a control.

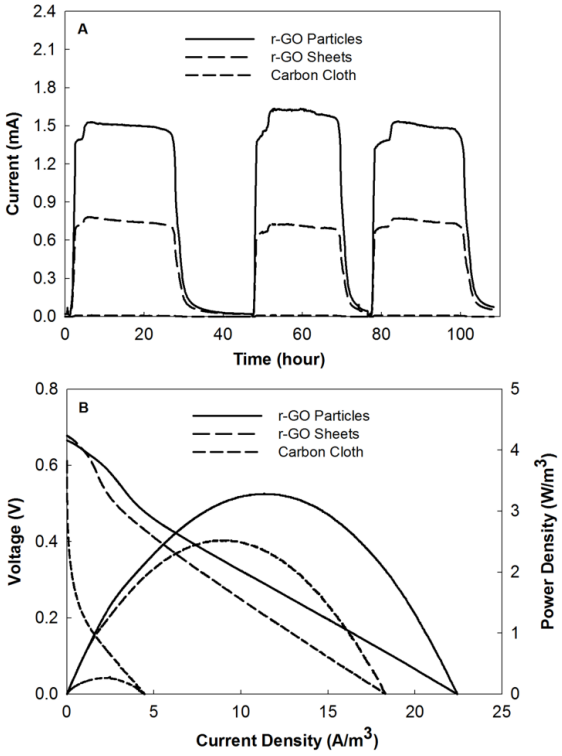

Figure 17. Electricity generation with grapheme-modified cathode electrodes: (A) current generation under 33 Ω; and (B) polarization curves.

To further confirm the findings from the polarization test, the cathode-MFC was operated under the 33 Ω external resistance with the second group of cathode electrodes (Figure 17A). Both the r-GO particles- and the r-GO sheets-modified cathode electrodes showed a batch profile of current generation over substrate consumption. The total charges of the r-GO particles-modified cathode electrode were 133.3 ± 8.7 C, twice as much as the r-GO sheets-modified cathode electrode (65.0 ± 7.3 C). No obvious electricity production was observed from the unmodified cathode electrode. In parallel with the anode-MFC, the cathode-MFC was operated for a period of 3 months and stable performance was achieved.

(2) Electrochemical analysis

The cathode-MFC was also characterized by CV and EIS. No distinct redox peak was observed from all three cathode electrodes during the *in situ* CV test, but the currents of the r-GO particles- and the r-GO sheets-modified cathode electrodes were much higher than the current of the unmodified electrode (Figure 18). It should be noted that the *in situ* CV test was conducted on carbon cloth that did not have a uniform surface like glass carbon electrodes used in the *ex situ* CV test; therefore, the results of the *in situ* CV test were more complex and no redox peaks did not necessarily mean no catalytic activities. The *ex situ* CV test of the r-GO particles clearly exhibited a reduction peak at -0.2 V (vs. Ag/AgCl) with oxygen gas but not with nitrogen gas (Figure 19). The CV of the Pt powder also showed a reduction peak close to -0.2 V (vs. Ag/AgCl) (Figure 20). EIS tests were carried out to determine the internal resistance of three electrodes (Figure 21) and the fitting parameters are shown in Table 4. The solution resistances of the r-GO

particles-modified cathode electrode (7 Ω) and the r-GO sheets-modified cathode electrode (9 Ω) were slightly lower than carbon cloth (11 Ω). Like the modified anode electrodes, the crumpled r-GO balls-modified cathode electrode had the lowest pore resistance (21 Ω). A significant difference between the modified and unmodified cathode electrodes occurred with the polarization resistance. The unmodified carbon cloth had a polarization resistance of 16680 Ω, several hundred times higher than those of the modified cathode electrodes.

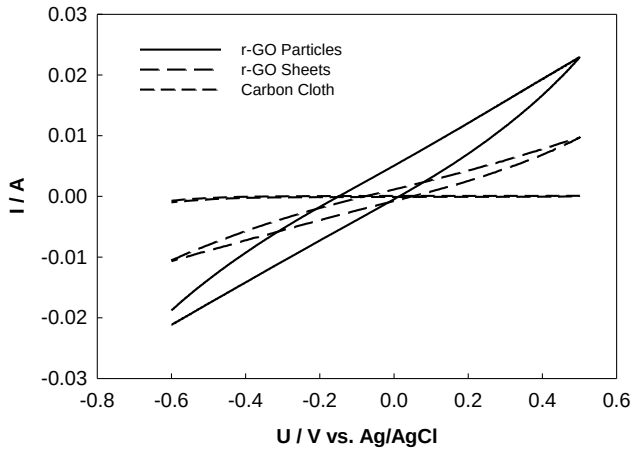

Figure 18. Cyclic voltammetry of the modified cathode electrodes in the cathode-MFC.

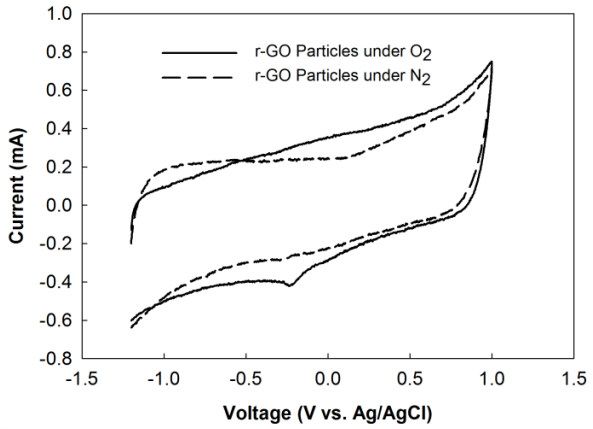

Figure 19. Cyclic voltammetry of r-GO particles with oxygen or nitrogen.

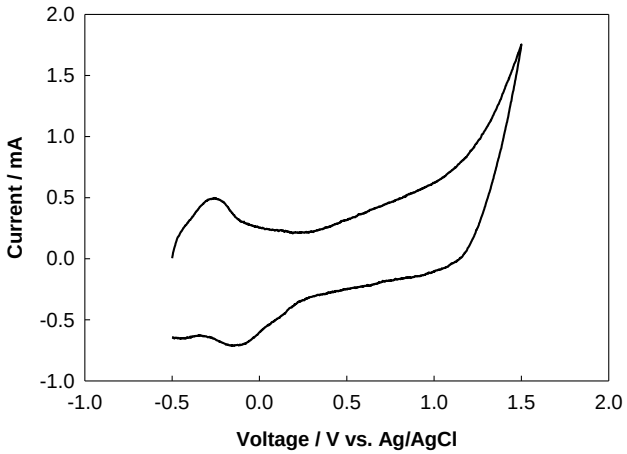

Figure 20. Cyclic voltammetry of the Pt electrode under oxygen condition in an electrochemical cell.

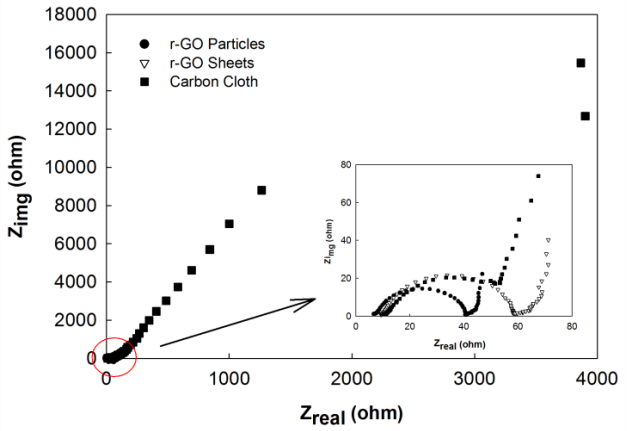

Figure 21. EIS (Nyquist plots) of the modified cathode electrodes. The insert shows the details at high frequency.

3.1.4 Discussion

The results have collectively demonstrated that graphene modification is generally beneficial to the electrode performance, with some difference between the anode and the cathode applications.

Graphene-modified anode electrodes could improve electricity generation compared with activated carbon modification, most likely because of graphene's superior properties, such as its large surface area and open structure. The results also confirmed the finding in a recent study that achieved a higher maximum power density with the graphene-modified stainless steel mesh (SSM) than plain SSM and polytetrafluoroethylene (PTFE) modified SSM [50]. The authors attributed the better performance to the fact that the graphene-modified electrode possessed a high surface area, facilitated bacterial adhesion, and exhibited an excellent efficiency of electron transfer. The electrodes modified by a porous layer of crumpled graphene particles used in our study have an even higher surface area than regular graphene because of its unique three-dimensional open structure [54], and thus is potentially more advantageous, as demonstrated by a higher electricity production with the r-GO particles-anode electrode than the r-GO sheets- and AC-anode electrodes.

The electrochemical analysis supported the finding with the best electrochemical activity and lowest impedance from the r-GO particles-anode electrode. Although no distinct redox peaks were observed from all three modified anode electrodes, the currents of the r-GO particles- and the r-GO sheets-modified anode electrodes were much higher than those of the AC-modified anode electrode, indicating that the graphene-modified electrode had a higher faradic charge capacity, which could be proportional to the electrode surface area [56]. With the same projected areas, the r-GO particles-modified anode electrode had the highest actual surface area [54], which also helped with biofilm formation. Its unique pore structure could facilitate bacterial adhesion and substrate

supply. As a result, in the anode-MFC, most of the charges were transferred through the r-GO particles-modified anode electrode during the oxidation of substrates. The low resistances of the r-GO particles- and the r-GO sheets-modified anode electrodes suggested a better mass transfer of fuel and ions, compared with activated carbon.

Graphene-modified cathode electrodes have exhibited catalytic activities of oxygen, which is supported by the *ex situ* CV test of r-GO particles that showed a reduction peak in oxygen but not in nitrogen gas. This reduction peak was similar to the one with the Pt CV test. Our results are also supported by a previous finding that graphene sheets had high catalytic activity for the reduction of oxygen [57]. The authors studied the electrochemical reduction of oxygen with graphene sheets by cyclic, rotating disk electrode, and rotating ring-disk electrode voltammetry. They found that graphene sheets could effectively catalyze the disproportionation of H_2O_2 and that such catalytic activity enables a 4-electron reduction of O_2 at a relatively low overpotential in neutral media. In the present study, the maximum power densities of the r-GO particles- and the r-GO sheets- modified cathode electrodes were about 60% of the Pt/C-modified cathode electrode, but much higher than the unmodified electrode, demonstrating that r-GO particles and r-GO sheets can improve the oxygen reduction reaction at the cathode of an MFC, although not as well as the Pt/C.

It is worth noting that the maximum power densities of r-GO particles- and r-GO sheets-modified cathode electrodes in Figure 17B (the cathode-MFC with CC as the control) were different from those in Figure 16 (the cathode-MFC with Pt/C as the control).

Because the Pt/C-modified cathode electrode dominated oxygen reduction in the cathode chamber, the difference between r-GO particles-modified and r-GO sheets-modified cathode electrodes was much smaller than that when they were compared with a Pt/C-modified cathode electrode. After changing Pt/C to bared carbon cloth (unmodified electrode), the main reaction in the cathode chamber was with r-GO particles-modified and r-GO sheets-modified cathode electrodes, as they were competing with each other and the difference between these two became apparent. The r-GO particles-modified cathode electrode performed the fastest electrode reaction rate and charge transfer rate compared with r-GO sheets- and unmodified cathode electrodes, suggested by the largest current from the *in situ* CV tests and the lowest resistance from EIS tests.

The EIS analysis also indicated different roles of graphene materials between anode and cathode modification. For anode modification, graphene helped to optimize the surface structure of the electrode, suggested by the lower pore resistances (R_{p1}). As a result, biofilm formation could be improved, leading to a reduced polarization resistance (R_{p2}) compared with the AC modification. For cathode modification, the effect of the electrode surface improvement was limited, indicated by the closeness of the three R_{p1} values, although graphene still improved the electrode surface. The key function of the graphene modification was to directly improve the cathode reaction through its catalytic function, which resulted in a great reduction of R_{p2} and significant higher electricity generation compared with the unmodified carbon cloth.

The r-GO particles are a novel type of graphene-based material with superior properties

and processability. The MFC tests have shown that r-GO particles can significantly enhance bioreaction/electrochemical kinetics and mass transfer because of a high surface area, open structure and high electrical conductivity; however, these characteristics highly depend on graphene processing history. In order to produce a high surface area, graphene oxide (the precursor of graphene) needs to be heated rapidly to trigger a violent gas evolution for efficient exfoliation; otherwise, the surface area of graphene reduces by more than 84% of its original surface area [54]. In contrast, r-GO particles always yielded a high surface area regardless of the heating rate [54]; therefore, r-GO particles are easier to prepare compared with regular graphene. In addition, due to their crumpled three-dimensional structure, r-GO particles possess a high surface area to facilitate the electron conductance and possibly biofilm formation in the anode and higher catalytic activity for reducing oxygen in the cathode. Although r-GO particles did not outperform the Pt/C for cathode reaction under the same loading rate in this study, the performance could be compensated for or improved by increasing the loading rate applied to the cathode electrode. The lower cost of graphene compared with Pt would make it a more viable option to increase graphene concentration for enhancing the electrode performance.

3.1.5 Conclusions

We demonstrated that r-GO particles and r-GO sheets could increase the power production in MFCs via modification of the anode or the cathode electrodes. Both graphene materials exhibited better electrochemical performance and lower impedance compared with activated carbon or unmodified electrode; in particular, r-GO particles, a novel structure of graphene, performed even better than regular r-GO sheets. With further

understanding of graphene's role in electron transfer and biofilm formation in MFCs, and reducing the cost of graphene preparation, graphene materials could be promising in the future design of large-scale MFC or MFC-related applications, such as microbial electrolysis cells and microbial desalination cells.

3.2 Carbon/Iron-based nanorod catalysts for hydrogen production in microbial electrolysis cells

(This section has been published as: Xiao, L., Wen, Z., Ci, S., Wen, Z., Chen, J. and He, Z. (2012) Carbon/Iron-based nanorod catalysts for hydrogen production in microbial electrolysis cells. ***Nano Energy***. 1, 751-756.)

3.2.1 Introduction

Microbial electrolysis cells (MECs) are bioelectrochemical devices that can produce hydrogen from organics via microbial metabolism [26]. Because of the electric potential supplied by the anode reaction, MECs require a voltage addition as low as 0.2 V from external sources to reduce protons to hydrogen gas [58], which is a significant advantage compared with hydrogen production via water electrolysis [59]. MECs offer opportunities to recover hydrogen as an energy carrier from biomass and wastewater; in particular, MECs can use fermenting products from biohydrogen-producing processes and thus maximize hydrogen production if linked to biohydrogen production. Recent advancement of MEC to a pilot test, although having problems with methanogens overgrowth, has provided valuable experiences in MEC scaling up and operation [60].

One of the key factors to MEC performance and application is the (cathode) catalyst for hydrogen production because of the large over potential of the hydrogen evolution reaction (HER) on plain carbon electrodes [26]. Platinum (Pt) is a commonly used and efficient catalyst, but the high cost associated with Pt material obstructs its application, especially for large-scale systems. Rapid development in material sciences introduced alternative catalysts to replace Pt in MECs; for instance, it was found that cobalt-based catalysts could catalyze hydrogen production in MECs, but not as well as Pt [61]. Nickel oxide catalysts prepared by electrodeposition were also studied in MECs [62]. The MECs with nickel alloy (NiMo) outperformed NiW cathode and achieved a comparable performance to the Pt cathode in terms of hydrogen production rate [63]. Another report found the Ni-W-P cathode demonstrated better electrocatalytic activity than the Ni-Ce-P cathode and achieved a comparable performance to the Pt cathode [64]. These studies demonstrate the potential of alternative catalysts for MECs and a strong need for developing new catalysts.

Derived from microbial fuel cells (MFCs), MECs inherit many similar features, including cathode catalysts, although with some differences. Nanoscale carbon materials such as carbon nanotubes (CNTs) have been studied to modify electrodes for improving electricity generation in MFCs [39]; however, there is no report using carbon nanomaterials as catalysts for hydrogen production in MECs. Recently, a family of Fe- and cobalt (Co)-based catalysts were synthesized to improve the cathodic oxygen reduction reaction (ORR). Consequently, we created a nitrogen-containing core-shell structured catalyst with iron-based composite (Fe/Fe_3C) nanorods as the core and graphite carbon as the shell, called N-Fe/Fe_3C@C [65]. The N-Fe/Fe_3C@C catalysts

achieved a comparable power production in an MFC to Pt/C catalyst, but outperformed Pt/C kinetically in current generation. Because of its superior performance in MFCs, in this study we examined hydrogen production using the N-Fe/Fe_3C@C as a cathode catalyst for HER in an MEC. For comparison, Pt/C, CNTs and unmodified cathodes were also investigated.

3.2.2 Materials and methods

Catalyst synthesis

Synthesis of N-Fe/Fe_3C@C nanorods started with drying the mixed solution of $FeCl_3$ and cyanamide. Further heat treatment under the argon protection led to the formation of C_3N_4 polymer-loading Fe-based nanoparticles, which then evolved into graphite-wrapping Fe-based nanoparticles, because of the decomposition of C_3N_4 polymer with Fe nanoparticles as catalysts. Further annealing treatment resulted in the oriented attachment of the Fe-based nanoparticles and finally produced the core-shell-structures N-Fe/Fe_3C@C nanorods (Figure 22). More details of N-Fe/Fe_3C@C preparation and characterization can be found in another of our studies [65].

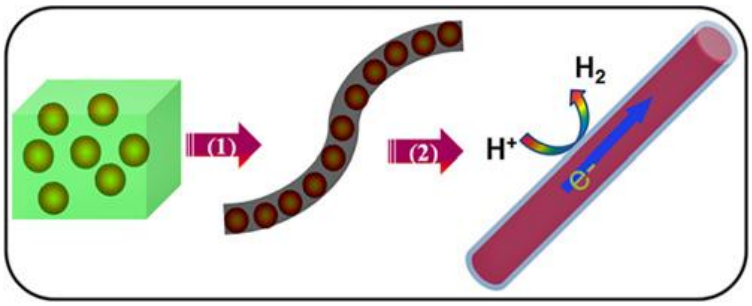

Figure 22. Schematic illustration of the formation of core-shell-structured N-Fe/Fe_3C@C nanorods: (1) The transformation of C_3N_4 polymer-loading Fe-based nanoparticles into graphite-wrapping Fe-based nanoparticles; (2) Oriented attachment of Fe-based nanoparticles and the formation of core-shell-structures N-Fe/Fe_3C@C nanorods.

Cathode electrode preparation

Carbon cloth (CC) electrodes (PANEX®30PW03, Zoltek, Corporation, St. Louis, MO, USA) were modified with N-Fe/Fe_3C@C, CNTs or Pt/C (10% Pt in carbon black) powder. An unmodified electrode (CC) was used as a control, and each electrode had a projected surface area of 12 cm^2. For modification, 60 mg of N-Fe/Fe_3C@C powder was mixed with 0.3 mL Nafion solution. This mixture was applied to the carbon cloth, dried in air for 24 hours, and then was ready for use. The final loading rate of the modifying material was ~5 mg cm^{-2}. Other modified electrodes (CNTs and Pt/C) were prepared using the same method.

MEC construction and operation

A two-chamber MEC was built with two glass bottles jointed by a cation exchange membrane (CEM) (Ultex CMI 7000, Membranes International, Inc., Glen Rock, NJ, USA). Each chamber had a liquid volume of 120 mL. The anode was a carbon brush

(Gordon Brush Mfg. Co., Inc., Commerce, CA). To develop the anode biofilm, the MEC was first operated as a two-chamber MFC. The anode was inoculated with the anaerobic sludge from a local municipal wastewater treatment plant (South Shore, Milwaukee, WI, USA). The nutrient solution in the anode chamber contained (per 1 L of DI water): sodium acetate, 1.0 g; NH_4Cl, 0.3 g; NaCl, 1.0 g; $MgSO_4$, 0.03 g; $CaCl_2$, 0.04 g; $NaHCO_3$, 0.2 g; KH_2PO_4, 5.3 g; K_2HPO_4, 10.7 g and 1 mL/L trace elements [35]. The cathode chamber was filled with 100 mM phosphate buffer solution (PBS: 5.3 g/L KH_2PO_4 H_2O and 10.7 g/L K_2HPO_4) and aerated with air. When the open cell voltage (OCV) reached 0.7 V, we switched the MFC to an MEC by removing aeration from its cathode and applying an external voltage of 0.8 V to the circuit via connecting the negative pole of a power supply (3644A, Circuit Specialists, Inc., Mesa, AZ, USA) to 10 Ω resistor, then to the cathode, and the positive pole to the anode. The MEC was operated in a batch mode at a room temperature of 20 ℃. The anode solution (same as the one used for MFC operation) was partially replaced (80 %) when the voltage dropped below 4 mV. Meanwhile, the cathode solution was completely replaced and then sparged with nitrogen gas for 15 min.

Measurement and analysis

The voltage across the resistor was recorded every 5 min by a digital multimeter (2700, Keithley Instruments, Inc., Cleveland, OH, USA). A potentiostat (Reference 600, Gamry Instruments, Warminster, PA, USA) performed the linear sweep voltammogram (LSV) at a scan rate of 5 mV/s with a three-electrode arrangement, including a working electrode

(modified electrode), a platinum electrode used as counter electrode, and an Ag/AgCl reference electrode (200 mV vs. SHE) in a separate beaker that contained N_2-saturated phosphate buffer solution (100 mM PBS, pH = 7.0). Gas production in the MEC was measured by water replacement using a graduated flask and the gas composition was analyzed by a gas chromatograph (Thermo Fisher Scientific, Waltham, MA, USA). Iron was analyzed using Ferrozine method [14]. The N-Fe/Fe_3C@C powder and N-Fe/Fe_3C@C-modified cathode were imaged using a scanning electron microscope (SEM) (Hitachi S4800, Japan). The morphology and nanostructures of the samples were characterized by using FEI Tecnai F20 ST 200 KeV high-resolution transmission electron microscope (HRTEM).

Several parameters were calculated as follows:

Total output coulombs (Q) is the integration of current over time: $Q = \int_{t=0}^{t} Idt$, where I is the current (A), t is the time (s). Coulombic recovery (CR) is defined as total output coulombs over total input coulombs in acetate: = Q/nFC_a, where n is the number of electrons released from each acetate (8), F is faradic constant (96, 485 C/mol e^-), and C_a is the total mole of the added acetate. Cathodic hydrogen recovery (R_{cat}) is the ratio between the electrons contained in the produced hydrogen gas and the electrons produced as current: $R_{cat} = 2n_{H_2}/(Q/F)$, where n_{H_2} is the mole of the produced hydrogen gas. The overall hydrogen recovery (R_{H_2}) represents the substrate used for hydrogen production: $R_{H_2} = R_{cat}CR$. The hydrogen production rate (Q_{H_2}) is the hydrogen production per cathode electrode area per time: $Q_{H_2} = V_{H_2}/A_{cat}t$, where V_{H2} is hydrogen volume (m^3), A_{cat} is the project surface area of the cathode electrode (m^2), and t is the time period of one cycle (d).

3.2.3 Results and discussions

Electrochemical and microscopy characterization of cathode electrodes

Linear sweep voltammetry (LSV) was used to characterize the electrochemical properties of these cathode materials. The bare CC showed a very small cathodic current and the CNT cathode had a slightly enhanced cathodic current; clearly, both the Pt/C- and the N-Fe/Fe3C@C cathodes displayed a much higher cathodic current than the other two cathodes (Figure 23). In more details, at the potential of - 0.9 V, the Pt/C- and the N-Fe/Fe3C@C exhibited a cathodic current of 0.059 A and 0.048 A, respectively, one order of magnitude higher than the corresponding cathodic current with the CC (1.92×10^{-5} A) and CNTs (0.0046 A). It should be noted the cathodic current can somehow reflect the activity of catalytic reduction of H^+; in this sense, the N-Fe/Fe3C@C behaved slightly lower than the Pt/C. Nevertheless, the N-Fe/Fe3C@C exhibited attractive properties for proton reduction compared with the bare CC and CNTs cathodes, which is also confirmed by the data on hydrogen production and MEC current generation, as discussed in the following section. To our surprise, conventional CNTs did not improve MEC cathodes as they do with MFC cathodes, indicating that CNTs might not possess the ability to catalyze proton reduction and their high surface that is beneficial to ORR in MFCs does not help hydrogen evolution in MECs.

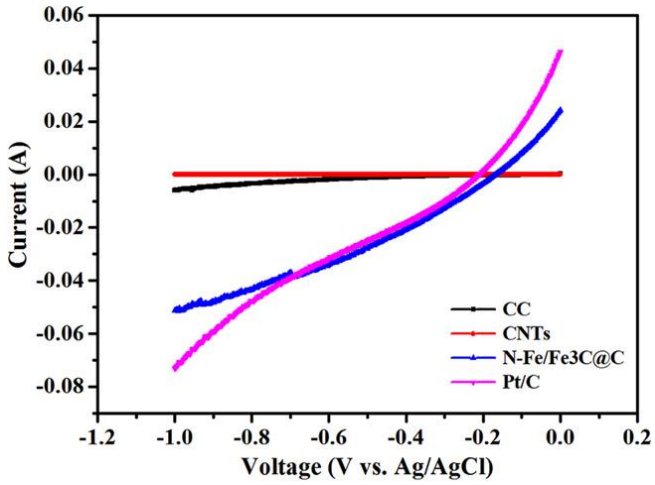

Figure 23. Linear sweep voltammetry of the four cathode electrodes in N_2-saturated phosphate buffer solution (100 mM PBS, pH = 7.0).

The N-Fe/Fe_3C@C had a solid rod morphology with iron-based composite (Fe/Fe_3C) nanorods as the core and graphite carbon as the shell. Figures 24a and 24b present the SEM and TEM images of the N-Fe/Fe_3C@C nanorods respectively, in which one can observe lots of nanorods accompanying with a few nanoparticles. Figures 24c and 24d display the TEM image of single N-Fe/Fe_3C@C nanorod; it can be seen that one film of graphite layers are covered on the core that have a crystalline spacing of about 0.21 nm, corresponding to crystalline face of Fe_3C.

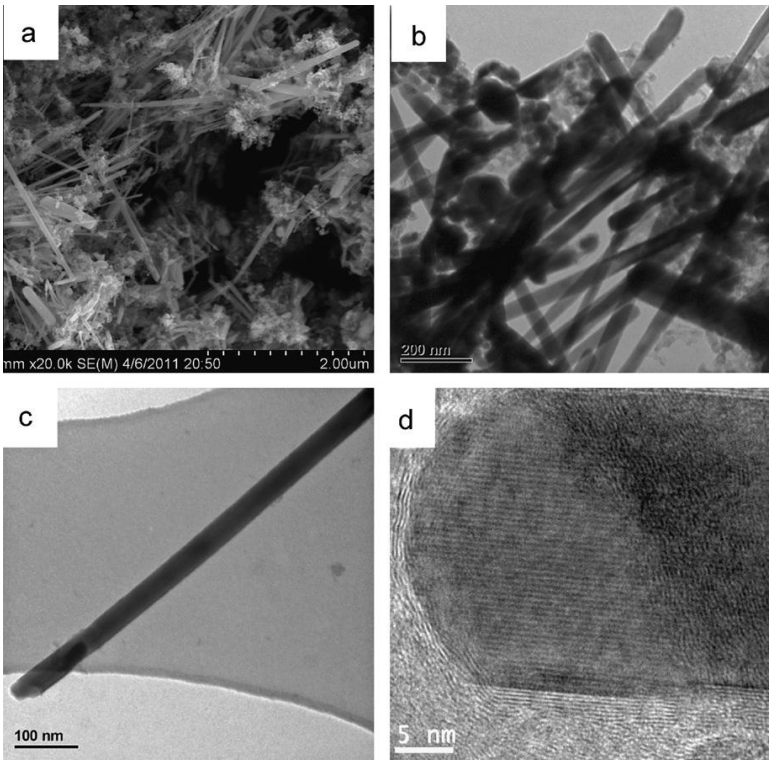

Figure 24. Scanning and transmission electron microscopy images of the N-Fe/Fe_3C@C catalysts.

Hydrogen production

When applying 0.8 V to the MEC, electric current was generated through the 10-Ω resistor, and this current was directly related to hydrogen production via electron transfer. A profile of current production was obtained in the batch operation mode: a rapid increase upon the replacement of a fresh anode solution, a gradual decrease due to the rising pH, and a rapid decrease because of the depletion of the anode substrate (Figure 25). The peak current density of the N-Fe/Fe_3C@C cathode was 2.60 ± 0.07 A m^{-2}, much higher than those of CNTs (1.30 ± 0.09 A m^{-2}) and CC cathodes (1.36 ± 0.10 A m^{-2}), although not comparable with that of the Pt/C cathode (3.50 ± 0.12 A m^{-2}). However, the

duration of current production with the Pt/C cathode was shorter than the N-Fe/Fe_3C@C cathode. As a result, the total charges produced with the N-Fe/Fe_3C@C cathode in one cycle amounted to 410.5 ± 7.3 C, higher than that of the Pt/C cathode (374.0 ± 24.2 C); therefore, the N-Fe/Fe_3C@C cathode had a higher coulombic recovery than the Pt/C cathode (Table 5). The CC and CNTs cathodes produced 253.6 ± 9.7 C and 228.6 ± 28.1 C, respectively.

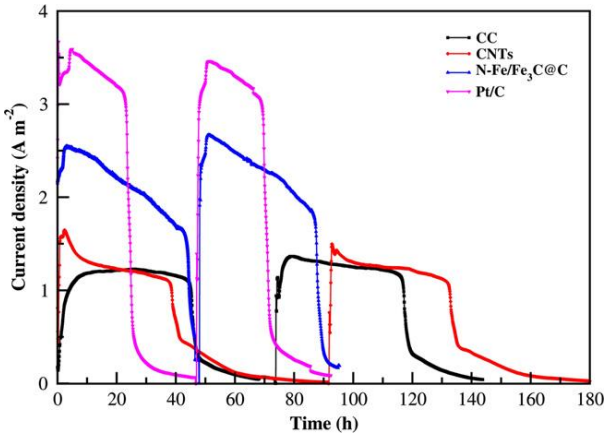

Figure 25. Current generation with the four cathode electrodes in the MEC at an external resistor of 10 Ω and an applied voltage of 0.8 V.

Table 5. Efficiencies and hydrogen production in the MEC with different cathodes.

	[1]CR (%)	[2]R_{cat} (%)	[3]R_{H2} (%)	[4]Q_{H2} (m^3 H_2 m^{-2} d^{-1})
CC	26.9 ± 1.1	67.7 ± 10.6	18.2 ± 2.4	0.0087 ± 0.0007
CNT	24.1 ± 3.0	66.6 ± 6.6	16.0 ± 2.1	0.0075 ± 0.0006
Pt/C	39.8 ± 2.6	81.6 ± 5.0	32.4 ± 1.9	0.0230 ± 0.0031
N-Fe/Fe_3C@C	43.6 ± 0.8	79.8 ± 8.4	34.8 ± 4.3	0.0181 ± 0.0011
N-Fe/Fe_3C@C*	38.1 ± 0.8	79.5 ± 0.8	30.3 ± 0.3	0.0144 ± 0.0002

*After 20-day operation
[1]C_R: Coulombic recovery
[2]R_{cat}: Cathodic hydrogen recovery
[3]R_{H2}: Hydrogen recovery
[4]Q_{H2}: Hydrogen production rate

Hydrogen production was monitored with all cathodes and the efficiencies are summarized in Table 5. Although both Pt/C and N-Fe/Fe_3C@C exhibited similar hydrogen recovery efficiency, the Pt/C cathode had a higher hydrogen production rate of 0.0230 ± 0.0031 $m^3 H_2$ m^{-3} d^{-1}. Even so, the hydrogen production rate of N-Fe/Fe_3C@C cathode (0.0181 ± 0.0011 $m^3 H_2$ m^{-3} d^{-1}) was about twice that of CNTs and CC cathodes.

Problems and perspectives of N-Fe/Fe_3C@C

An extended MEC operation for more than 20 days resulted in a decrease in both the total charges produced with the N-Fe/Fe_3C@C cathode to 358.7 ± 7.7 C and the hydrogen production rate (Table 5), indicating the catalyst has an issue with stability. It was observed that yellowish-green particles appeared on the surface of the N-Fe/Fe_3C@C cathode. The analysis suggested that those particles contained only Fe(II), which was likely a result of Fe(III) reduction during the MEC operation; however, this phenomenon was not found with the MFC test, and the N-Fe/Fe_3C@C cathode was stable after operating for more than six months [65]. Fe(III) is a major functional component in the N-Fe/Fe_3C@C. During the MFC cathode operation, oxygen is a preferable electron acceptor and has a higher reduction potential than Fe(III); thus, Fe(III) is not electrochemically reduced. In the MEC cathode, Fe(III) could be reduced by accepting electrons from the cathode electrode, although this was shown as a minor and slow effect. The presence of Fe(II) in the MEC cathode was also due to the absence of oxygen that could oxidize Fe(II) to Fe(III). Nevertheless, the N-Fe/Fe_3C@C exhibited remarkable

improvement in catalytic activities for hydrogen production compared with CC and CNTs, although not as good as Pt/C.

A great advantage of the N-Fe/Fe_3C@C is its low cost. We estimate that it costs less than $2 for the raw-materials to prepare 1 g N-Fe/Fe3C@C, while 1 g of 10% Platinum on Vulcan XC-72 costs about $46 (www.fuelcellstore.com), which is more than 20 times that of N-Fe/Fe3C@C. Considering the procedure of the N-Fe/Fe_3C@C preparation is simple, and only electricity is consumed, the total cost could be very attractive compared with the Pt/C catalysts. The cost of the cathode catalyst is critical to capital investment of large-scale MEC applications, and the tradeoff between expense and performance must be considered.

3.2.4. Conclusions

In this study we demonstrated that the N-Fe/Fe_3C@C could catalyze the hydrogen production in an MEC via modifying the cathode electrode. The rate and efficiency of hydrogen production with the N-Fe/Fe_3C@C cathode was slightly lower than that of the Pt/C cathode, but much higher than those of CNTs and unmodified cathodes. Although instability of the N-Fe/Fe_3C@C was observed, its low cost will compensate for lower performance compared with the Pt/C catalysts. Thus, this Fe-based core-shell catalyst could be promising for hydrogen production in MECs.

4 Integrated photo-bioelectrochemical systems

4.1 Integrated photo-bioelectrochemical system for contaminants removal and bioenergy production

(This section has been published as: Xiao, L., Young, E. B., Berges, J. A. and He, Z. (2012) Integrated photo-bioelectrochemical system for contaminants removal and bioenergy production. ***Evironmental Science & Technology***. 46, 11459-11466.)

4.1.1 Introduction

Municipal wastewater treatment plants play a critical role in environmental protection, but the operation of such plants consumes an extensive amount of energy [66]. An ongoing challenge to sustainability is to improve the efficiency of wastewater management to reduce energy demands and to increase energy recovery from waste. To address this challenge, the key research tasks include: optimizing a more energy-efficient process of removing dissolved organics from wastewater and reducing aeration, which represents an important, electricity-demanding step in most municipal wastewater treatment facilities; developing better processes for capturing the energy bonded within the organic contaminants of wastewater to produce electric energy; and improving nutrient (chiefly inorganic nitrogen and phosphorus) removal/recovery from wastewater by using a process that consumes fewer resources (e.g., aeration required for nitrification [67], and chemicals for denitrification and phosphorus precipitation). These key challenges have been addressed in various ways, but primarily in distinct and separated approaches (e.g., anaerobic digesters, and algal bioreactors in different locations). A system that aims to integrate these approaches may increase efficiency, and save energy and resources.

To achieve such a system, we can synergistically link microbial fuel cells (MFCs) [12] with algal bioreactors [68] for wastewater treatment and bioenergy production. MFCs will remove organics and provide nutrients and carbon dioxide to grow algae in the bioreactor, and algal bioreactors will remove nutrients and provide dissolved oxygen to the MFC cathode reaction. MFCs can effectively remove various organic substrates [20], but nutrient removal is generally limited under an anaerobic condition with a few specially designed nutrient removal processes [69][70][71][72]. Algal treatment of wastewater has a long history, especially in removing nutrients, and provides additional services by using photosynthesis to fix carbon dioxide into organic compounds for fuel biomass production [73]. Microalgae can assimilate significant amounts of nutrients because of high N and P demand for synthesis of proteins (45-60% of microalgae dry weight), nucleic acids, phospholipids, and other cellular constituents [74]. The algal biomass produced from bioreactors also can be used for producing biofuels, including biodiesel [75][76].

Linking MFCs to algal growth can be accomplished in several ways. First, algal biomass can be used as a fuel in MFCs, but the efficiency of energy production is very low due to the low transfer of chemical energy from algae to electrochemically active bacteria [77][78]. Second, electrodes can be installed in algal bioreactors for electricity generation [79]; however, mixing algae with electrochemically active bacteria will adversely affect anode reactions because of dissolved oxygen produced by algae [80], and the presence of organic compounds will stimulate the growth of heterotrophic bacteria that compete with algae for nutrients. Third, MFCs and algal bioreactors can be installed separately and the algal bioreactor can receive MFC effluent; in this way, the intrinsic problems with each

process are not solved. For instance, in a membrane-based MFC, its cathode requires an additional supply of water and oxygen, as well as pH buffering, and algal bioreactors need pH buffering when CO_2 is added.

To address these intrinsic problems, we have developed an integrated photo-bioelectrochemical (IPB) system. Instead of simply connecting the two processes in series, the IPB system involves a unique integration of MFCs within an algal bioreactor, leading to a potentially more efficient system that can achieve both waste treatment and bioenergy production (Figure 26). In this system, wastewater is fed into the MFCs where organic contaminants are oxidized; the remaining inorganic nutrients are then discharged into the algal bioreactor for algal growth, which strips nutrients out of the water before the treated effluent is released for final tertiary treatment (e.g., disinfection). Installing MFCs inside an algal bioreactor would have algae producing oxygen used by the MFCs for their cathode reactions, thereby reducing the need for aeration. If additional CO_2 (e.g., waste gas from power plants) is added to the algal bioreactor for algal growth, the pH of the algal growth medium could become acidic, thereby inhibiting algal growth; MFC cathodic reactions can buffer the pH by adding alkalinity resulting from oxygen reduction. Through this combination, the two treatment processes are cooperatively linked for the same purpose of treating wastewater, with two different bioenergy products: bioelectricity from the MFCs, and algal biomass for use in biofuels production.

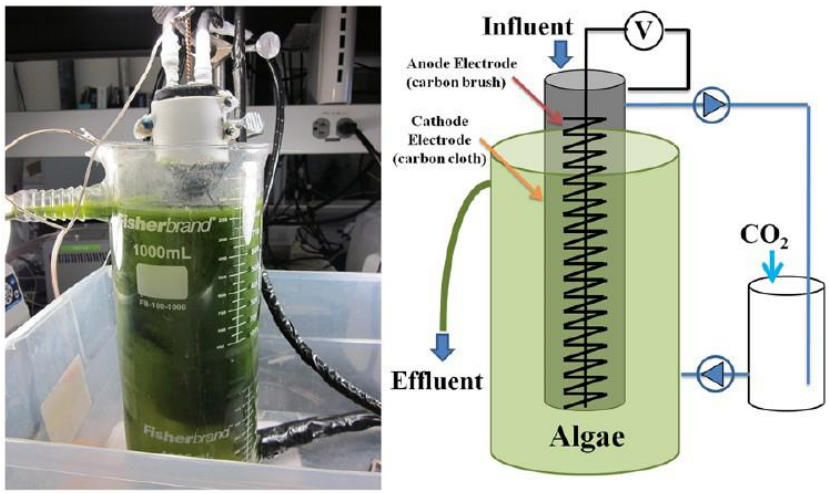

Figure 26. Experimental setup (left) and schematic (right) of the IPB system.

In this study, we operated a bench-scale IPB system for more than 360 days with three primary objectives: (1) to examine the long-term system performance of organic/nutrient removal and energy production; (2) to understand the effects of illumination or aeration on the IPB system; and (3) to understand the microbial composition of the biofilm attached on the cathode electrode and planktonic cells in the cathode compartment (algal bioreactor).

4.1.2 Materials and methods

IPB system setup

The IPB system consisted of a single-chamber tubular MFC installed in a glass beaker, which functioned as both the cathode compartment and the algal bioreactor (Figure 26). The MFC was constructed based on a cation exchange membrane tube (CEM, Ultrex

CMI7000, Membranes International, Inc., Glen Rock, NJ) with a diameter of 4.5 cm and a height of 20 cm, resulting in an anode liquid volume of ~ 300 mL. A 20 cm long carbon brush (Gordon Brush Mfg. Co., Inc., Commerce, CA) was used as the anode electrode. Before use, the carbon brush electrode was pretreated by immersing in acetone overnight and heating at 450 ℃ for 30 min. The cathode electrode was a layer of carbon cloth with Pt/C as catalysts that wrapped the CEM tube. To coat the Pt catalyst to the cathode electrode, Pt/C powder was mixed with Nafion solution and then applied to the carbon cloth surface with a brush to a final loading rate of ~ 0.5 mg Pt/cm^2. The anode and cathode electrodes were connected by copper wires to an external circuit across a 100 Ω resistance. The glass beaker that held the MFC had a diameter of 10 cm and height of 29 cm, with a liquid volume of 1700 mL. Three compact fluorescent bulbs (32 W, 120 V, Energy Wiser, color temperature 4000 K, Bulbrute Industries, Inc., China) were installed around the cathode to provide an average irradiance of 13 W m^{-2} on a 16-h on/8-h off cycle, unless noted elsewhere.

Operating conditions

The IPB system was continuously operated with a synthetic solution at about 20 ℃. The anode compartment was inoculated with the anaerobic sludge from a local municipal wastewater treatment plant (South Shore, Milwaukee, WI, USA). The cathode compartment was initially inoculated with the green algae *Pseudokirchneriella subcapitata* (Korshikov) Hindak (CPCC 37) obtained from the Canadian Phycological Culture Collection (www.phycol.ca) and previously maintained in axenic culture. The

synthetic solution had 2.48 mS/cm conductivity and pH of 7.8, and contained (per L of tap water): sodium acetate, 0.35 g; NH_4Cl, 0.2 g; NaCl, 0.5 g; $MgSO_4$, 0.015 g; $CaCl_2$, 0.02 g; $NaHCO_3$, 0.6 g; KH_2PO_4, 0.027 g and 1 mL/L trace elements [35]. This solution was fed into the anode of the MFC at a flow rate of 0.4 mL/min (with an anolyte recirculation rate of 30 mL/min), resulting in a hydraulic retention time (HRT) of 12.5 hours and an organic loading rate of 0.51 kg COD/m^3/d in the anode compartment. The effluent of the anode flowed into a 500 mL beaker where CO_2 was bubbled by a gas diffuser to provide inorganic carbon for algal growth and then pumped into the cathode of the MFC at the same flow rate of the anode feeding. The catholyte was mixed by a magnetic stirrer.

Measurement and analysis

The cell voltage was recorded every 5 min by a digital multimeter (2700, Keithley Instruments, Inc., Cleveland, OH, USA). The concentrations of soluble COD, ammonium nitrogen, nitrite nitrogen, nitrate nitrogen, and phosphate were measured according to the manufacturer's instructions using a DR/890 datalogging colorimeter (Hach Company, Loveland, CO, USA). The pH, temperature, and dissolved oxygen (DO) were measured using a 556 MPS hand-held multiparameter instrument (YSI Incorporated, Yellow Spring, OH, USA). The concentration of algal mass was measured as absorbance at 680 nm in a 1100 spectrophotometer (Unico, Dayton, NJ, USA) and converted to biomass using the standard curve shown in Figure 27.

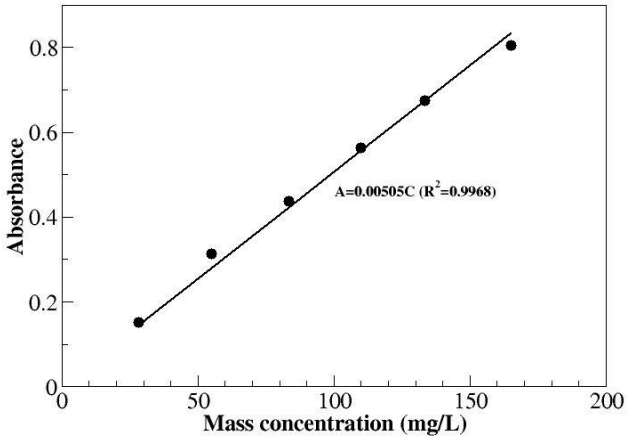

Figure 27. The standard curve of algal mass vs. absorbance.

Power density and current density was based on the anode liquid volume, according to a previous study [33]. The efficiency of organic-to-electricity was expressed by coulombic recovery (CR) and coulombic efficiency (CE), calculated as the follows:

$$CR = \frac{Q_{output}}{Q_{input}} = \frac{\sum I(A)t(s)}{96485\left(\frac{C}{mol\ e^-}\right) \times COD_{total}(mol) \times 4(\frac{mol\ e^-}{mol\ O_2})}$$

$$CE = \frac{Q_{output}}{Q_{input-r}} = \frac{\sum I(A)t\ (s)}{96485(\frac{C}{mol\ e^-}) \times COD_{removed}(mol) \times 4(\frac{mol\ e^-}{mol\ O_2})}$$

Where Q_{output} is the produced charge, Q_{input} is the total charge available in the added organic compounds, $Q_{input-r}$ is the total charge available in the removed organic compounds, I is electric current and t is time. COD_{total} is the total COD input to the anode compartment in the period of time t, and calculated based on the initial COD concentration multiplied by the initial anolyte volume. $COD_{removed}$ is the removed COD

within time t. The removed COD was also expressed in percentage as a ratio of initial COD input and final COD remained.

Energy consumption in the IPB system was mainly due to the recirculation of the anolyte by pumps and mixing catholyte which also was estimated according to a recirculation rate of 120 mL/min. Power requirement by the recirculation pump was estimated as [81]:

$$P = \frac{Q\gamma E}{1000}$$

where P is power requirement (kW), Q is flow rate (m^3/s), γ is 9800 N/m^3, and E is the hydraulic pressure head (m). For the IPB system, Q was 0.0018 m^3/s (30 mL/min) for anode recirculation and 0.0072 m^3/s (120 mL/min) for cathode recirculation, and the measured hydraulic pressure head loss was 0.055 m for the anode and 0.07 m for the cathode; thus, the total power required for the anode recirculation pump was 0.9702 W and the cathode recirculation pump was 4.9392 W.

Scanning electron microscopy (SEM)

Small pieces of the cathode electrode with biofilm were cut off and suspended cells in the catholyte were collected through filtration using 0.2 μm filters. Those samples were fixed with 2.5% glutaraldehyde for one night and 1% OsO_4 for one hour, and then dehydrated with a graded ethanol series: 10%, 25%, 50%, 75%, 95%, 100% and 100%. The samples were critical-point dried via liquid CO_2 in a Balzers CPD 020 critical point drying apparatus (Balzers Union, Liechtenstein). After drying, the samples were coated with 5.0

nm Iridium in the Emitech K575X Sputter Coater (Emitech, Polaron, Britain). The morphology of microorganisms was observed by SEM (S-4800 Hitachi, Japan).

Cathode microbial analysis

Samples were collected at day 179 and 278. Algal-bacterial communities associated with biofilm on the cathode electrode were scraped off using a sterile spatula and transferred to microcentrifuge tubes. Communities in the cathode suspension were sampled by collecting 5 - 20 mL from the liquid using a sterile syringe, and filtering this volume through a 0.22 mm membrane filter (make/brand) and the filter folded and transferred to a microcentrifuge tube. All samples were immediately frozen at -80^{o}C until analysis. Frozen samples were thawed on ice and DNA was extracted using the FastDNA® spin kit for Soil (MP Biomedicals, Solon, OH), and purified using a Powerclean® DNA clean-up kit (MO BIO Laboratories Inc., Carlsbad, CA). DNA concentrations were measured using NanoDrop® ND-1000 (Thermo Fisher Scientific Inc., Pittsburg, PA). DNA was used for genetic analysis using 16S rRNA gene clone libraries. Extracted DNA was amplified using universal bacterial 16S rRNA primers 8F and 1492R [82]. PCR products was purified using QIAGEN PCR purification kit (Qiagen Inc., Valencia, CA) and cloned into pCR2.1 vector using the TOPO® TA cloning kit (Invitrogen, Carlsbad, CA). Plasmid DNA was isolated using a manual method adapted to a 96-well format [83]. Sequencing was carried out from the 8F and 1492R primers using the ABI Big Dye Terminator Kit (Applied Biosystems, Foster City, CA) on an ABI Prism 3700xi (Applied Biosystems, Foster City, CA), which generated approximately 800 bp reads. Sequences

were trimmed for quality using PHRED [84]. After this quality control, DNA sequences were examined using NCBI BLAST algorithm [85] and the Ribosomal Database Project II Classifier [86] at a confidence level of 80%, to identify similar sequences and identify bacterial sequences to taxonomic level of genus, where possible.

4.1.3 Results and discussion

Performance of the IPB system

The IPB system was operated for more than 360 days and its electricity production was affected by illumination and organic input. To exhibit more details, electricity production, DO, pH and temperature for a period of 4 d are shown in Figure 28. The electricity produced by the MFC exhibited a day-night profile, affected by illumination (16-h light : 8-h dark) (Fig. 2A). The peak power density reached 2.2 ± 0.2 W/m^3 under illumination. Because no aeration was provided in this period, the cathode reaction relied on the dissolved oxygen (DO) produced by algae in the cathode compartment. Similar to current generation, the DO concentration varied on a day-night basis, and under illumination DO concentration reached 20 mg/L (Fig. 28B), more than twice the saturated DO in DI water at the same temperature, which has been observed in other algal bioreactors [87]. When the light was turned off, the DO gradually dropped to below 1 mg/L, resulting in a power density of 0.1 ± 0.0 W/m^3 in the dark. Although oxygen in the air could be dissolved in the catholyte and contributed to electricity generation, this contribution was much smaller compared with the algae-produced oxygen, as demonstrated by the low electricity generation in the dark, even with active aeration (Figure 30). Therefore, it is reasonable

to conclude that algae can provide a substantial amount of oxygen to the cathode reaction under illumination.

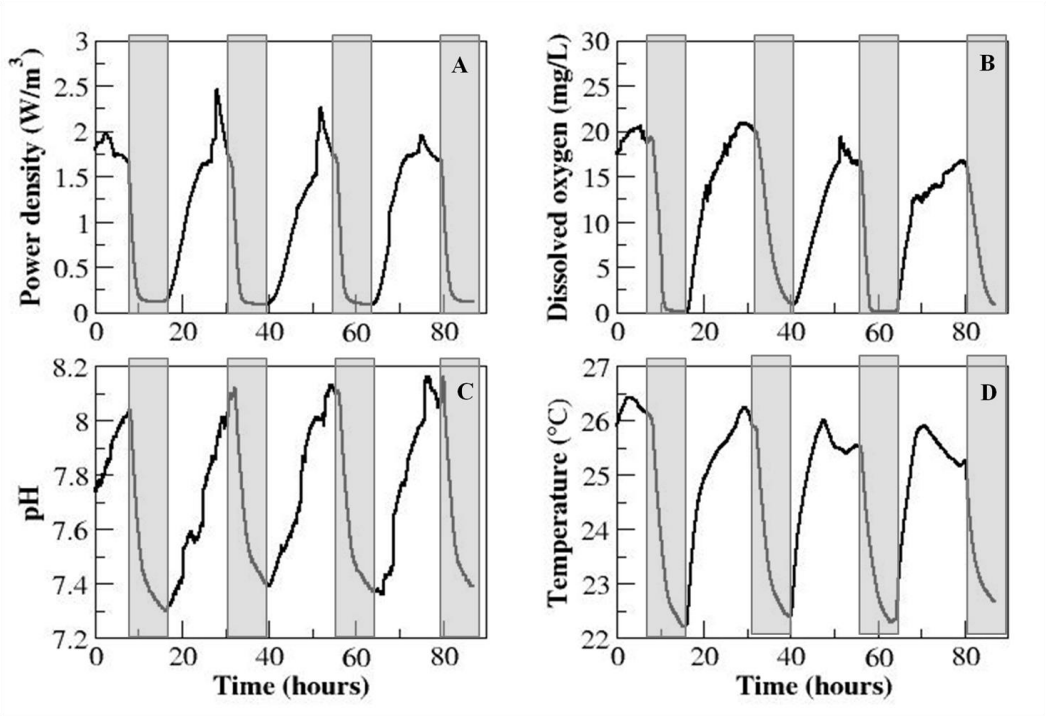

Figure 28. The performance and operating parameters of the IPB system: power density, dissolved oxygen, pH and temperature. The white indicates the illuminated period and the shadow indicates the dark period.

The pH of the catholyte (algal growth medium) varied between 7.3 and 8.2 (Figure 28C), a result of the combined effect of the cathode oxygen reduction and CO_2 buffering: the MFC cathode reaction could elevate the pH of the catholyte to above 11 [88] and the anode effluent saturated with CO_2 had a low pH of ~ 4; when the low pH anode effluent entered the cathode compartment, the oxygen reduction increased the pH to levels appropriate for algal growth (7~9 [89]). On the other hand, the low pH of the anode effluent also benefited the cathode reaction by providing more protons. The addition of

CO_2 not only provides carbon source for algal growth, but also buffers the catholyte and thus eliminates the use of an expensive buffer solution that is not practical for large scale application [90][91]. A potential source of CO_2 is combustion of digester biogas, or flue gas if the MFC system can be installed adjacent to power plants. In addition, biological processes such as nitrification could also provide protons and thus lower the pH of the catholyte. The illumination also changed the temperature of the catholyte with an increase from ~ 22 to ~ 26 ℃ from dark to under illumination (Figure 28D). Such an increase in temperature could benefit the anode microbes when heat is transferred into the anode compartment through the CEM and electrolyte.

The IPB system effectively reduced the concentrations of both organics and nutrients. The anode removed 92.4% of SCOD and decreased its concentration from 266.7 to 22.0 ±13.7 mg/L, which was further reduced to 20.2 ±2.9 mg/L by the cathode (Table 6). The average CE was 7.7%, and the average CR was 7.2%. Almost all of ammonium (98.6%) was removed through either algal uptake or nitrification. It is interesting to note that the anode effluent contained less than half of the initial ammonium concentration; because anaerobic ammonium oxidation has not been well demonstrated in the anode of an MFC [80], we believe that the ammonium loss was due to ammonium transport into the cathode compartment through the cation exchange membrane[72]. Nitrification was expected to occur in the cathode because of the presence of both dissolved oxygen and bacteria. Denitrification, on the other hand, would be very limited because of the DO. The growth of some algae is faster with ammonium than with nitrate, and the presence of ammonium higher than 1 μM could inhibit nitrate uptake [92][93], resulting in the observed nitrate accumulation to 19.3±1.8 mg/L. The removal of total nitrogen by the

IPB system was about 63%. The concentration of phosphate was decreased by 82.3% in the IPB system, including a 27% reduction in the anode compartment likely due to the bacterial uptake, and a 55% reduction in the cathode compartment because of the algal uptake. The final phosphate concentration was 1.1 ± 0.2 mg/L; future studies will include a more detailed analysis of total phosphorus fractions, including organic phosphorus that can be released under an anaerobic condition. The IPB system produced an algal biomass of 128 ± 36 mg/L (or 43.37 mg/L/day based on the liquid volume of the algal bioreactor), which was comparable with other algal bioreactors fed on wastewater [73].

Table 6. Characteristics of the synthetic solution when flowing through the IPB system. The error term is standard deviation.

	SCOD (mg/L)	NH_4^+-N (mg/L)	NO_3^--N (mg/L)	NO_2^--N (mg/L)	PO_4^{3-}-P (mg/L)	Biomass (mg/L)
Anode Influent	266.7	52.3	N/D	N/D	6.2	N/A
Anode Effluent	22.0 ± 13.7	20.3 ± 0.5	N/D	N/D	4.5 ± 0.2	N/A
Cathode Effluent	20.2 ± 2.9	0.7 ± 0.8	19.3 ± 1.8	N/D	1.1 ± 0.2	128 ±36

N/D: not detected;
N/A: not available.

Effects of illumination on the IPB system

To understand the influence of illumination on the IPB system, we created two scenarios: keeping constant illumination, or increasing the frequency of light/dark cycles. When the illumination was extended to 24 h/day, the power density gradually decreased with time

(Figure 29A); within 2 days, the accumulated electricity production improved, compared with the on/off illumination, but for a period of 7 days, the total electricity production was not much higher (Table 7), because of the low power output after 2 days. Likewise, the DO concentration also decreased. The similar trend between electricity and DO confirmed that photosynthetic O_2 production determined the power density in the IPB system. Research found that some algae require a dark period for division, which could be inhibited by high light intensity and continuous illumination [94]. The continuous illumination also promoted nitrification in the catholyte. The highest concentration of nitrate in the effluent during this period was 32.2 mg NO_3^--N /L, which was about 1.7 times that of the 19.3 mg NO_3^--N /L shown in Table 6. It was previously reported that the presence of algae inhibited the growth of nitrifying bacteria because of faster algal growth rate and toxicity to nitrifiers [95]; our results confirmed that decreased photosynthesis (and algal growth) could benefit nitrifying bacteria, as shown by a higher nitrate concentration under constant illumination.

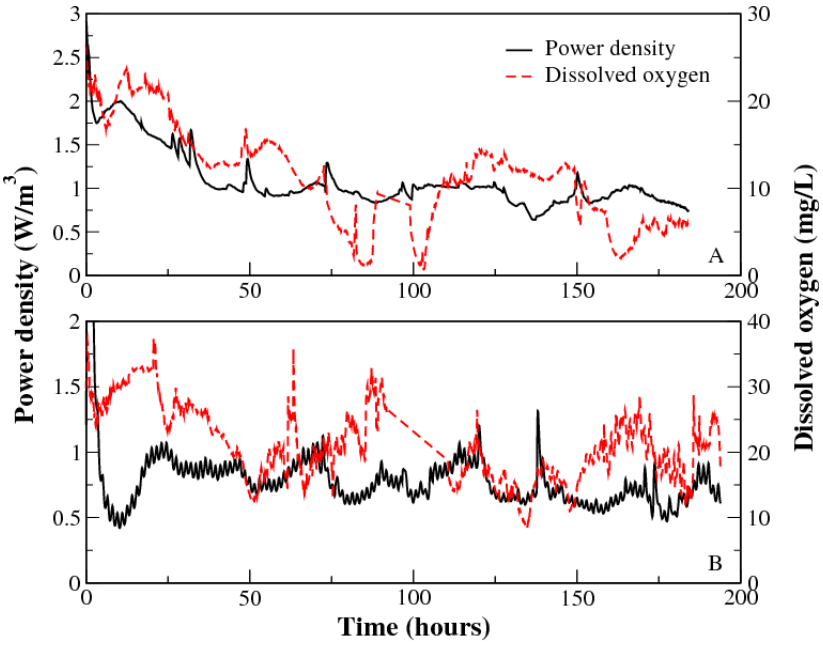

Figure 29. Power density (black solid line) and the DO (red dashed line) during the continuous illumination (A) and the increased light/dark cycle (B).

Table 7. Energy production and consumption in the IPB system under different illumination and aeration operating conditions.

		16-h on/8-h off (kWh/m^3)	24 h/d on (kWh/m^3)	1-h on/0.5-h off (kWh/m^3)	Night Aeration[1] (kWh/m^3)
Input	Pump[2]	-0.011	-0.011	-0.011	-0.011
	Mixing[3]	-0.057	-0.057	-0.057	-0.057
	Aeration	N/A	N/A	N/A	-0.004
Output	Electricity	0.012	0.013	0.01	0.021
	Biomass[4]	0.081	0.057	0.073	0.085
Net	Total	0.025	0.002	0.015	0.034
	Electricity[5]	-0.056	-0.055	-0.058	-0.051

[1] Aeration rate of 30 cc/min and 16-h on/8-h off illumination

[2] Estimated according to hydraulic head loss and theoretic equation (in supporting information)

[3] Estimated according to energy consumption by a recirculation rate of 120 mL/min

[4] Energy consumption during treating algal biomass is not included

[5] Excluding the energy production from biomass

When the frequency of the light/dark cycles was increased to 1-h light/0.5-h dark, the electricity production maintained between 0.5 and 1 W/m^3 (Figure 29B). The average DO concentration stayed around 20 mg/L (Figure 29B), much higher than under continuous illumination (Figure 29A), suggesting that the dark condition was beneficial to net algal oxygen production [96]. The concentration of nitrate decreased to 17.6 mg/L at the end of the increased light/dark cycle period, suggesting that the improved algal activities slowed down nitrification, compared with continuous illumination.

Aeration in the dark

We investigated the effects of intermittent aeration (in the dark) on the production of electricity and algal biomass, using three aeration rates, 30, 50 and 100 mL/min (Figure 30). As expected, the aeration increased the DO at night, as well as the power production. At 30 mL/min aeration, the electric power was improved by about 40% compared with no aeration (Table 7). The highest DO in the dark with 100 mL/min aeration was about 8 mg/L (Figure 30A), much lower than during algal photosynthesis under illumination, indicating that algal production of DO would be more promising than mechanical aeration. Aeration also encouraged algal growth and improved biomass production by ~ 5% (Table 7). However, aeration consumed additional electric energy, so an analysis of energy balance with this approach in the IPB system would be needed.

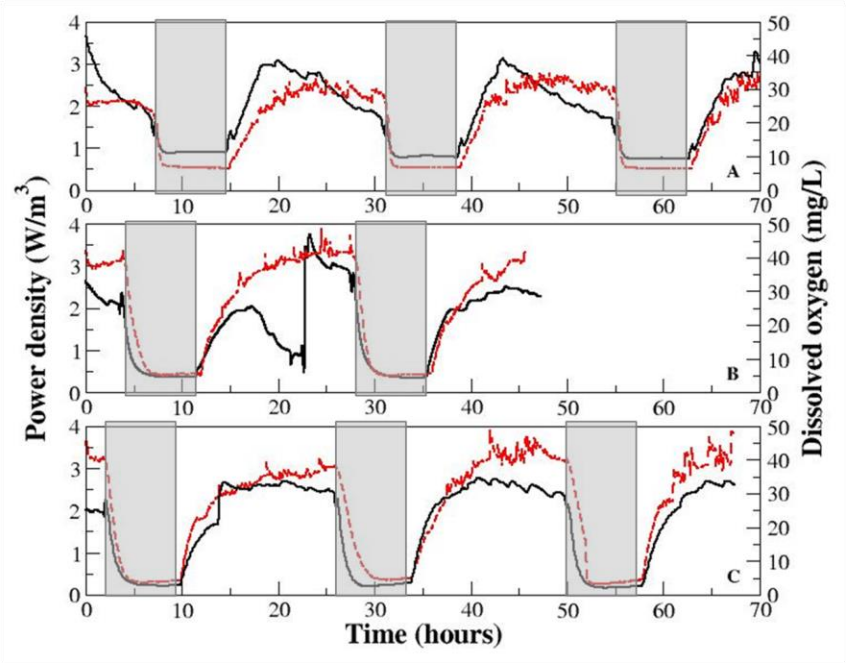

Figure 30. Power density (black solid line) and the DO (red dashed line) during the aeration in the dark at three aeration rates: (A) 100 mL/min, (B) 50 mL/min and (C) 30 mL/min. The shadow indicates the dark period.

Energy balance

Table 7 summarizes energy production and consumption in the IPB system under four different conditions. It must be noted that this is a preliminary analysis and a precise energy analysis is very difficult for a bench-scale system. Energy production consists of two parts, electric energy and biomass energy. Electric energy was calculated according to the power production of the MFC while energy trapped in algal biomass was estimated based on the assumption that biomass contains 20% oil that is converted to biodiesel ($E_{biodiesel}$ is ~37800 MJ/ton) [75][97] and a conversion efficiency of 30% from diesel to electricity. Energy consumption was mainly due to the pumping system (recirculation and feeding) and was estimated according to a previous publication [81] (more details in the

Supporting Information). The energy consumption of mixing was estimated according to a catholyte recirculation rate of 120 mL/min, which was experimentally found to maintain a similar system performance to that with the mechanic mixing. Energy consumption of the intermittent aeration was estimated according to an aeration efficiency of 1.2 kg O_2/kWh [98].

In general, the IPB system could theoretically produce more energy than it consumed, and the intermittent aeration was beneficial with a larger net energy balance through improving both the electricity generation and the algal growth. The electricity produced in the MFC accounted for 14-29% of the energy consumption, depending on the operating condition. The algal biomass provided much more energy than the MFC. Considering that energy consumption during the conversion of algal biomass to biodiesel was not included in Table 7, the actual energy from algal biomass would be less. If the energy production in the MFC can be improved by 5-10 times to 0.06-0.12 kWh/m^3, which may be possible through optimizing configuration and operation, the IPB system will achieve energy neutrality based on the electricity generation alone, with additional economic benefits obtained from the algal biomass. To evaluate the energy benefits of the IPB system, we also need to consider the energy saving. It has been reported that anaerobic treatment of low-strength wastewater consumes much less energy (e.g., 0.058 kWh/m^3 in an anaerobic membrane bioreactor [81]) than activated sludge treatment (~ 0.6 kWh/m^3 [99]). Therefore, the energy saved by omitting the aeration provides additional significance for the application of an IPB system.

Analysis of cathode microbial communities

Because the anode microbial communities have been well documented [100], in this study we focused on the cathode microbes, which are important to comprehend the interaction and the competition between algae and bacteria. A large number of sequences (up to 50% from each sample) were identified as 'chloroplast', derived from organellar DNA extracted from the Chlorophyte algae present in the MFC cathode (*Chlamydomonas reinhardtii* and *Pseudokirchneriella subcapitata*), evident in the SEM images (Figure 31). The presence of *Chlamydomonas reinhardtii* could be from the anode inocula. These were not included in the analysis of bacteria.

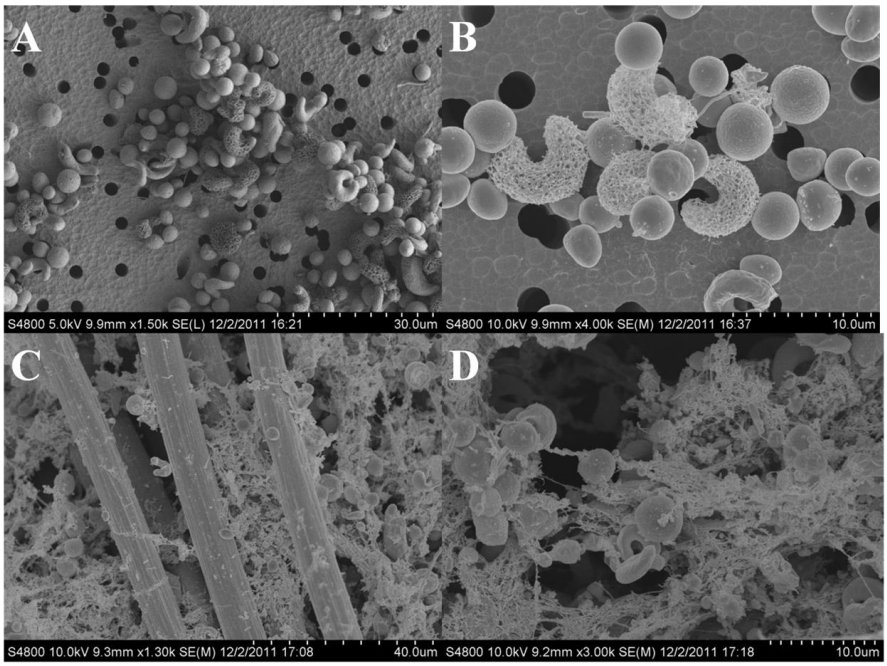

Figure 31. SEM pictures of suspended cells (A and B) collected on filter membrane and biofilm on the cathode electrode (C and D). Note presence of both bacteria and algal cells (spherical *Chlamydomonas reinhardtii* and crescent-shaped *Pseudokirchneriella subcapitata).*

Of the bacteria present in the biofilm on the cathode electrode, and in the catholyte suspension, there were diverse bacterial taxa representing groups typical of aquatic and soil bacterial communities, shown as pooled taxa from each of three replicates in Figure 32. The dominant classes were the alpha-, beta- and gamma-Proteobacteria along with Acidobacteria_Gp3, which together represented between 68 and 90% of bacterial sequences identified in replicate samples. The family Xanthomonadaceae was the dominant family in all samples, with 49 and 26% of total taxa in pooled samples from membrane and suspension communities, respectively, and a mean of triplicate samples from electrodes of 46.0 ± 20.2% and 30.7 ± 5.5% in suspension. This was especially due to sequences identified as *Aquimonas,* which was the most abundant genus in both the electrode (37.5 ± 23.9%) and the suspension communities (28.1 ± 6.6%). Additional BLAST searches using individual sequences did not clarify which species of this genus were present. *Aquimonas* is a common aquatic bacterial genus, with a capacity for nitrate reduction [101], which may be important in inorganic N cycling within the algal-bacterial cathode communities. Also within the Xanthomonadaceae, *Pseudofulvimonas* was also present in both communities (6.7 ± 3.3 in electrode samples, 2.6 ± 0.6 in suspended samples). The next most abundant family in the catholyte suspension was the Rhodobacteraceae, representing 24.4 ± 17.0% of the sequences in the suspended samples but only 1.1 ± 1.9% in the cathode electrode samples. The most common Rhodobacteraceae genus was *Rhodobacter,* which was abundant (17.1 ± 12.5%) in the catholyte suspension but rare in the cathode electrode community (<1% of total sequences). Additional BLAST searches suggested possibly *R. changlensis*, a non-motile purple non-sulfur bacterium which, like other *Rhodobacter* species, can be photosynthetic

[102]. Another Rhodobacteraceae genus, *Pannonibacter*, was also well represented (3.8 ± 3.3 %) in suspension but was absent from the cathode electrode. The Acidobacteria_gp3 unclassified family was the second most abundant in the electrode community comprising 13.5 ± 9.5% of the sequences but only 4.6 ± 2.3% of the sequences identified in the catholyte suspension samples. Comamonadaceae was the third most abundant bacterial family in the catholyte suspension communities (12.3 ± 6.9% of total) and the fourth most common in the communities on the electrode (5.1 ± 1.9 %). This family was dominated by the genus *Hydrogenophaga*, found in both the suspension and the cathode electrode, and known to be a common aquatic and soil bacterium capable of H-oxidation [103]. The common soil bacterial genus *Brevundimonas* (Caulobacteraceae) was identified in both the electrode (4.6 ± 3.9%) and the suspension (3.5 ± 1.6) samples. *Brevundimonas* species have been demonstrated to perform enhanced biological phosphorus removal from wastewater [104] and provide biomass for removal of heavy metals from wastewater [105].

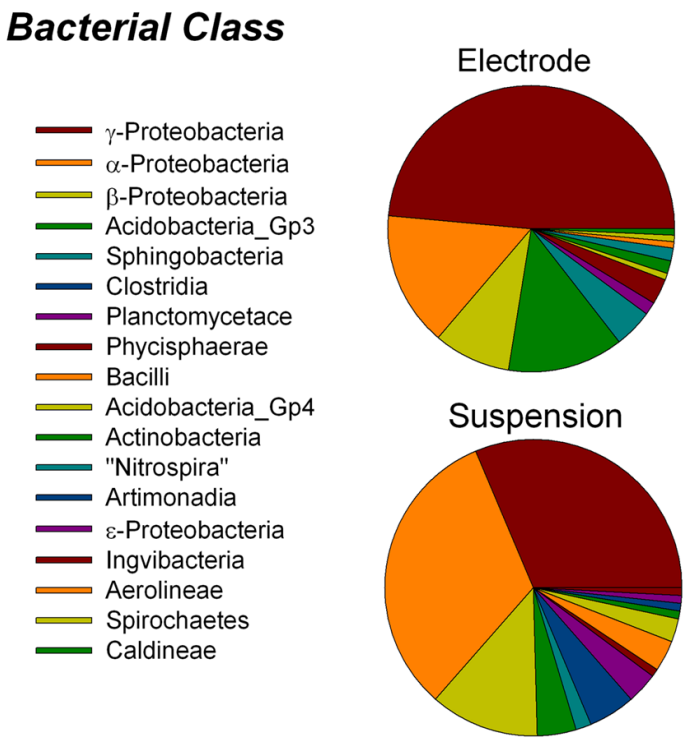

Figure 32. Distribution of bacterial classes between electrode and suspension communities. Taxa were identified from analysis of partial rRNA gene sequences from clone libraries of generated from DNA extracted from samples collected from each community. Results shown are total sequences for 3 replicate libraries from each community.

An amino-acid utilizing anaerobic bacterium, *Anaeromusa*, and other anaerobes of the class Clostridia (genus *Proteiniclasticum*) were found in suspension samples, but not in the electrode community. This was despite obviously aerobic conditions present due to algal photosynthesis. However, daily excursions into low oxygen conditions (Figure 26) during the dark phase may have promoted the survival of this bacterium.

Aside from the abundant *Aquimonas*, which could have been involved in the reduction of nitrate to nitrite, other key taxa known to be involved in the nitrogen transformations

were identified. *Nitrosomonas* (1.4% of sequences in the electrode samples) can oxidize ammonium to nitrite; *N. europaea* is known to degrade a variety of organic compounds pollutants [106]. *Nitrospira*, also 1.4% of sequences in the electrode samples, could have been oxidizing nitrite to nitrate. Sequences identified as *Mesorhizobium*, a gram-negative soil bacterium, were found in the suspension samples and could indicate the presence of a diazotrophic species; however, high fixed nitrogen concentrations were maintained in the catholyte (e.g., up to 20-30 mg NO_3^--N /L), so fixation of N_2 in the cathode would have been unlikely.

Despite the reported abundance of Firmicutes and Bacteroidetes in the sewerage water from South Shore treatment plant [107], which was the source of sludge as inoculum for the anode, these phyla were not well represented in the cathode electrode and the suspension communities. Firmicutes were absent from the electrode samples and were only 9.4% of the sequences identified in the suspension communities (comprising Classes Clostridia 5.1% and Bacilli 4.3% of the total suspension sample sequences). This result compares with 76% of the suspension sequences as phylum Proteobacteria. Bacteriodetes were represented as 6.9% of the sequences in the electrode communities but only 2 sequences in one sample of the suspension community (1.7% of total). Of the Bacteriodetes, Chitinophagaceae and Sphingomondaceae were the identified families; Sphingomonodaceae was absent from the suspension samples. The low relative abundance of Firmicutes and Bacteriodetes, which are commonly found in MFC anodes [108][109][110], likely resulted from the aerobic condition and the low organic contents in the cathode.

The combined algal and bacterial metabolic activities in the IPB system provide conditions that promote shifts in abundance of the different bacterial taxa. Our future studies will better understand the (cathode) bacterial functions in correlation with the IPB performance (e.g., nutrient removal and algal growth).

4.2 Integrated photo-bioelectrochemical system affected by algal sources

4.2.1 Introduction

Freshwater, essential substrate to all life on earth, is critical to human health and the prosperity of society. However, pollutants and waste due to industrial development and overpopulation are becoming serious threats to global freshwater resources and aquatic ecosystems. Consequently, a number of wastewater treatment technologies have been developed in the past several decades, but most require a considerable energy input. However the wastewater contains organic matter and some nutrients, so it is also a potential energy source [99]. The aim of sustainable wastewater treatment is to not only clean up the polluted water, but also recover energy from contaminants, thereby offsetting energy consumption.

Recently, microbial fuel cells (MFCs) have drawn much attention as a novel technology for extracting useful energy from wastewater. MFCs are bio-electrochemical reactors in

which bacteria oxidize organic compounds in the anode chamber and generate protons and electrons that are transported to the cathode to reduce oxygen to water [111]. Electron flow from the anode to the cathode generates an electric current or power if a load is connected [112]. The power output in lab-scale MFCs has improved significantly from several W m^{-3} to more than 1 kW m^{-3} [91]. It has been observed that electricity-generating processes in MFCs can stimulate the oxidation of organic matter and achieve higher organic removal [33]. Nutrient removal by MFCs focuses on removing nitrate to N_2 gas through a denitrifying cathode, therefore, ammonium present in fuel must be oxidized to nitrate either in a separate nitrification reactor or in the cathode with a strictly controlled aeration [113][67]. Transformations of phosphorus, on the other hand, have not been investigated in MFCs.

Fortunately, current studies on algae provide a complementary tool to MFCs in removing nutrients from wastewater. Algal treatment of wastewater has a long history, especially in removing nutrients, and both open-flow systems and closed bioreactors have been used [68]. Algal bioreactors are typically based on algae using photosynthesis to fix carbon dioxide into organic compounds to fuel biomass growth. During algal growth, concentrations of dissolved nutrients, nitrogen (N) and phosphorus (P), are drawn down by algal uptake. Microalgae can assimilate significant amounts of nutrients because of high N and P demand for synthesis of proteins (45-60% of microalgae dry weight), nucleic acids, phospholipids, and other cellular constituents [74]. The algal biomass produced from bioreactors can also be used for producing biofuels, including biodiesel [114][76].

In 2008, Strik and coworkers combined an algal bioreactor with an MFC and called it a photosynthetic algal microbial fuel cell (PAMFC) [77]. In their system, algae only grew in the bioreactor and were fed as the substrate to the anode of MFCs. Two years later, Wang and coworkers set up a microbial carbon capture cell (MCC), in which *Chlorella vulgaris* was used to capture CO_2 and produce O_2 for the cathode of MFCs [115]. This indicated that algae can grow in the cathode of MFCs and provide oxygen for the cathodic reaction. Based on this idea, Zhang and coworkers used algae in the cathode of a sediment MFC without a membrane, and algae directly used the CO_2 produced by the anode [116]. In their photomicrobial fuel cell (PFC), algae was not only used to capture CO_2 and produce O_2, but also to remove the nutrients from the wastewater [116].

Our previous work developed an integrated photo-bioelectrochemical (IPB) system to synergistically link an MFC with an algal bioreactor for wastewater treatment and bioenergy production [117]. During the one-year operation, the IPB system removed more than 92% of organics, 98% of ammonium nitrogen and 82% of phosphate in synthetic wastewater solution, and produced a maximum power density of 2.2 W m^{-3} and 128 mg L^{-1} of algal biomass. However, the system also produced 19.3 mg L^{-1} nitrate nitrogen, which was unexpected and the electricity energy was still very low. Moreover, although the algal and bacterial composition of the biofilm attached on the cathode electrode and planktonic cells in the cathode compartment was analyzed, The interactions algae and bacteria and their effects on the performance of IPB system were still unclear. So in this study, small-diameter tubular MFC with an anion exchange membrane was set up in the IPB system to improve the electricity generation and three different algal

sources were tested in the IPB system in order to better understand the interactions of algae and bacteria in the IPB system.

4.2.2 Materials and methods

IPB system setup

The IPB system consisted of a single-chamber tubular MFC installed in a glass beaker, which functioned as both the cathode compartment and the algal bioreactor as described previously [117]. The MFC was constructed with an anion exchange membrane tube (AEM, Ultrex CMI7000, Membranes International, Inc., Glen Rock, NJ) containing an interior supporter of a polyvinyl chloride (PVC) tube with a diameter of 2.54 cm and a height of 24 cm, resulting in an anode liquid volume of about 180 mL. A 20 cm-long carbon brush (Gordon Brush Mfg. Co., Inc., Commerce, CA) was used as the anode electrode. The carbon brush electrode was pretreated by immersing in acetone overnight and heated to 450 ℃ for 30 min. The cathode electrode was a layer of carbon cloth with Pt/C as the catalyst that wrapped the AEM tube. To coat the Pt catalyst to the cathode electrode, Pt/C powder was mixed with Nafion solution, and then applied to the carbon cloth surface with a brush to a final loading rate of ~ 0.5 mg Pt cm^{-2}. The anode and cathode electrodes were connected by copper wires to an external circuit across a 100 Ω resistance. The glass beaker that held the MFC had a diameter of 10 cm and height of 29 cm, with a liquid volume of 1800 mL. A compact fluorescent bulb (32 W, 120 V, Energy Wiser, color temperature 4000 K, Bulbrute Industries, Inc., China) was installed nearby the cathode to provide the light on a 16-h on/8-h off cycle.

Operating conditions

The IPB system was continuously operated with a synthetic solution at about 20 ℃. The anode compartment was inoculated with the anaerobic sludge from a local municipal wastewater treatment plant (South Shore, Milwaukee, WI, USA). The cathode compartment was initially inoculated with algal and bacteria mixed solutions from different sources: Sherwood #2 for stage I, Francisville #3 for stage II and WWExp for stage III. The synthetic solution contained (per L of tap water): sodium acetate, 0.35 g; NH_4Cl, 0.2 g; NaCl, 0.5 g; $MgSO_4$, 0.015 g; $CaCl_2$, 0.02 g; $NaHCO_3$, 2.6 g; KH_2PO_4, 0.027 g and 1 mL L^{-1} trace elements [35]. This solution was fed into the anode of the MFC at a flow rate of 0.4 mL min^{-1} (with an anolyte recirculation rate of 30 mL min^{-1}), resulting in a hydraulic retention time (HRT) of 7.5 hours and an organic loading rate of 0.87 kg COD/m^3/d in the anode compartment. The effluent of the anode flowed into a 200 mL beaker and then directly pumped into the cathode of the MFC at the same flow rate of the anode feeding. The catholyte was mixed by a magnetic stirrer.

Measurement and analysis

The cell voltage was recorded every 5 min by a digital multimeter (2700, Keithley Instruments, Inc., Cleveland, OH, USA). The concentrations of soluble COD, ammonium nitrogen, nitrite nitrogen, nitrate nitrogen, and phosphate were measured according to the manufacturer's instructions using a DR/890 datalogging colorimeter (Hach Company, Loveland, CO, USA). The pH, temperature, and dissolved oxygen (DO) were measured using a 556 MPS hand-held multiparameter instrument (YSI Incorporated, Yellow Spring,

OH, USA). The concentration of algal mass was measured as absorbance at 680 nm in an 1100 spectrophotometer (Unico, Dayton, NJ, USA) and converted to biomass as our previous study [117]. According to our previous study [117], power density and current density was based on the anode liquid volume, and the normalized energy recovery (NER) was based on the volume of treated water.

4.2.3 Results and discussion

Performance of IPB system with Sherwood #2 algal source

Compared to our previous study, the IPB system produced much higher power density (8.44 ± 0.20 W m^{-3} under the light showed in Figure 33A), which was about four times as much as that in our previous study [117]. And the NER of the electricity (0.055 ± 0.001 kWh m^{-3}) was also much higher than the previous study (0.012 kWh m^{-3}). This means the new configuration of the MFC reactor successfully improved the electricity performance of the IPB system. The small diameter shortens the distance between the anode electrode and cathode electrode, which can significantly improve the performance of the MFC [24]. It is worth noting that the power density without the light was still very high, about 5 W m^{-3}, which was more than half of the power density under the light. Compared to the previous IPB system [117], a little taller tubular MFC, which has larger cathode area above the water level, can help absorb more oxygen to participate in the cathode reaction without additional oxygen supply.

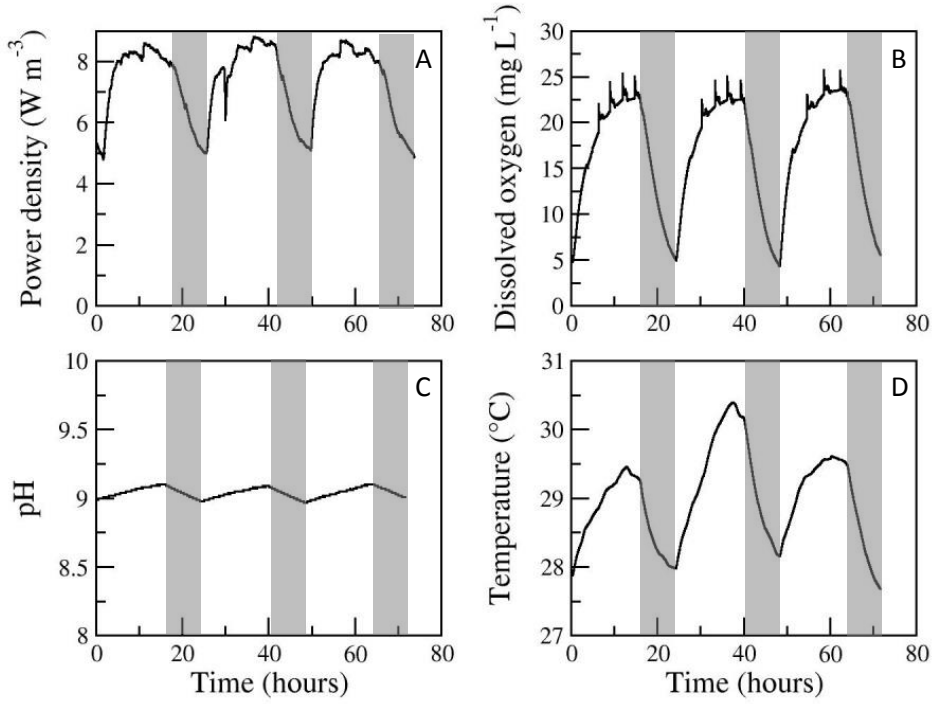

Figure 33. The performance and operating parameters of the IPB system in stage I.

The dissolved oxygen (DO) was above 20 mg L^{-1} under the light, which was similar to the previous study [117]. However, we found that the DO was not exhausted during the dark time and the lowest DO concentration was about 5 mg L^{-1} (Figure 33B). This means that the sum of the amount of DO left in the cathode part when the light was shut down and the amount of the absorbed oxygen from the environment during the dark was larger than the total DO demand for the respiration of algae and the cathode reaction of the MFC, which may be because the low biomass concentration (53.3±8.9 mg L^{-1}) in the cathode part reduced the DO consumption and the cathode electrode above the water level increased the oxygen absorption. The pH showed very little difference between the

condition under the light and that under the dark (Figure 33C), due to the small difference of cathode reaction rates (shown as the magnitude of the power density) under these two conditions. The temperature fluctuated slightly because of not very constant room temperature and some additional heat provided by the light (Figure 33D).

The IPB system can efficiently remove the organics and nutrients which have been proved in the previous study [117]. Table 8 showed that about 91.0% of COD was removed by the anode part of the MFC, while some COD was produced in or transferred from the anode to the cathode part. There was not any ammonia in the cathode effluent, which meant that 100% of ammonia nitrogen was removed by the IPB system. There was 0.2 mg L^{-1} nitrate nitrogen detected in the anode effluent and 12.9 mg L^{-1} nitrate nitrogen in the cathode part, which showed that some nitrate produced in the cathode part was transferred to the anode part through the AEM. And the denitrified bacteria in the anode chamber can take up the nitrate under the anaerobic condition, so the nitrate concentration in the anode effluent was very low. Compared to the MFC with CEM used in the previous study, AEM significant decreased the nitrate concentration in the final effluent. However, very little phosphate was removed by this IPB and the concentration of PO_4^{3-}-P in the final effluent was still very high (4.4 mg L^{-1}).

Table 8. Characteristics of the synthetic solution when flowing through the IPB system; the error term is standard deviation.

		COD (mg L^{-1})	NH_4^+-N (mg L^{-1})	NO_3^--N (mg L^{-1})	PO_4^{3-}-P (mg L^{-1})	Biomass (mg L^{-1})
Anode influent		266.7	52.3	N/D	6.2	N/A
Stage I	Anode effluent	24.0 ±8.1	44.3 ±2.0	0.2 ±0.2	5.5 ±0.5	N/A
	Cathode effluent	32.5 ±8.5	N/D	12.9 ±0.6	4.4 ±0.4	53.3 ±8.9
Stage II	Anode effluent	22.7 ±4.0	42.3 ±1.2	0.1 ±0.1	5.8 ±0.9	N/A
	Cathode effluent	39.0 ±7.7	N/D	5.9 ±1.8	3.5 ±0.9	5.9 ±1.2

Performance of IPB system with Francisville #3 algal source

The power density produced by the IPB system in stage II was 8.70 ±0.17 W m^{-3} under the light condition and the NER was 0.061 ±0.001 kWh m^{-3}, a little higher than that in stage I (Figure 34A). This means that the electricity generation of the IPB system was still limited by the cathode compartment and Francisville #3 algal source could help the MFC produce more electricity compared to Sherwood #2 algal source. A significant difference between Francisville #3 and Sherwood #2 algal sources was that there was very little suspended biomass in the cathode compartment (5.9 ±1.2 mg L^{-1}) for Francisville #3. It proved that the algae attached on the cathode electrode made the main contribution to the electricity generation in the IPB system, while the suspended algae in the cathode solution played a minor role.

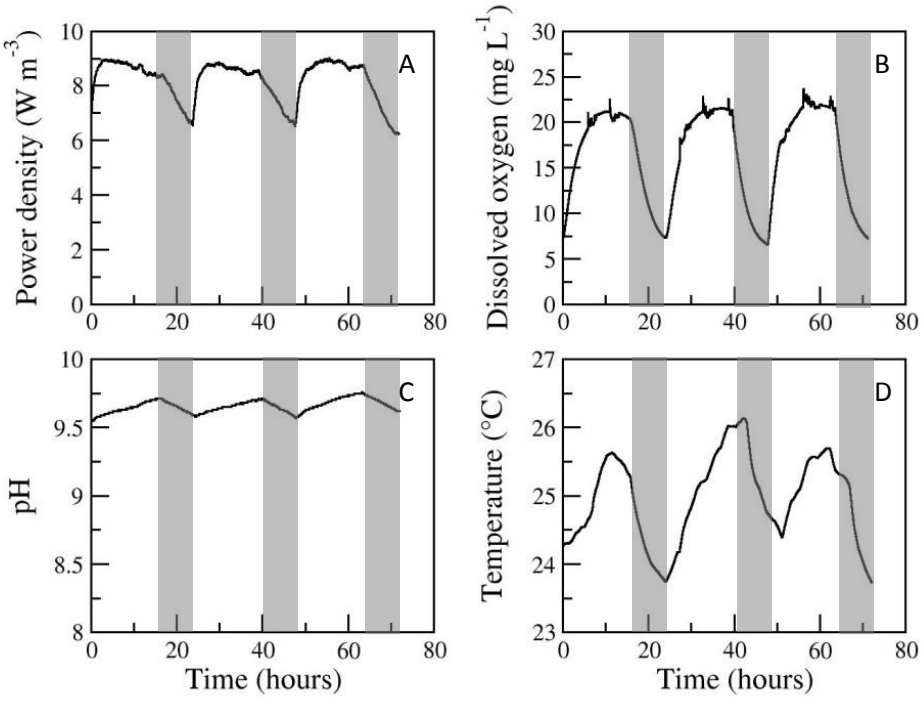

Figure 34. The performance and operating parameters of the IPB system in stage II.

The DO concentration in stage II was a little lower than that in stage I (Figure 34B), probably because of the lower concentration of suspended algae and a little higher cathode reaction rate. Because the power density was higher under the light in stage II than that in stage I and the cathode reaction consumed protons, the pH (around 9.7) of the cathode solution was also a little higher than that in stage I. Note that, compared to stage I in August, the temperature in stage II was lower simply because the room temperature was lower in stage II at the end of September.

Similar to stage I, most of organics (91.5%) was removed by the MFC and the COD concentration in the cathode effluent was a little higher than that in the anode effluent

(Table 8). 100% NH_4^+-N was removed by the system, while only 43.5% of PO_4^{3-}-P was removed. Therefore, the algae from Francisville #3 were not good at taking up the phosphate either. In the final effluent, the nitrate nitrogen concentration was only 5.9 mg L^{-1} (Table 8), much lower than that in stage I and the previous study.

4.2.4 Future Work

Algae from WWExp will be tested in the IPB system during the stage III experiment. The community analysis will be performed on the algae and bacteria in the cathode compartment. The morphology of microorganisms will be observed by scanning electron microscopy (SEM).

5 Perspective

During my Ph.D. study, a lot of effort was made to improve the energy performance of bioelectrochemical systems (BES), and a new system was developed to integrate the algal technology and MFCs, which was called integrated photo-bioelectrochemical (IPB) system. However, it still has a long way to go to realize the application of the IPB system at large scales.

Firstly, the electricity generated from the system is still low. Although the power density higher than 1 kW m^{-3} has been achieved with a very small-scale MFC (2.5 mL) by Liu and coworkers [91], the electrical energy generated from it was very low. And it is known that the large-scale MFCs generally have low power output [34]. The maximum power density of the IPB system in section 4.1 was about 3 W m^{-3} and the maximum NER_V was 0.021 kWh m^{-3}, which was still far from the application. The energy balance showed that the electricity generation could not even cover the energy needed for the operation of the IPB system. So more research is needed for improving the electricity generation from IPB systems. New reactors and experiments need to be designed to produce more electricity. For example, the use of spiral spacers to create a helical flow which can improve electricity generation in MFCs was approved in the work of Zhang et al. [34]. The electrode material is also an area to study where significant improvements can be achieved.

Secondly, for applications, large-scale IPB system needs to be set up and real wastewater needs to be tested in the IPB system. The wastewater flow rate of the IPB system showed in section 4 is only 0.4 mL min^{-1}, which is far below actual wastewater flow in

wastewater treatment plants. The size of current system does not have enough capacity for high wastewater flow rate, so developing large-scale reactor is the only way for the application of IPB systems. However, there are some challenges during the scaling up, such as how well the materials perform at large scale and their longevity. Only artificial wastewater was tested in our studies on IPB systems, which is much simpler than real wastewater. The real wastewater contains various types of wastes and communities, which may affect the performance of IPB systems.

Thirdly, in IPB systems, algal activities determine the removal of nutrients, biomass production and DO supply to the cathode reaction of the MFC. However, algae inevitably contact with large amount of bacteria coming from anode effluent and surrounding environment, so characterizing how algae and bacteria interact is essential for optimizing the IPB system. And an efficient separation method also needs to be developed to harvest the biomass from the IPB system. From the results in section 4.1, we noticed that the main energy obtained from the IPB system was the biomass, which was 80-88% of total energy output. However, the energy balance shown in section 4.1 did not include the energy consumption during the separation of the biomass from the water. This process has several high energy-demanding solutions such as centrifuging. So developing a low-cost and low-energy-consumption separation technology is a big challenge for the application of IPB systems.

Lastly, the materials used in the IPB system are still expensive. Platinum, as an expensive metal, is used as the catalyst on the cathode electrode of the IPB system. Nafion, the price of which is about 2 to 3 dollars per milliliter, is used as the binder. Compared to other carbon electrodes, such as carbon cloth, carbon brush is also relatively expensive. So

cheap but efficient catalysts for oxygen reduction need to be tested in the IPB system. Other cheap binders, such as polytetrafluoroethylene (PTFE), can be used to replace Nafion. We also need to consider the energy cost of operation. In our study of IPB system in section 4.1, the main energy cost came from mixing. Seeking a low energy cost mixing method is also a big challenge.

References

[1] K. Bilen, O. Ozyurt, K. Bakirci, S. Karsli, S. Erdogan, M. Yilmaz, et al., Energy production, consumption, and environmental pollution for sustainable development: A case study in Turkey, Renew. Sustain. Energy Rev. 12 (2008) 1529–1561.

[2] P. Weisz, Basic choices and constraints on long-term energy supplies, Phys. Today. (2004) 47–52.

[3] EIA, International Energy Outlook 2008, U.S. Energy Inf. Adm. (2008).

[4] D. Pant, A. Singh, G. Van Bogaert, S. Irving Olsen, P. Singh Nigam, L. Diels, et al., Bioelectrochemical systems (BES) for sustainable energy production and product recovery from organic wastes and industrial wastewaters, RSC Adv. 2 (2012) 1248.

[5] EIA, Monthly Energy Review, U.S. Energy Inf. Adm. (2013).

[6] Z. Du, H. Li, T. Gu, A state of the art review on microbial fuel cells : A promising technology for wastewater treatment and bioenergy, Biotechnol. Adv. 25 (2007) 464–482.

[7] M.C. Potter, Electrical Effects Accompanying the decomposition of organic compounds, Proc. R. Soc. London. 84 (1911) 260–276.

[8] H.B. Kim, H.J. Kim, M.S. Hyun, D.H. Park, Direct electrode reaction of Fe(III)-reducing bacterium, shewanella putrefaciens, J. Microbiol. Biotechnol. 9 (1999) 127–131.

[9] B.H. Kim, D.H. Park, P.K. Shin, I.S. Chang, H.J. Kim, Mediatoe-less biofuel cell, U.S. Patent 5976719, 1999.

[10] B.E. Logan, Microbial fuel cells, Hoboken, John Wiley & Sons, Inc., 2008.

[11] H. Liu, R. Ramnarayanan, B.E. Logan, Production of electricity during wastewater treatment using a single chamber microbial fuel cell, Environ. Sci. Technol. 38 (2004) 2281–2285.

[12] B.E. Logan, B. Hamelers, R. Rozendal, U. Schröder, J. Keller, S. Freguia, et al., Microbial fuel cells: methodology and technology, Environ. Sci. Technol. 40 (2006) 5181–5192.

[13] B. Logan, S. Cheng, V. Watson, G. Estadt, Graphite Fiber Brush Anodes for Increased Power Production in Air-Cathode Microbial Fuel Cells, Environ. Sci. Technol. 41 (2007) 3341–3346.

[14] Y. Qiao, C. Li, S. Bao, Q. Bao, Carbon nanotube/polyaniline composit as anode material for microbial fuel cells, J. Power Sources. 179 (2007) 79–84.

[15] Y. Qiao, S. Bao, C. Li, X. Cui, Z. Lu, J. Guo, Nanostructured polyaniline/titanium dioxide composite anode for microbial fuel cells, ACS Nano. 2 (2007) 113–119.

[16] L. Mao, D. Zhang, T. Sotomura, K. Nakatsu, N. Koshiba, T. Ohsaka, Mechanistic study of the reduction of oxygen in air electrode with manganese oxides as electrocatalysts, Electrochim. Acta. 48 (2003) 1015–1021.

[17] B.H. Kim, I.S. Chang, G.M. Gadd, Challenges in microbial fuel cell development and operation, Appl. Microbiol. Biotechnol. 76 (2007) 485–494.

[18] A. Ter Heijne, H.V.M. Hamelers, V. De Wilde, R. a Rozendal, C.J.N. Buisman, A bipolar membrane combined with ferric iron reduction as an efficient cathode system in microbial fuel cells, Environ. Sci. Technol. 40 (2006) 5200–5205.

[19] F. Zhang, K. Brastad, Z. He, Integrating forward osmosis into microbial fuel cells for wastewater treatment, water extraction and bioelectricity generation, Environ. Sci. Technol. 45 (2011) 6690–6696.

[20] D. Pant, G. Van Bogaert, L. Diels, K. Vanbroekhoven, A review of the substrates used in microbial fuel cells (MFCs) for sustainable energy production, Bioresour. Technol. 101 (2010) 1533–1543.

[21] Z. Ge, J. Li, L. Xiao, Y. Tong, Z. He, Recovery of Electrical Energy in Microbial Fuel Cells: a Brief Review, Environ. Sci. Technol. Lett. (2013).

[22] A.P. Borole, G. Reguera, B. Ringeisen, Z.-W. Wang, Y. Feng, B.H. Kim, Electroactive biofilms: Current status and future research needs, Energy Environ. Sci. 4 (2011) 4813.

[23] B.C. Jong, B.H. Kim, I.S. Chang, P.W.Y. Liew, Y.F. Choo, G.S. Kang, Enrichment, performance, and microbial diversity of a thermophilic mediatorless microbial fuel cell, Environ. Sci. Technol. 40 (2006) 6449–6454.

[24] H. Liu, S. Cheng, B. Logan, Power generation in fed-batch microbial fuel cells as a function of ionic strength, temperature, and reactor configuration, Environ. Sci. Technol. 39 (2005) 5488–5493.

[25] H. Moon, I. Chang, B. Kim, Continuous electricity production from artificial wastewater using a mediator-less microbial fuel cell, Bioresour. Technol. 97 (2006) 621–627.

[26] B.E. Logan, D. Call, S. Cheng, H.V.M. Hamelers, T.H.J. a. Sleutels, A.W. Jeremiasse, et al., Microbial Electrolysis Cells for High Yield Hydrogen Gas Production from Organic Matter, Environ. Sci. Technol. 42 (2008) 8630–8640.

[27] B. Logan, K. Rabaey, Conversion of wastes into bioelectricity and chemicals by using microbial electrochemical technologies, Science 337 (2012) 686-690.

[28] B.E. Logan, Scaling up microbial fuel cells and other bioelectrochemical systems, Appl. Microbiol. Biotechnol. 85 (2010) 1665–1671.

[29] H. Wang, J. Park, Z. Ren, Active Energy Harvesting from Microbial Fuel Cells at the Maximum Power Point without Using Resistors, Environ. Sci. Technol. 46 (2012) 5247–5252.

[30] Z. Ge, Q. Ping, L. Xiao, Z. He, Reducing effluent discharge and recovering bioenergy in an osmotic microbial fuel cell treating domestic wastewater, Desalination 312 (2013) 52–59.

[31] Z. He, Mincrobial Fuel Cells: Now Let us Talk about Energy, Environ. Sci. Technol. 47 (2013) 332–333.

[32] A.K. Plappally, J.H. Lienhard, Energy Requiements for Water Production, Treatment, End Use, Reclamation, and Disposal, Renew. Sustain. Energy Rev. 16 (2012) 4818–4848.

[33] F. Zhang, K.S. Jacobson, P. Torres, Z. He, Effects of anolyte recirculation rates and catholytes on electricity generation in a litre-scale upflow microbial fuel cell, Energy Environ. Sci. 3 (2010) 1347.

[34] F. Zhang, Z. Ge, J. Grimaud, J. Hurst, Z. He, Improving Electricity Production in Tubular Microbial Fuel Cells through Optimizing the Anolyte Flow with Spiral Spacers, Bioresour. Technol. 134 (2013) 251–256.

[35] Z. He, S.D. Minteer, L.T. Angenent, Electricity generation from artificial wastewater using an upflow microbial fuel cell, Environ. Sci. Technol. 39 (2005) 5262–5267.

[36] Z. Ge, F. Zhang, J. Grimaud, J. Hurst, Z. He, Long-term investigation of microbial fuel cells treating primary sludge or digested sludge, Bioresour. Technol. 136 (2013) 509–514.

[37] L.T. Angenent, K. Karim, M.H. Al-Dahhan, B.A. Wrenn, R. Dom ́guez-Espinosa, Production of bioenergy and biochemicals from industrial and agricultural wastewater., Trends Biotechnol. 22 (2004) 477–485.

[38] L. Fu, S.-J. You, G.-Q. Zhang, F.-L. Yang, X.-H. Fang, PB/PANI-modified Electrode Used as a Novel Oxygen- Reduction Cathode in Microbial Fuel Cell, Biosens. Bioelectron. 26 (2011) 1975–1979.

[39] M. Zhou, M. Chi, J. Luo, H. He, T. Jin, An overview of electrode materials in microbial fuel cells, J. Power Sources. 196 (2011) 4427–4435.

[40] X. Xie, M. Ye, L. Hu, N. Liu, J.R. McDonough, W. Chen, et al., Carbon Nanotube-coated Macroporous Sponge for Microbial Fuel Cell Electrodes, Energy Environ. Sci. 5 (2012) 5265–5270.

[41] C. Feng, L. Ma, F. Li, H. Mai, X. Lang, S. Fan, A polypyrrole/anthraquinone-2,6-disulphonic disodium salt (PPy/AQDS)-modified anode to improve performance of microbial fuel cells, Biosens. Bioelectron. 25 (2010) 1516–1520.

[42] H.-Y. Tsai, C.-C. Wu, C.-Y. Lee, E.P. Shih, Microbial fuel cell performance of multiwall carbon nanotubes on carbon cloth as electrodes, J. Power Sources. 194 (2009) 199–205.

[43] H. Wang, Z. Wu, A. Plaseied, P. Jenkins, L. Simpson, C. Engtrakul, et al., Carbon nanotube modified air-cathodes for electricity production in microbial fuel cells, J. Power Sources. 196 (2011) 7465–7469.

[44] A.K. Geim, K.S. Novoselov, The rise of graphene., Nat. Mater. 6 (2007) 183–191.

[45] K.S. Novoselov, A.K. Geim, S. V Morozov, D. Jiang, Y. Zhang, S. V Dubonos, et al., Electric field effect in atomically thin carbon films, Science. 306 (2004) 666–669.

[46] M. Pumera, Electrochemistry of graphene: new horizons for sensing and energy storage, Chem. Rec. 9 (2009) 211–223.

[47] S.-M. Paek, E. Yoo, I. Honma, Enhanced cyclic performance and lithium storage capacity of SnO2/graphene nanoporous electrodes with three-dimensionally delaminated flexible structure, Nano Lett. 9 (2009) 72–75.

[48] X. Wang, L. Zhi, K. Müllen, Transparent, conductive graphene electrodes for dye-sensitized solar cells, Nano Lett. 8 (2008) 323–327.

[49] L.L. Zhang, R. Zhou, X.S. Zhao, Graphene-based materials as supercapacitor electrodes, J. Mater. Chem. 20 (2010) 5983–5992.

[50] Y. Zhang, G. Mo, X. Li, W. Zhang, J. Zhang, J. Ye, et al., A graphene modified anode to improve the performance of microbial fuel cells, J. Power Sources. 196 (2011) 5402–5407.

[51] Y.-X. Huang, X.-W. Liu, J.-F. Xie, G.-P. Sheng, G.-Y. Wang, Y.-Y. Zhang, et al., Graphene oxide nanoribbons greatly enhance extracellular electron transfer in bio-electrochemical systems, Chem. Commun. (Camb). 47 (2011) 5795–5797.

[52] F. Kim, J. Luo, R. Cruz-Silva, L.J. Cote, K. Sohn, J. Huang, Self-Propagating Domino-like Reactions in Oxidized Graphite, Adv. Funct. Mater. 20 (2010) 2867–2873.

[53] D. Li, R.B. Kaner, Graphene-Based Material, Science 320 (2008) 1170–1171.

[54] J. Luo, H.D. Jang, T. Sun, L. Xiao, Z. He, A.P. Katsoulidis, et al., Compression and aggregation-resistant particles of crumpled soft sheets., ACS Nano. 5 (2011) 8943–8949.

[55] Z. He, N. Wagner, S.D. Minteer, L.T. Angenent, An upflow microbial fuel cell with an interior cathode: assessment of the internal resistance by impedance spectroscopy., Environ. Sci. Technol. 40 (2006) 5212–5217.

[56] M. Sun, F. Zhang, Z.-H. Tong, G.-P. Sheng, Y.-Z. Chen, Y. Zhao, et al., A gold-sputtered carbon paper as an anode for improved electricity generation from a microbial fuel cell inoculated with Shewanella oneidensis MR-1., Biosens. Bioelectron. 26 (2010) 338–343.

[57] J. Wu, Y. Wang, D. Zhang, B. Hou, Studies on the electrochemical reduction of oxygen catalyzed by reduced graphene sheets in neutral media, J. Power Sources. 196 (2011) 1141–1144.

[58] H. Liu, S. Grot, B.E. Logan, Electrochemically assisted microbial production of hydrogen from acetate, Environ. Sci. Technol. 39 (2005) 4317–4320.

[59] H. Liu, H. Hu, J. Chignell, Microbial electrolysis: novel technology for hydrogen production from biomass, Biofuels. 1 (2010) 129–142.

[60] R.D. Cusick, B. Bryan, D.S. Parker, M.D. Merrill, M. Mehanna, P.D. Kiely, et al., Performance of a pilot-scale continuous flow microbial electrolysis cell fed winery wastewater., Appl. Microbiol. Biotechnol. 89 (2011) 2053–2063.

[61] S. Cheng, B. Logan, Evaluation of catalysts and membranes for high yield biohydrogen production via electrohydrogenesis in microbial electrolysis cells (MECs), Water Sci. Technol. 58 (2008) 853–858.

[62] P.A. Selembo, M.D. Merrill, B.E. Logan, The use of stainless steel and nickel alloys as low-cost cathodes in microbial electrolysis cells, J. Power Sources. 190 (2009) 271–278.

[63] H. Hu, Y. Fan, H. Liu, Hydrogen production in single-chamber tubular microbial electrolysis cells using non-precious-metal catalysts, Int. J. Hydrogen Energy. 34 (2009) 8535–8542.

[64] L. Wang, Y. Chen, Y. Ye, B. Lu, S. Zhu, S. Shen, Evaluation of low-cost cathode catalysts for high yield biohydrogen production in microbial electrolysis cell, Water Sci. Technol. 63 (2011) 440–448.

[65] Z. Wen, S. Ci, F. Zhang, X. Feng, S. Cui, S. Mao, et al., Nitrogen-Enriched Core-Shell Structured Fe/Fe(3)C-C Nanorods as Advanced Electrocatalysts for Oxygen Reduction Reaction, Adv. Mater. 24 (2012) 1399–1404.

[66] B.E. Logan, Exoelectrogenic bacteria that power microbial fuel cells, Nat. Rev. Microbiol. 7 (2009) 375–381.

[67] B. Virdis, K. Rabaey, R. a Rozendal, Z. Yuan, J. Keller, Simultaneous nitrification, denitrification and carbon removal in microbial fuel cells, Water Res. 44 (2010) 2970–2980.

[68] J.P. Hoffmann, Wastewater treatment with suspended and nonsuspended algae, J. Phycol. 34 (1998) 757–763.

[69] P. Clauwaert, K. Rabaey, P. Aelterman, L. de Schamphelaire, T.H. Pham, P. Boeckx, et al., Biological denitrification in microbial fuel cells., Environ. Sci. Technol. 41 (2007) 3354–3360.

[70] F. Zhang, Z. He, Simultaneous nitrification and denitrification with electricity generation in dual-cathode microbial fuel cells, J. Chem. Technol. Biotechnol. 87 (2012) 153–159.

[71] R.D. Cusick, B.E. Logan, Phosphate recovery as struvite within a single chamber microbial electrolysis cell, Bioresour. Technol. 107 (2012) 110–115.

[72] P. Kuntke, K.M. Smiech, H. Bruning, G. Zeeman, M. Saakes, T.H.J. Sleutels, et al., Ammonium recovery and energy production from urine by a microbial fuel cell, Water Res. 46 (2012) 2627–2636.

[73] C.U. Ugwu, H. Aoyagi, H. Uchiyama, Photobioreactors for mass cultivation of algae, Bioresour. Technol. 99 (2008) 4021–4028.

[74] R. Muñoz, B. Guieysse, Algal-bacterial processes for the treatment of hazardous contaminants: a review, Water Res. 40 (2006) 2799–2815.

[75] Y. Chisti, Biodiesel from microalgae., Biotechnol. Adv. 25 (2007) 294–306.

[76] B.E. Rittmann, Opportunities for renewable bioenergy using microorganisms., Biotechnol. Bioeng. 100 (2008) 203–212.

[77] D. Strik, H. Terlouw, H. Hamelers, C. Buisman, Renewable sustainable biocatalyzed electricity production in a photosynthetic algal microbial fuel cell (PAMFC), Appl. Microbiol. Biotechnol. 81 (2008) 659–668.

[78] S.B. Velasquez-Orta, T.P. Curtis, B.E. Logan, Energy from algae using microbial fuel cells, Biotechnol. Bioeng. 103 (2009) 1068–1076.

[79] Y. Zhang, J.S. Noori, I. Angelidaki, Simultaneous organic carbon, nutrients removal and energy production in a photomicrobial fuel cell (PFC), Energy Environ. Sci. 4 (2011) 4340–4346.

[80] Z. He, J. Kan, Y. Wang, Y. Huang, F. Mansfeld, K.H. Nealson, Electricity Production Coupled to Ammonium in a Microbial Fuel Cell, Environ. Sci. Technol. 43 (2009) 3391–3397.

[81] J. Kim, K. Kim, H. Ye, E. Lee, C. Shin, P.L. McCarty, et al., Anaerobic Fluidized Bed Membrane Bioreactor for Wastewater Treatment, Environ. Sci. Technol. 45 (2011) 576–581.

[82] B.C. Crump, E.V. Armbrust, J.A. Baross, Phylogenetic Analysis of Particle-Attached and Free-Living Bacterial Communities in the Columbia River, Its Estuary, and the Adjacent Coastal Ocean, Appl. Environ. Microbiol. 65 (1999) 3192–3204.

[83] J. Sambrook, D. Russell, Molecular Cloning: A Laboratory Manual, 3rd ed., New York, Cold Spring Harbor, 2001.

[84] B. Ewing, P. Green, Base-calling of Automated Sequencer Traces Using Phred. II. Error Probabilities, Genome Res. 8 (1998) 186–194.

[85] S.F. Altschul, W. Gish, W. Miller, E.W. Myers, D.J. Lipman, Basic Local Alinment Search Tool, J. Mol. Biol. 215 (1990) 403–410.

[86] Q. Wang, G.M. Garrity, J.M. Tiedje, J.R. Cole, Naive Bayesian Classifier for Rapid Assignment of rRNA Sequences into the New Bacterial Taxonomy, Appl. Environ. Microbiol. 73 (2007) 5261–5267.

[87] J.B.K. Park, R.J. Craggs, Wastewater treatment and algal production in high rate algal ponds with carbon dioxide addition, Water Sci. Technol. 61 (2010) 633–639.

[88] R.A. Rozendal, H.V.M. Hamelers, C.J.N. Buisman, Effects of Membrane Cation Transport on pH and Microbial Fuel Cell Performance, Environ. Sci. Technol. 40 (2006) 5206–5211.

[89] J.B.K. Park, R.J. Craggs, A.N. Shilton, Wastewater treatment high rate algal ponds for biofuel production., Bioresour. Technol. 102 (2011) 35–42.

[90] J.J. Fornero, M. Rosenbaum, M.A. Cotta, L.T. Angenent, Carbon Dioxide Addition to Microbial Fuel Cell Cathodes Maintains Sustainable Catholyte pH and Improves Anolyte pH, Alkalinity, and Conductivity, Environ. Sci. Technol. 44 (2010) 2728–2734.

[91] Y. Fan, H. Hu, H. Liu, Enhanced Coulombic efficiency and power density of air-cathode microbial fuel cells with an improved cell configuration, Cell. 171 (2007) 348–354.

[92] K.Y. Chan, K.H. Wong, P.K. Wong, Nitrogen and Phosphorus Removal from Sewage Effluent with High Salinity by Chlorella Salina, Environ. Pollut. 18 (1979) 139–146.

[93] Q. Dortch, The Interaction Between Ammonium and Nitrate Uptake in Phytoplankton, Mar. Ecol. Prog. Ser. 61 (1990) 183–201.

[94] S.W. Chisholm, Temporal Patterns of Cell Division in Unicellular Algae, Can Bull Fish Aquat Sci. 210 (1981) 150–181.

[95] O. Choi, A. Das, C.P. Yu, Z. Hu, Nitrifying Bacterial Growth Inhibition in the Presence of Algae and Cyanobacteria, Biotechnol. Bioeng. 107 (2010) 1004–1011.

[96] E. Molina, J. Fernández, F.G. Ación, Y. Chisti, Tubular photobioreactor design for algal cultures, J. Biotechnol. 92 (2001) 113–131.

[97] Y. Chisti, Biodiesel from Microalgae Beats Bioethanol, Trends Biotechnol. 26 (2008) 126–131.

[98] J.T. Force, Design of Munnicipal Wastewater Treatment Plants: WEF Manual of Practice No.8, Alexandria, Water Environment Federation, 1998.

[99] P.L. McCarty, J. Bae, J. Kim, Domestic wastewater treatment as a net energy producer--can this be achieved?, Environ. Sci. Technol. 45 (2011) 7100–7106.

[100] B. Logan, J. Regan, Electricity-producing Bacterial Communities in Microbial Fuel Cells, Trends Microbiol. 14 (2006) 512–518.

[101] P.R. LaSala, J. Segal, F.S. Han, J.J. Tarrand, X.Y. Han, First Reported Infections Caused by Three Newly Described Genera in the Family Xanthomonadaceae, J Clin Microbiol. 45 (2007) 641–654.

[102] P. Anil Kumar, T.N. Srinivas, C. Sasikala, V. Ramana Ch, Rhodobacter Changlensis sp. nov., A Psychrotolerant, Phototrophic Alphaproteobacterium From the Himalayas of India, Int J Syst Evol Microbiol. 57 (2007) 2568–2571.

[103] K.S. Yoon, N. Tsukada, Y. Sakai, M. Ishii, Y. Igarashi, H. Nishihara, Isolation and Characterization of A New Facultatively Autotrophic Hydrogen-oxidizing Betaproteobacterium, Hydrogenophaga sp. AH-24, FEMS Microbiol Lett. 278 (2008) 94–100.

[104] S.H. Ryu, M. Park, J.R. Lee, P.Y. Yun, C.O. Jeon, Brevundimonas Aveniformis sp. nov., A Stalked Species Isolated from Activated Sludge, Int J Syst Evol Microbiol. 57 (2007) 1561–1565.

[105] N. Singh, R. Gadi, Bioremediation of Ni(II) and Cu(II) from Wastewater by the Nonliving Biomass of Brevundimonas Vesicularis, J. Environ. Chem. Ecotoxicol. 4 (2012) 137–142.

[106] P. Chain, J. Lamerdin, F. Larimer, W. Regala, V. Lao, M. Land, et al., Complete Genome Sequence of the Ammonia-oxidizing Bacterium and Obligate Chemolithoautotroph Nitrosomonas Europaea, J Bacteriol. 185 (2003) 2759–2773.

[107] S.L. McLellan, S.M. Huse, S.R. Mueller-Spitz, E.N. Andreishcheva, M.L. Sogin, Diversity and Population Structure of Sewage-derived Microorganisms in Wastewater Treatment Plant Influent, Env. Microbiol. 12 (2010) 378–392.

[108] Y. Sun, J. Wei, P. Liang, X. Huang, Electricity Generation and Microbial Community Changes in Microbial Fuel Cells Packed with Different Anodic Materials, Bioresour. Technol. 102 (2011) 10886–10891.

[109] J. Kan, L. Hsu, A.C. Cheung, M. Pirbazari, K.H. Nealson, Current Production by Bacterial Communities in Microbial Fuel Cells Enriched from Wastewater Sludge with Different Electron Donors, Environ. Sci. Technol. 45 (2011) 1139–1146.

[110] S. Ishii, S. Suzuki, T.M. Norden-Krichmar, K.H. Nealson, Y. Sekiguchi, Y.A. Gorby, et al., Functionally Stable and Phylogenetically Diverse Microbial Enrichments from Microbial Fuel Cells During Wastewater Treatment, PLoS One. 7 (2012) 30495.

[111] B. Logan, B. Hamelers, B. Rozendal, U. Schroder, J. Keller, S. Freguia, et al., Microbial Fuel Cells : Methodology and Technology, Environ. Sci. Technol. 40 (2006) 5181–5192.

[112] K. Rabaey, W. Verstraete, Microbial fuel cells: novel biotechnology for energy generation, Trends Biotechnol. 23 (2005) 291–298.

[113] P. Clauwaert, K. Rabaey, P. Aelterman, L. de Schamphelaire, T.H. Pham, P. Boeckx, et al., Biological denitrification in microbial fuel cells, Environ. Sci. Technol. 41 (2007) 3354–3360.

[114] Y. Chisti, Biodiesel from microalgae, Biotechnol. Adv. 25 (2007) 294–306.

[115] X. Wang, Y. Feng, J. Liu, H. Lee, C. Li, N. Li, et al., Sequestration of CO2 discharged from anode by algal cathode in microbial carbon capture cells (MCCs), Biosens. Bioelectron. 25 (2010) 2639–2643.

[116] Y. Zhang, J.S. Noori, I. Angelidaki, Simultaneous organic carbon, nutrients removal and energy production in a photomicrobial fuel cell (PFC), Energy Environ. Sci. 4 (2011) 4340-4346.

[117] L. Xiao, E.B. Young, J.A. Berges, Z. He, Integrated photo-bioelectrochemical system for contaminants removal and bioenergy production, Environ. Sci. Technol. 46 (2012) 11459–11466.

CURRICULUM VITAE

Li Xiao

Place of birth: Gaoyou, Jiangsu, P.R. China

Education

B.S., University of Science and Technology of China, Hefei, Anhui, China, July 2009
Major: Chemistry

Ph.D., University of Wisconsin-Milwaukee, Milwaukee, WI, USA, December 2013
Major: Engineering

Dissertation Title: Recovering Bioresources from Integrated Photo-Bioelectrochemical System

Publications:

1. Xiao, L., Ge, Z., Kelly, P., Zhang, F. and He, Z. (2013) Evaluation of normalized energy recovery (NER) in tubular microbial fuel cells affected by reactor dimensions or substrates. Submitted.
2. Ge, Z., Li, J., Xiao, L., Tong, Y. and He, Z. (2013) Recovery of electrical energy in microbial fuel cells: a brief review. ***Evironmental Science & Technology Letters***. In Press.
3. Yossan, S., Xiao, L., Prasertsan, P. and He, Z. (2013) Hydrogen production in microbial electrolysis cells: choice of catholyte. ***International Journal of Hydrogen Energy***. 38, 9619-9624.
4. Ge, Z., Ping, Q., Xiao, L. and He, Z. (2013) Reducing effluent discharge and recovering bioenergy in an osmotic microbial fuel cell treating domestic wastewater. ***Desalination***. 312, 1584-1590.
5. Xiao, L., Young, E. B., Berges, J. A. and He, Z. (2012) Integrated photo-bioelectrochemical system for contaminants removal and bioenergy production. ***Evironmental Science & Technology***. 46, 11459-11466.
6. Xiao, L., Wen, Z., Ci, S., Wen, Z., Chen, J. and He, Z. (2012) Carbon/Iron-based nanorod catalysts for hydrogen production in microbial electrolysis cells. ***Nano Energy***. 1, 751-756.
7. Xiao, L., Damien, J., Luo, J., Jang, H. D., Huang, J. and He, Z. (2012) Crumpled graphene particles for microbial fuel cell electrodes. ***Journal of Power Sources***. 208, 187-192.
8. Luo, J., Jang, H., Sun, T., Xiao, L., He, Z. Katsoulidis, A., Kanatzidis, M., Gibson, J.M., and Huang, J. (2011) Compression and aggregation-resistant particles of crumpled soft sheets. ***ACS Nano***. 5, 8943-8949. (Cover Article)